Order Number 1335437

A non-plugging annulus control valve for extrusion of polymers and slurries

Wong, Joseph Man, M.S.

The University of Arizona, 1986

U·M·I
300 N. Zeeb Rd.
Ann Arbor, MI 48106

A NON-PLUGGING ANNULUS CONTROL VALVE FOR EXTRUSION OF POLYMERS AND SLURRIES

by

Joseph Man Wong

A Thesis Submitted to the Faculty of the

DEPARTMENT OF CHEMICAL ENGINEERING

In Partial Fulfillment of the Requirements
For the Degree of

MASTER OF SCIENCE

In the Graduate College

THE UNIVERSITY OF ARIZONA

1 9 8 6

STATEMENT BY AUTHOR

This thesis has been submitted in partial fulfillment of requirements for an advanced degree at The University of Arizona and is deposited in the University Library to be made available to borrowers under rules of the Library.

Brief quotations from this thesis are allowable without special permission, provided that accurate acknowledgment of source is made. Requests for permission for extended quotation from or reproduction of this manuscript in whole or in part may be granted by the copyright holder.

SIGNED: Joseph M Wong

APPROVAL BY THESIS DIRECTOR

This thesis has been approved on the date shown below:

D. H. White

D. H. WHITE
Professor of Chemical Engineering

12/12/86

Date

ACKNOWLEDGMENTS

I wish to express my sincere appreciation to Dr. Donald H. White, research advisor, for his guidance, advice, support, and the opportunity of taking part in this rewarding research project.

Special thanks go to Dr. David Wolf, Visiting Professor, for his recommendations and his comments in reviewing the original manuscript.

Finally, my deepest thanks go to my parents for their many years of continuous moral support and encouragement.

TABLE OF CONTENTS

		Page
	LIST OF ILLUSTRATIONS	vi
	LIST OF TABLES	ix
	ABSTRACT	x
1.	INTRODUCTION	1
	1.1 Statement of the Problem	3
	1.2 Objective and Scope of Research	5
2.	RHEOLOGY	7
	2.1 Rheological Equation of State	7
	2.2 Effect of Temperature on Viscosity	13
	2.3 Effect of Pressure on Viscosity	14
3.	PLASTICATING EXTRUDER	16
	3.1 Fundamentals of Extrusion	16
	3.2 Mathematical Modeling of the Metering Zone	19
	3.2.1 The Single-Screw Geometry	20
	3.2.2 Isothermal Flow of Newtonian Fluids	22
	3.2.3 Isothermal Flow of Non-Newtonian Fluids	25
4.	THEORY OF VALVE DESIGN	30
	4.1 Control Valve Characteristics	30
	4.2 Valve Seals	32
	4.2.1 Factors Governing Effective Closure	32
	4.2.2 Stuffing Box and Gland Seal	34
	4.2.3 Factors Governing Gasket Seal	36
	4.3 Mechanical Considerations	37
5.	DEVELOPMENT OF A NON-PLUGGING ANNULAR CONTROL VALVE	38
	5.1 Isothermal Flow Between Coaxial Cylinders	40
	5.2 Modeling of the Flow Through Each Valve Section	44
	5.3 Installed Valve Characteristic	46
	5.4 Design Criterion	49
	5.5 Results of Parametric Evaluation	51

TABLE OF CONTENTS--Continued

		Page
6.	EXPERIMENTAL PROCEDURES AND RESULTS	66
	6.1 Description of Apparatus	66
	6.2 Experimental Procedures	67
	6.3 Experimental Results	70
	6.3.1 Dow Low-Density Polyethylene	71
	6.3.2 Sawdust and Polyethylene	75
	6.3.3 Albany Wood Flour and Polyethylene	77
	6.3.4 Albany Wood Flour and Vacuum Bottom	84
	6.4 Viscosity of Wood Slurries	86
7.	CONCLUSIONS AND RECOMMENDATIONS	90
	7.1 Conclusions	90
	7.2 Recommendations	91
	APPENDIX A: COMPUTER CODE AND SIMULATION RESULTS	93
	APPENDIX B: TABULATED EXPERIMENTAL RESULTS	106
	NOMENCLATURE	118
	REFERENCES	121

LIST OF ILLUSTRATIONS

Figure		Page
1.1	The overall flow diagram of the Advanced Extruder-Reactor Biomass Liquefaction Unit	2
1.2	Installed valve characteristic of a needle type extruder valve	4
2.1	Steady-state laminar velocity profile for drag flow . . .	8
2.2	Logarithmic flow curve for Alathon 14 LDPE at 126°C . . .	12
3.1	Schematic diagram of a single-screw plasticating extruder	17
3.2	Geometry of a single screw (double flighted)	21
3.3	Geometry of the "unwound" helical screw channel	21
3.4	Dimensionless flow rate as a function of pressure gradient calculated by Griffith (1962)	27
3.5	Dimensionless flow rate as a function of pressure gradient calculated by Middleman (1977)	29
4.1	Inherent flow characteristic of valves	31
4.2	Stuffing box and gland assembly	35
5.1	Conceptualized diagram of the annular control valve . . .	39
5.2	Fredrickson-Bird Y factor for flow of power-law fluids inside annulus	42
5.3	Radial position $r = \lambda R$ at which the shear stress is zero .	43
5.4	Schematic flow diagram detailing the procedure used to calculate the installed valve characteristic	48
5.5	Logarithmic flow curves for a Dow type 955 LDPE and a Dupont Alathon 3 LDPE	50
5.6	Simulated valve characteristics for different conical angle φ	53

LIST OF ILLUSTRATIONS--Continued

Figure		Page
5.7	Simulated valve characteristics for two different annular spacings	54
5.8	Simulated valve characteristics for different annular radii	56
5.9	Simulated valve characteristics for different annular length L_a	57
5.10	Simulated valve characteristic for the extrusion of a Dupont Alathon 3 LDPE	59
5.11	Detailed diagram of the annular valve	60
5.12	Detailed drawing of the valve body	61
5.13	Detailed drawing of the valve trim	62
5.14	Detailed drawing of the removable conical valve plug	63
5.15	Detailed drawing of the valve bonnet	64
5.16	Detailed drawing of the gland assembly	65
6.1	Schematic diagram of the instrumentation and apparatus layout	68
6.2	Schematic of detail mounting of instrumentation on the extruder barrel	69
6.3	Valve characteristics for the extrusion of a Dow LDPE at different temperatures	73
6.4	Flow rate as a function of valve opening	74
6.5	Valve characteristics for the extrusion of a 40:60 wt % sawdust/LDPE regrind at different screw RPM	76
6.6	Flow rate as a function of screw RPM	78
6.7	Valve characteristics for the extrusion of Albany wood flour/LDPE slurry at different concentrations	79
6.8	Valve characteristics for the extrusion of a 60:40 wt % WF/LDPE slurry at different RPM	81

LIST OF ILLUSTRATIONS--Continued

Figure		Page
6.9	Valve hysteresis for the extrusion of a 60:40 wt % WF/LDPE at 60 RPM	82
6.10	Effect of the conical geometry for the extrusion of a 60:40 wt % WF/LDPE slurry at 40 RPM	83
6.11	Valve characteristic for the extrusion of a 40:60 wt % WF/VB slurry at 40 RPM	85

LIST OF TABLES

Table		Page
2.1	Summary of rheological relations for time-independent non-Newtonian fluids in Cartesian coordinates	10
5.1	Power-law parameters for a Dow type 955 LDPE at 175°C and a Dupont Alathon 3 LDPE at 190°C	51
5.2	The screw dimensions for the metering zone of the Prodex extruder	52
6.1	Apparent viscosity of wood slurries	89

ABSTRACT

An annular control valve was developed for the extrusion of wood slurries and polymers. The objective was to determine the optimal valve geometry: 1) to provide a linear pressure drop across the valve as a function of valve opening and 2) to eliminate the problem of valve plugging caused by the high solid content of the wood slurries.

The approach was to model the non-Newtonian flow in a plasticating single-screw extruder. A finite-difference scheme was developed to model the flow through annular surfaces. The two flow equations were solved simultaneously and a parametric study was performed to determine the optimal valve geometry.

The valve operability was evaluated for the extrusion of various mixtures of low-density polyethylene, sawdust, wood flour, and vacuum bottom. The experimental results were in good agreement with the model. In general, a linear valve characteristic was observed and the problem of valve plugging was not evident.

CHAPTER 1

INTRODUCTION

The Department of Chemical Engineering at The University of Arizona has developed an Advanced Extruder-Reactor Biomass Liquefaction System to convert wood flour into a liquid oil product by direct liquefaction. The unique aspect of the system involves a modified single-screw plasticating extruder similar to those used in the polymer industry to pump and transport a highly concentrated and viscous wood slurry into a 3000 psi pressure reactor. The modified extruder has been shown to be capable of pumping slurries as high as 60 wt % wood flour. The overall schematic diagram of the system is shown in Figure 1.1. A detailed description was given by Battelle Labs (1981).

The extreme process conditions and hazardous materials encountered in the system have prompted the design of an automatic control system. Experience with the operation of the experimental unit has shown that a major control parameter is the extruder outlet pressure. Variations in the nature of raw material, such as bulk density and concentration, tend to cause the pressure generated by the extruder to fluctuate. A non-plugging control valve was developed in this research to help stabilize the pressure.

In many extrusion processes, the pressure generated by the extruder can be established by the use of screen packs. The type and size of screen are determined by a trial-and-error procedure to produce

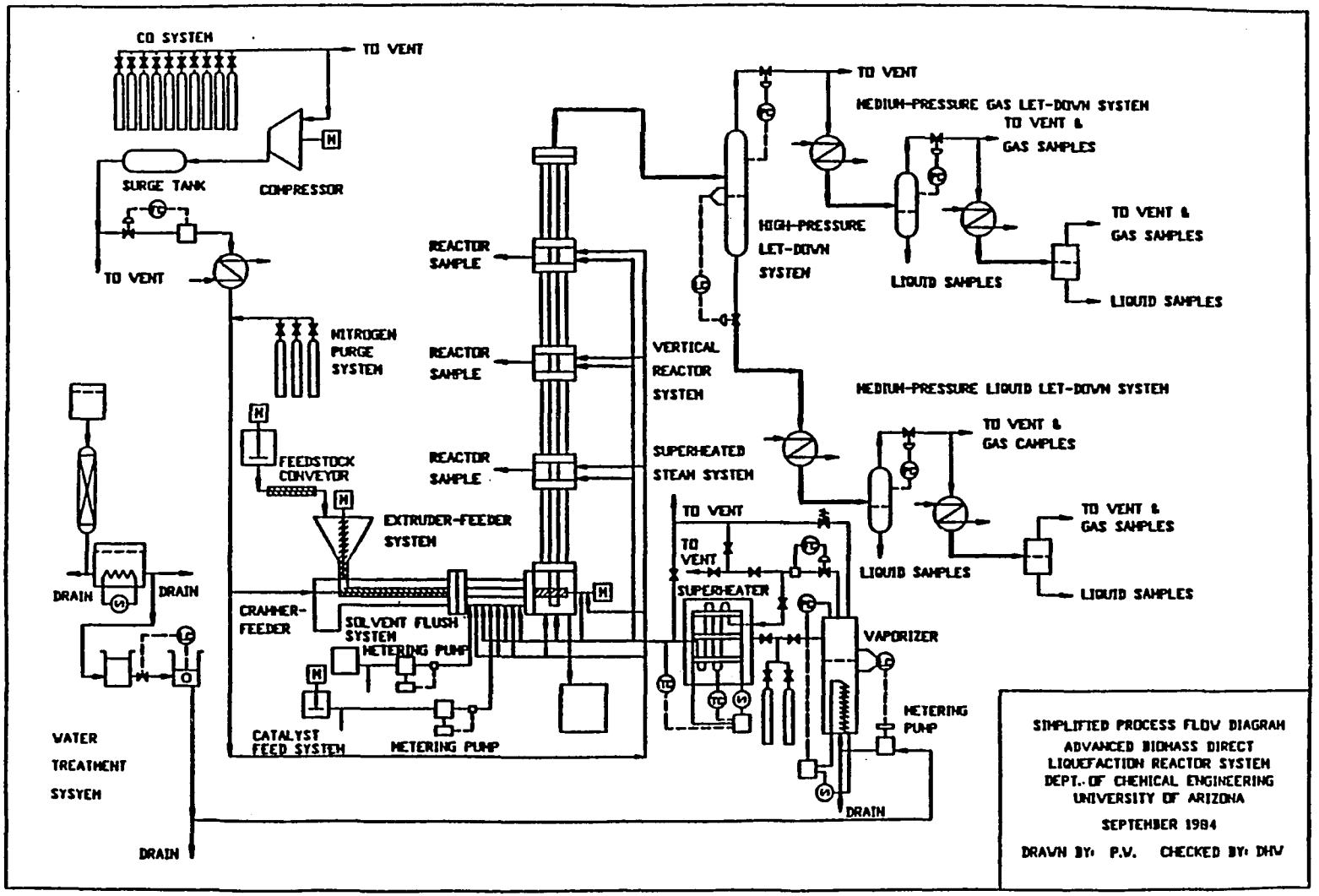

Figure 1.1 The overall flow diagram of the Advanced Extruder-Reactor Biomass Liquefaction Unit.

the required pressure drop. The application of a valve or a gear pump has gained popularity in recent extruder design. The use of a valve is of interest in microprocessor control of extrusion processes. A valve represents a suitable method of changing the pressure drop and, consequently, the extruder outlet pressure.

1.1 Statement of the Problem

One of the difficulties in using a valve is the non-linearity between the valve restriction and the pressure drop across the valve. It is important to recognize that the pressure profile inside the extruder is influenced by many parameters, such as temperature profile, rheology, and flow rate. Increasing the pressure drop by increasing the valve restriction would also reduce the melt viscosity to counteract the increase in pressure drop. In addition, the valve restriction would generate different shear behavior on the non-Newtonian material flowing through the valve, which will also affect the pressure drop. This non-linear and interactive response of the control variable to the controlling element makes controlling the extruder pressure a difficult issue.

The non-linear characteristic is illustrated in Figure 1.2 for the extrusion of a Dow low-density polyethylene (LDPE). A valve with a needle-type configuration was installed at the extruder outlet to control the pressure. The results for the pressure drop across the valve as a function of valve restriction are shown. The valve has an on-off characteristic and is not suitable for control applications. A relatively small change in valve restriction will result in an exponential

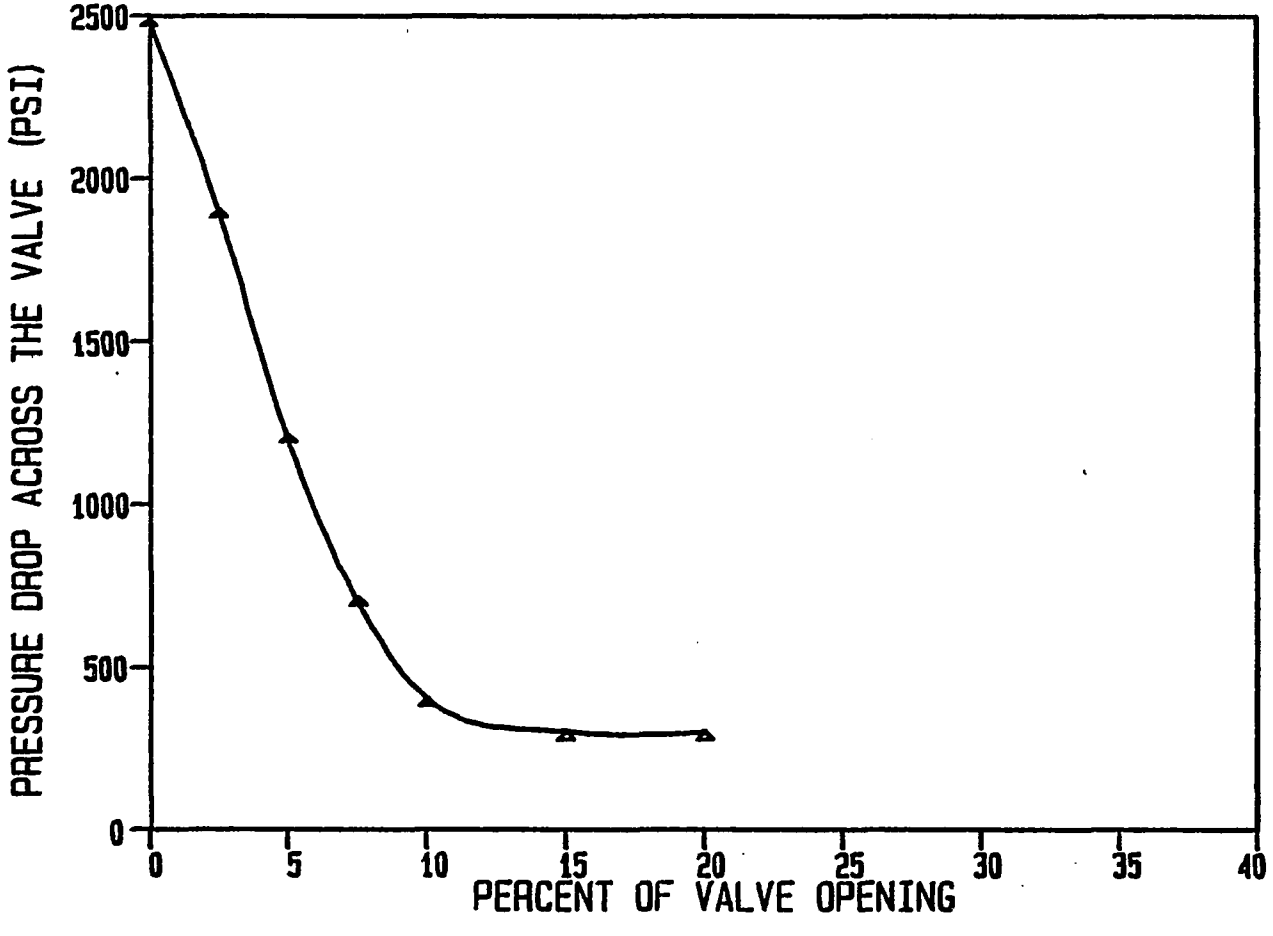

Figure 1.2 Installed valve characteristic of a needle type extruder valve.

decrease in the pressure drop. Similar results have been reported by Patterson, Branchi, and Paris (1979).

Another major problem of using a commercially available valve is the plugging of the valve orifice by the high solids content of the wood slurries. Experience with the operation of the biomass liquefaction unit has shown that plugging of pipelines, fittings, and valves is a major problem. The appropriate valve configuration must be sized to minimize this problem.

1.2 Objective and Scope of Research

In view of the above-stated problems, the objective of the research was to develop a valve suitable for controlling the extruder outlet pressure. The criterion was to determine the optimal valve geometry which has a linear pressure drop as a function of valve restriction. The motivation was for the extrusion of wood slurries in the biomass liquefaction process. However, this development was not restricted to the extrusion of slurries, but would also be applicable to the polymer industry.

The approach taken was to model the non-Newtonian flow in a plasticating single-screw extruder. A finite-difference method was also developed to model the flow through an annular valve geometry. The two flow equations were coupled to establish the installed valve characteristic. Parametric studies were performed on various valve dimensions to determine the optimal valve geometry. This analysis was complicated by the lack of reliable rheological properties for the wood slurries. It was observed that wood slurries behave as pseudoplastic fluids at low

shear rate and the rheology could be predicted by the power-law equation. In view of this, the rheological properties of a Dow LDPE were selected for design purposes. Polyethylene is a pseudoplastic fluid and the power-law model was equally applicable. The goal then became the design of a control valve for the extrusion of polyethylene. Engineering judgment and flexibility in valve design were applied. In this fashion, it was believed that the valve could also be used for the extrusion of wood slurries and other polymers. Experiments were conducted with the Dow LDPE to verify the validity of the model. Additional experiments were performed on wood slurries to determine operating characteristics.

CHAPTER 2

RHEOLOGY

2.1 Rheological Equation of State

Rheology is the science of deformation and flow of materials. The rheology of a fluid is the fashion in which it deforms and flows in response to an applied shear stress. A rheological equation is a mathematical description of shear stress and shear rate. Many fluids can be described accurately by a linear relation between shear stress and shear rate. For a case of drag flow between parallel plates as illustrated in Figure 2.1, the rheological equation is:

$$\tau_{yx} = - \mu \frac{dv_x}{dy} \qquad [2.1]$$

where τ_{yx} is the shear stress defined as the shear force per unit area applied to the lower plate. The shear rate $\dot{\gamma}$ is defined as the derivative of the velocity gradient:

$$\dot{\gamma} = \frac{dv_x}{dy} \qquad [2.2]$$

The proportionality constant μ is defined as the viscosity of the fluid. This class of fluids is generally referred to as Newtonian. There are many types of fluids, particularly those of polymer melts, slurries, and asphalts, which do not exhibit this behavior. A great deal of research effort has been expended to develop rheological equations which govern the complex behavior of non-Newtonian fluids.

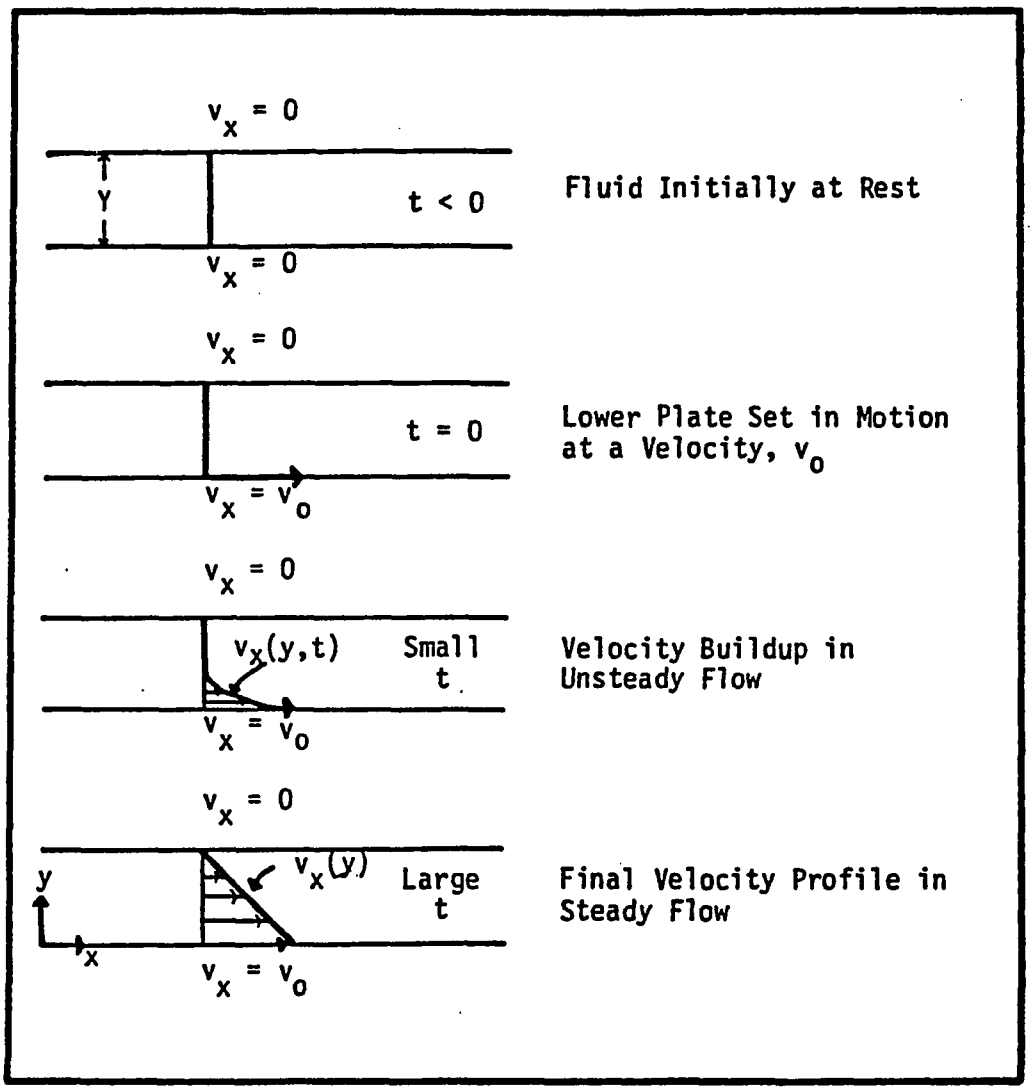

Figure 2.1 Steady-state laminar velocity profile for drag flow.

The approach commonly taken is the generalization of the Newtonian model:

$$\tau = - \eta\dot{\gamma} \qquad [2.3]$$

where η is the apparent viscosity. In general, researchers have separated fluids in which η depends on the previous shear history of the fluids as well as on the shear rate and those fluids in which η depends on shear rate only. The first category is known as time-dependent fluids. Those materials are further divided into two classifications, thixotropic fluids and rheopectic fluids, depending upon whether the shear stresses decrease or increase with time. The second category is commonly referred to as time-independent fluids. Most polymer melts are under this classification and will be discussed below.

Many rheological equations have been proposed to predict non-Newtonian flow behavior. Skelland (1967) has summarized the results. A partial list of the rheological equations applicable to time-independent fluids is shown in Table 2.1. Due to the mathematical complexity, most of these equations are rarely used. The most common rheological equation is the power-law or the Ostwald and de Waele model. For the flow behavior depicted in Figure 2.1, the power-law equation is:

$$\tau_{yx} = - m|\dot{\gamma}|^{n-1} \dot{\gamma} \qquad [2.4]$$

The absolute sign is required because the shear rate may be negative. If the shear rate is positive, the above equation can be written as:

$$\tau = - m\dot{\gamma}^{n} \qquad [2.5]$$

The power-law model relates the shear rate and shear stress through two empirical constants, the fluid behavior index n, and the consistency index m. The apparent viscosity is defined by:

Table 2.1 Summary of rheological relations for time-independent non-Newtonian fluids in Cartesian coordinates.

1.	Newtonian	$\tau = -\mu\dot{\gamma}$	
2.	Bingham plastic	$\tau = -\mu\dot{\gamma} + \tau_o$	if $\lvert\tau\rvert > \tau_o$
		$\tau = \tau_o$	if $\lvert\tau\rvert < \tau_o$
3.	Power law	$\tau = -n\dot{\gamma}^n$	
4.	Reiner-Philipoff	$\tau = [\mu_\infty + \frac{\mu_o - \mu_\infty}{1 + (\tau/B)^2}]\dot{\gamma}$	
5.	Powell-Frying	$\tau = \mu_\infty[\frac{\text{arc sinh } (\mu_o\dot{\gamma}/B)}{(\mu_o\dot{\gamma}/B)}]\dot{\gamma}$	
6.	Ellis	$\tau = [\frac{\mu_o}{1 + (\mu_o/\eta_o)\lvert\tau\rvert^{m-1}}]\dot{\gamma}$	

$$\eta = m\dot{\gamma}^{n-1} \qquad [2.6]$$

For most polymeric materials, the exponent n is less than unity and the apparent viscosity decreases with increasing shear rate. This behavior is known as pseudoplastic. If the exponent n is greater than unity or the apparent viscosity increases with increasing shear rate, this behavior is classified as dilatant.

The two empirical constants can be determined by taking the logarithm of Equation 2.5:

$$\log (-\tau) = n \log (\dot{\gamma}) + \log m \qquad [2.7]$$

A plot of log $(-\tau)$ versus log $\dot{\gamma}$, which is called a logarithmic flow curve, will give a straight line over a short shear rate range with a slope of n. The consistency index m can be obtained from the same graph, since $m = -\tau$ at $\dot{\gamma} = 1$.

In view of the simplicity, most polymer rheology could be approximated by the power-law behavior. Logarithmic flow curves for most polymer melts often appear to be linear if restricted to a few decades of shear rate. However, if extended over several decades, most polymer melts appear to give curves. A logarithmic flow curve for a Dupont Alathon-14 low-density polyethylene is shown in Figure 2.2. At very low shear rates, the slope of the curve is unity, indicating Newtonian behavior. At higher shear rates, the slope of the curve becomes less than unity, reflecting pseudoplastic behavior. At the higher spectrum, the slope continually decreases, indicating a greater deviation from Newtonian fluids.

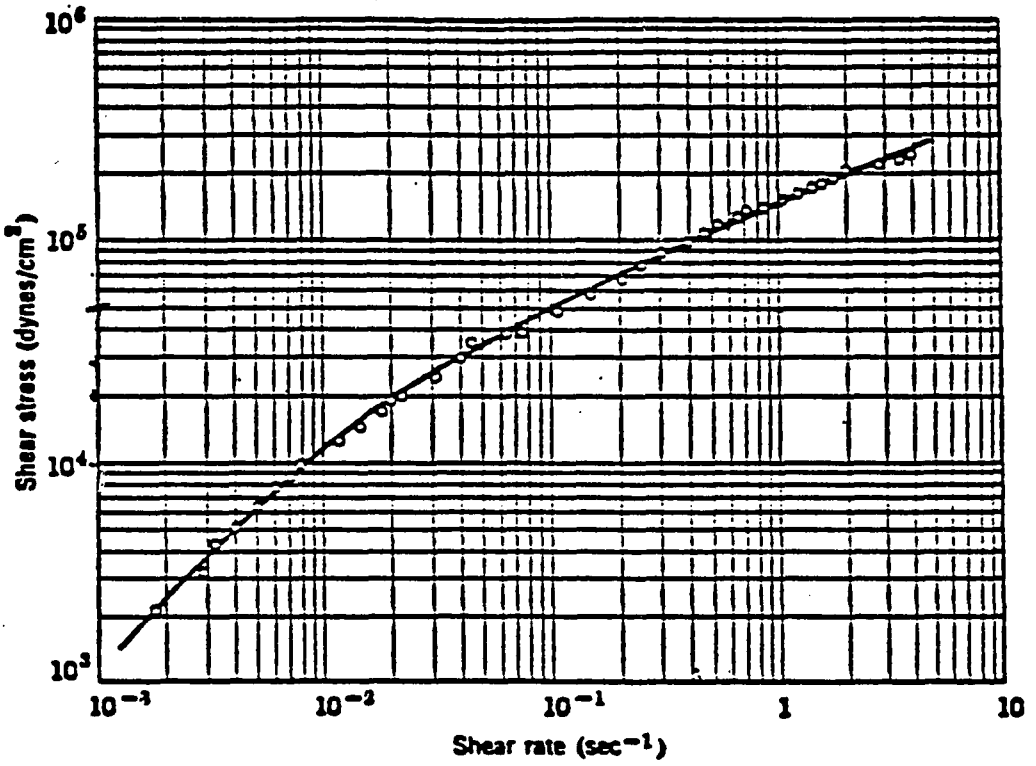

Figure 2.2 Logarithmic flow curve for Alathon 14 LDPE at 126°C. -- From McKelvey (1962, p. 34).

2.2 Effect of Temperature on Viscosity

The dependence of viscosity on temperature cannot be underestimated. Eyring, Glasstone, and Lardle (1941) have derived an Arrhenius equation expressing the effect of temperature for Newtonian fluids:

$$\mu = Ae^{E/RT} \qquad [2.8]$$

where A is an empirical coefficient depending upon the nature of the fluids, E is an activation energy for flow, and R is the universal gas constant. The validity of the Arrhenius equation can be tested by plotting log μ versus the reciprocal of temperature. For most liquids following the Newtonian model, a relatively straight line over a temperature of 100°F is observed.

Apparent viscosity of a non-Newtonian fluid is a function of shear rate or shear stress. This relation can be expressed as:

$$\eta = \eta_1(\tau, T) \qquad [2.9]$$

or

$$\eta = \eta_2(\dot{\gamma}, T)$$

Consequently, the viscosity-temperature relation can be studied either at constant shear rate or at constant shear stress. In either case, the relation can be expressed by the Arrhenius equations:

$$\eta = Ae^{E_\tau/RT} \qquad [2.10]$$

$$\eta = Ae^{E_{\dot{\gamma}}/RT}$$

The first expression relates the apparent viscosity with temperature at constant shear stress and the latter expresses the viscosity-temperature

dependence at constant shear rate. In general, the activation energies are related by:

$$\frac{E_\tau}{E^*_{\dot\gamma}} = 1 - \dot\gamma \left(\frac{\partial n}{\partial \tau} \right)_T \qquad [2.11]$$

If the fluids obey the power-law model, the ratio of the activation energies becomes:

$$E_\tau = \frac{1}{n} E^*_{\dot\gamma} \qquad [2.12]$$

For a temperature change of ΔT at constant shear rate, the viscosity change is given by:

$$\ln \left(\frac{n_2}{n_1} \right) = \frac{E^*_{\dot\gamma} \Delta T}{R T_2 T_1} \qquad [2.13]$$

Similarly, for an incremental temperature change of ΔT at constant shear stress:

$$\ln \left(\frac{n_2}{n_1} \right) = - \frac{E_\tau \Delta T}{R T_1 T_2} \qquad [2.14]$$

2.3 Effect of Pressure on Viscosity

The viscosity of polymer melts will ultimately depend on the molecular attractive forces and the intermolecular distance. Compression of polymer melts will result in an increase of polymer viscosity. The importance of this concept can be illustrated by the negligible change in viscosity with temperature at constant volume:

$$\left(\frac{\partial \mu}{\partial T} \right)_v = 0 \qquad [2.15]$$

Since the compressibility of polymer melts is higher at operating temperature, it is apparent that viscosity is even more affected. Most

polymer processes take place at high pressure; therefore, it is important to examine the pressure dependence of viscosity.

Cogswell (1973) has summarized experiments in which viscosity changes with temperature at constant pressure $(\partial\eta/\partial T)_p$ and viscosity changes with pressure at constant temperature $(\partial\eta/\partial P)_T$ are recorded. He observed that viscosity gradients appear to have a linear response when log η is plotted versus either pressure or temperature. Based on this observation, he suggested that the effect of pressure on viscosity can be related to the temperature effect through a coefficient - $(\Delta T/\Delta P)_\eta$. Thus, the increase in pressure has an equivalent effect on viscosity to that of decreasing temperature. It is further observed that - $(\Delta T/\Delta P)_\eta$ appears to be independent of the molecular weight and the type of polymer. Cogswell estimated a coefficient of 5.2×10^{-7} °C/Nm^{-2} for a low-density polyethylene at 220°C. If this polymer is extruded at 3000 psi, this is equivalent to a temperature drop of 12°C.

Another popular method to approximate the pressure dependence of viscosity is Eyring's "hole theory":

$$\mu_p = \mu_{po}\, e^{b(P-P_o)} \qquad [2.16]$$

where μ_p and μ_{po} are the viscosity at the operating pressure p and atmospheric pressure po. The "b" is a pressure coefficient which depends on the hole volume v_H and absolute temperature:

$$b = \frac{v_H}{RT} \qquad [2.17]$$

Pressure coefficients for common polymer melts were measured by Semjonow (1965).

CHAPTER 3

PLASTICATING EXTRUDER

3.1 Fundamentals of Extrusion

A plasticating extruder has many functions; it can operate as a mixer, a reactor, or a pump. In the biomass liquefaction unit, the extruder functions both as a preheater and as a screw pump. The principal objective of a plasticating extruder is to transport and melt solid polymeric materials in the form of pellet or powder into a homogeneous fluid at a pressure, temperature, and flow rate suitable for the next stage of operation. In most polymer processes, the next stage of operation is the formation of polymeric products by means of a die. Plastic film, pipe, and plastic-coated wire are examples of common products manufactured by the extruder.

The most widely used extruder is the single-screw plasticating extruder shown in Figure 3.1. The solid polymer is transported along the extruder by the relative motion of the screw and the barrel. The screw is driven by a motor and gear reducer system. The extruder barrel is equipped with a cooling and heating system to control the operating temperature. As the polymer is conveyed along the screw channel, a homogeneous melt is produced by the heat supplied by the barrel and the heat generated by the shearing action of the screw.

The plasticating screw is divided into three regions: the feed zone, the compression or melting zone, and the metering zone. Each zone

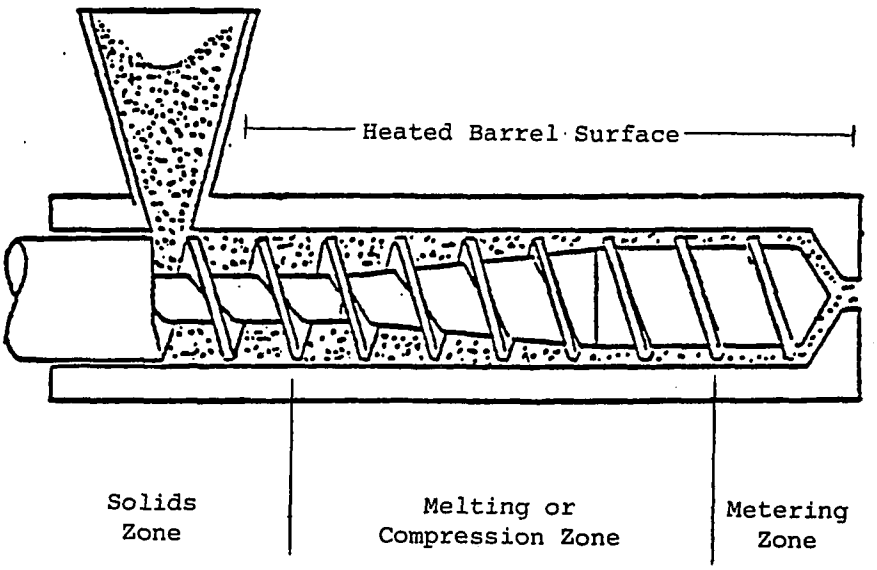

Figure 3.1 Schematic diagram of a single-screw plasticating extruder.

has a unique design and configuration, depending upon its function and the physical properties of the polymers. In general, the channel depth is greatest in the feed zone and gradually decreases in the compression zone to compensate for the change in the different conveying characteristics between the solid and the polymer melt.

Solid transport occurs in the feeding zone. Its function is to convey solid polymers from the extruder hopper to the compression region where the polymers begin to melt. The important factor in solid transport is the coefficient of friction between the polymers and the contact surfaces. It is believed that solid polymers compact together to form a plug that is acted upon by the frictional forces between the polymers and the surfaces of the screw and the barrel. The most recent solid-conveying model was proposed by Agur and Vlachopoulous (1982), in which they assumed that the solid bed is isothermal and travels as a solid plug with constant velocity.

The function of the melting zone is to produce a uniform polymer melt at a desirable temperature. There are two mechanisms by which melting occurs. The first involves the conduction of heat from the extruder barrel. The second method comes from the dissipation of mechanical energy into heat due to the viscous shear action on the screw near the barrel and by viscous shear in the melt itself. The coexistence of polymer melt and polymer pellets complicates the modeling of the melting zone. Maddock (1959) was the first to present a qualitative description of the melting mechanism generally accepted today. According to his theory, the solid polymer begins to melt in a thin film of fluid formed between the extruder barrel and the moving polymer

pellets. The advancing screw flight continuously melts the melted film and forces the polymer melt downward along the flight surface and into a circulating melt pool. The polymer melt is collected at the rear of the channel where the forward portion remains filled with solid pellets. As the polymer conveys along the screw, the thickness of the melt increases, while the thickness of the solid bed decreases. Eventually, a homogeneous melt is produced.

Based on Maddock's (1959) observations, various mathematical models have been formulated by Tadmore and Klein (1970) and Donovan (1971). The use of their models requires a lengthy iterative numerical computation procedure. Since the differential equations describing the melting region are too complex to yield exact analytical solutions, Mount, Walson, and Chung (1982) have proposed an approximated solution by seeking asymptotically limiting cases. The accuracy of their model has proved to be satisfactory. A review of the different melting models was presented by Lindt (1985).

3.2 Mathematical Modeling of the Metering Zone

The metering zone is the most important section of a plasticating extruder and, consequently, a detailed treatment is presented. This zone usually determines the output characteristic of the process. In the metering zone, three major flow components can be identified: drag flow, pressure flow, and leakage flow. Drag flow is the forward conveying motion caused by the relative action between the rotating screw and the statinary barrel. Pressure flow is a backflow along the screw channel caused by the pressure difference between the inlet and

the extruder outlet. Leakage flow is the result of the pressure difference between successive turns of the channel which causes a backward leakage between the flight of the screw and the inner extruder barrel. This leakage flow is usually a small fraction of the total flow and is ignored.

3.2.1 The Single-Screw Geometry

Figure 3.2 illustrates a typical double-flighted screw geometry with the reference axis shown. The z-component is directed along the screw helix and is referred to as the helical screw axis. The x-axis is perpendicular to the helical screw axis. The y-component is directed outward towards the extruder barrel. The principal screw geometries are the channel width W, the inside diameter of the barrel D, the annular distance between the root of the screw and the barrel surface H, the clearance between the crest of the screw flight and the inner barrel δ_f, the width of the screw flight measured normal to the helical screw axis e, and the helical screw angle Θ. It is important to note that the channel geometries could vary along the entire screw.

In the modeling of the flow behavior along the metering zone of an extruder, certain geometric simplifications prove necessary. A considerable amount of flow complexity could be resolved if the ratio of channel depth to screw diameter is small, such that the curvature effect of the helical channel around the screw is ignored. This is analogous to unwinding the helical screw channel and laying it flat, as illustrated in Figure 3.3. The barrel is conceptualized as an infinite plate stacked on top of the screw channels. It is also assumed that there is

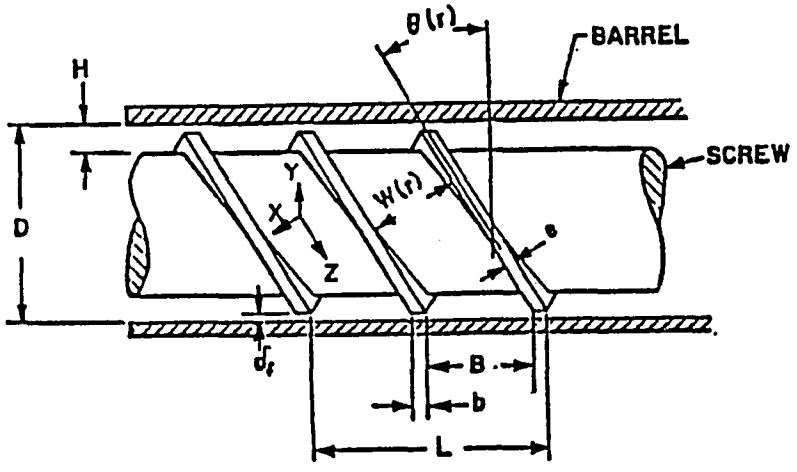

Figure 3.2 Geometry of a single screw (double flighted) -- From Tadmore and Klein (1970, p. 40).

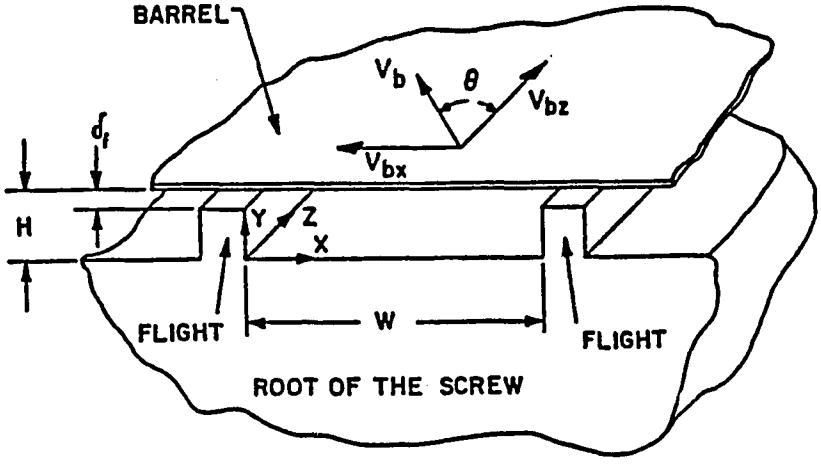

Figure 3.3 Geometry of the "unwound" helical screw channel. -- From Tadmore and Klein (1970, p. 185).

no clearance between the crest of the screw flight and the barrel. This is equivalent to ignoring leakage flow. The problem then becomes the analysis of the pressure flow and the drag flow in a rectangular channel. The relative motion of the screw and barrel becomes identical to a steady motion of the barrel moving at the helical angle Θ relative to the helical screw axis z. Thus, a drag flow will be observed with components in the x- and z-directions.

Because of the high viscosity of the polymer melts, the flow inside the metering zone is laminar. The steady-state motion for the cases of isothermal Newtonian fluid and the non-Newtonian fluid will be presented.

3.2.2 Isothermal Flow of Newtonian Fluids

For a Newtonian fluid, the steady-state momentum equation along the helical screw axis z can be written as:

$$\rho[v_x(\frac{\partial v_z}{\partial x}) + v_y(\frac{\partial v_z}{\partial y}) + v_z(\frac{\partial v_z}{\partial z})]$$

$$= -(\frac{\partial p}{\partial z}) + \mu[\frac{\partial^2 v_z}{\partial x^2} + \frac{\partial^2 v_z}{\partial y^2} + \frac{\partial^2 v_z}{\partial z^2}] \qquad [3.1]$$

The inertial terms appearing in the left-hand side are generally neglected due to the highly viscous flow. It is also important to assume that the screw geometry is uniform throughout the metering zone and that v_z is not a function of z. Equation 3.1 then becomes:

$$\frac{\partial p}{\partial z} = \mu[\frac{\partial^2 v_z}{\partial x^2} + \frac{\partial^2 v_z}{\partial y^2}] \qquad [3.2]$$

The boundary conditions are:

$$v_z\ (0,y) = 0 \qquad v_z\ (x,0) = 0$$

$$v_z\ (W,y) = 0 \qquad v_z\ (x,H) = V_b$$

where V_b is the screw velocity directed along the helical screw axis z. The solution to the equation can be obtained through the method of separation of variables.

The velocity component can be separated into a pressure term v_p and a drag term v_D:

$$v_z = v_D + v_p$$

The pressure flow component becomes:

$$\frac{\partial^2 v_p}{\partial x^2} + \frac{\partial^2 v_p}{\partial y^2} = \frac{1}{\mu}\left(\frac{\partial p}{\partial z}\right) \qquad [3.3]$$

and the drag flow component becomes:

$$\frac{\partial^2 v_D}{\partial x^2} + \frac{\partial^2 v_D}{\partial y^2} = 0 \qquad [3.4]$$

The boundary conditions are:

$$v_p\ (0,y) = 0 \qquad v_D\ (0,y) = 0$$

$$v_p\ (W,y) = 0 \qquad v_D\ (W,y) = 0$$

$$v_p\ (x,0) = 0 \qquad v_D\ (x,0) = 0$$

$$v_p\ (x,H) = 0 \qquad v_D\ (x,H) = V_b$$

The solutions which satisfied the above equations were expressed in Tadmore and Gogos (1979). The solutions are given by an infinite Fourier series, and the most useful result is the volumetric flow rate, following from:

$$Q = \int_0^W \int_0^h v_z(x,y)\,dxdy \qquad [3.5]$$

The result is:

$$Q = \frac{V_b WH}{2} F_D - \frac{WH^3 \Delta p}{12 \mu L} F_p \qquad [3.6]$$

The first term in Equation 3.6 represents the drag flow component and the latter is the pressure flow. V_b can be related to the screw speed in revolutions per unit time:

$$V_b = \pi DN \cos \Theta \qquad [3.7]$$

where μ is the fluid viscosity and L is the length of the metering zone. The parameters F_D and F_p are the drag flow and pressure flow shape factors, respectively. The shape factors can be expressed as infinite series:

$$F_d = \frac{16}{\pi^3 (H/W)} \sum_{i=1,3}^{W} \frac{1}{i^3} \tanh \left[\frac{\delta \pi (H/W)}{2} \right] \qquad [3.8]$$

$$F_p = 1 - \frac{192 (H/W)}{\pi^5} \sum_{i=1,3}^{W} \frac{1}{i^3} \tanh \left[\frac{\delta \pi}{2 (H/W)} \right] \qquad [3.9]$$

The theoretical values of F_d and F_p are between zero and unity, depending upon the aspect ratio (H/W).

In many applications, the flow in the extruder can be approximated by the simplified flow theory. The development of the model is analogous to the previous theory with the added assumption that the variation of v_z with respect to x is negligible. Equation 3.3 can be simplified to:

$$\frac{1}{\mu} \left(\frac{\partial p}{\partial z} \right) = \frac{d^2 v_z}{dy^2} \qquad [3.10]$$

$$v_z (0) = 0$$

$$v_z (H) = V_b$$

The solution to the simplified flow theory is analogous to Equation 3.6 with the shape factors equal to unity, which is applicable to screws having a small (H/W) value.

3.2.3 Isothermal Flow of Non-Newtonian Fluids

For the Newtonian fluids, the validity of the rectangular channel approximation has been confirmed by numerous experiments. However, most polymer melts are non-Newtonian, such that a non-Newtonian model is needed. There have been many attempts to modify the non-Newtonian viscosity and superimpose it with the Newtonian equation. In the approach taken by Booy (1981), he estimated an effective viscosity for the flow of non-Newtonian fluids. This effective viscosity is equivalent to the Newtonian viscosity that would give the same screw performance with non-Newtonian flow at the same operating conditions. Once the effective viscosity is determined, it can be inserted into the pressure term of the simplified Newtonian equation.

In a more recent approach, Shirato, Murase, and Iwata (1983) estimated an average differential viscosity based on the power-law model:

$$\bar{\mu} = mn\left(\frac{V_b}{H}\right)^{n-1} \qquad [3.11]$$

In most circumstances, the above approximations are inadequate in predicting non-Newtonian flow. A theoretical model is required.

There are many publications dealing with the modeling of non-Newtonian flow inside a plasticating extruder. In most cases, the

"parallel plate" approximation is necessary. It is also important to reiterate and state additional assumptions which prove helpful:

1. Inertial terms are neglected.
2. The velocity profile is fully developed along the helical screw axis; therefore, the velocity components are not functions of z.
3. The aspect ratio W/H is large enough such that the velocity components v_x and v_z are independent of x and are functions of y only.

For a power-law fluid flowing in a rectangular channel, the velocity profiles along the helical screw axis z and axial axis x are:

$$0 = - \frac{\partial p}{\partial x} + m \frac{\partial}{\partial y} \left\{ \left[\left(\frac{\partial v_x}{\partial y} \right)^2 + \left(\frac{\partial v_z}{\partial y} \right)^2 \right]^{(n-1)/2} \frac{\partial v_x}{\partial y} \right\} \qquad [3.12]$$

$$0 = - \frac{\partial p}{\partial z} + m \frac{\partial}{\partial y} \left\{ \left[\left(\frac{\partial v_x}{\partial y} \right)^2 + \left(\frac{\partial v_z}{\partial y} \right)^2 \right]^{(n-1)/2} \frac{\partial v_z}{\partial y} \right\} \qquad [3.13]$$

Since the variables v_x and v_z appear in Equations 3.12 and 3.13, the two equations are coupled. Analytical solution is not possible. A numerical procedure was taken by Griffith (1962). Some of his results are summarized in Figure 3.4, where the ratio of the total flow to drag flow is plotted against a dimensionless group G_z defined as:

$$G_z = \frac{\Delta p H^{n+1}}{L m V_b} \qquad [3.14]$$

$$Q_D = \frac{V_b W H}{2} \qquad [3.15]$$

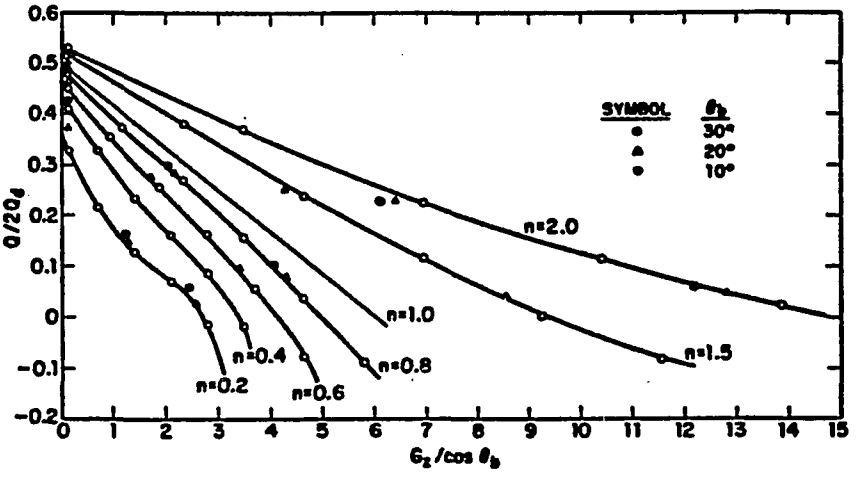

Figure 3.4 Dimensionless flow rate as a function of pressure gradient calculated by Griffith (1962). -- From Tadmore and Klein (1970, p. 185).

A simpler approach was taken by Middleman (1977). In this analysis, Equation 3.12 and Equation 3.13 are uncoupled by assuming that the cross-channel flow v_x is unimportant. The result becomes:

$$0 = - \frac{dp}{dz} + m \frac{d}{dy} \left(\left| \frac{dv_z}{dy} \right|^{n-1} \frac{dv_z}{dy} \right) \qquad [3.16]$$

The analytical solution is:

$$\pi_Q = \frac{\pi_p^s}{s+1} \left[\frac{\xi^{s+2} + (1 - \xi)^{s+2}}{s+2} - \xi^{s+1} \right] \qquad [3.17]$$

where $s = 1/n$, and π_Q and π_p are dimensionless numbers defined by:

$$\pi_Q = \frac{Q}{WHV_b} \qquad [3.18]$$

$$\pi_p = \frac{\Delta p H^2}{L \bar{\mu}_s V_b} \qquad [3.19]$$

Also:

$$\bar{\mu}_s = m \left(\frac{V_b}{H} \right)^{n-1} \qquad [3.20]$$

ξ is calculated from:

$$\xi^{s+2} - (1 - \xi)^{s+1} + \frac{s+1}{\pi_p s} = 0 \qquad [3.21]$$

A plot of π_Q and π_p as a function of the fluid behavior index n is reproduced from Middleman (1977) and is shown in Figure 3.5. It is apparent that non-Newtonian fluids tend to have complex flow behavior as compared to the straight line of the Newtonian fluids.

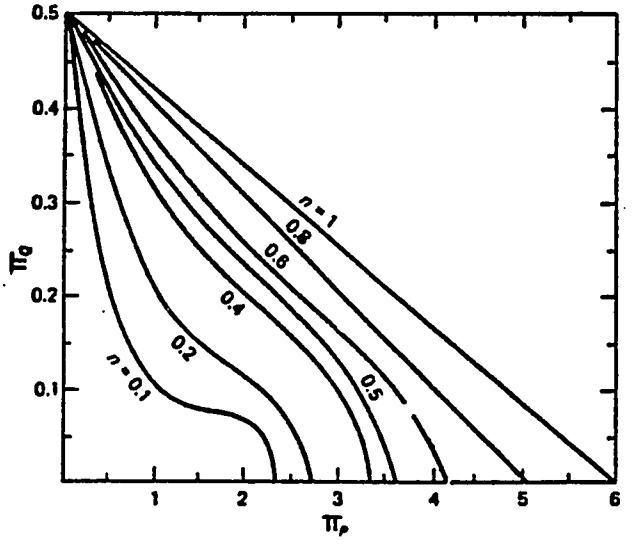

Figure 3.5 Dimensionless flow rate as a function of pressure gradient calculated by Middleman (1977). -- From Middleman (1970, p. 142).

CHAPTER 4

THEORY OF VALVE DESIGN

A control valve consists of two major components, a valve body and an actuator. The valve body is the portion that controls the passage of fluids. It consists of the valve housing, the internal trim, and the bonnet assembly. The theory of valve design can be divided into three problems. The most important is the design of the flow control elements, which requires the selection or the geometric specifications of the valve plug and the valve seating to provide a suitable flow characteristic. The second is the design of various sealing methods to prevent the leakage of process fluids. Equally important is the mechanical design of the valve housing to meet the pressure, temperature, and corrosion requirements.

4.1 Control Valve Characteristics

A major area of valve design is the geometric specifications of the valve plug and internal valve housing. The valve plug and valve housing are usually shaped to control the process fluids with a given flow characteristic. The inherent flow characteristic is defined as the relationship between the percentage of valve opening and the total flow across the valve at a constant pressure drop across the valve. In general, three types of inherent flow characteristics are available. These are the quick-opening, linear, and equal-percentage as shown in Figure 4.1. The quick-opening is commonly used for on-off control

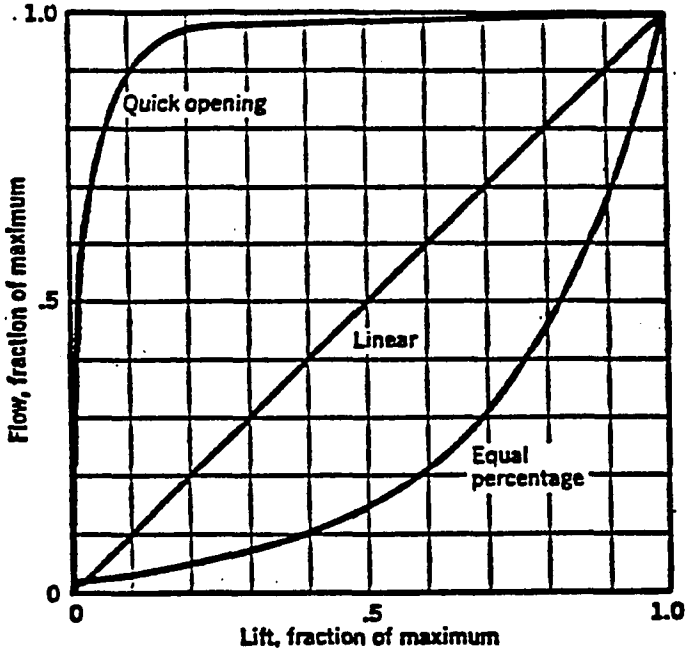

Figure 4.1 Inherent flow characteristic of valves. -- From Pearson (1978, p. 17).

applications because of the significant increase in flow rate for a relatively small change in valve position. The linear flow characteristic has a linear relation between the flow capacity and valve position. An equal-percentage flow characteristic increases the flow rate by the same percentage for each equal increment of valve lift.

In most valve applications, the pressure drop across the valve is also a function of valve opening. The flow across the valve is obviously affected by the pressure drop. Therefore, the operating conditions of the process where the valve is installed must be taken into consideration. This is generally referred to as the installed flow characteristic.

4.2 Valve Seals

4.2.1 Factors Governing Effective Closure

There are three critical locations in a valve where sealing is needed. A sealing method is necessary to prevent the leakage of process fluids downstream when the valve is in a closed position. If the valve contains a stem which actuates the valve plug from outside the valve body, a packing material compressed against the stem is commonly used. A seal is also required for the connection between the valve bonnet and the valve body.

In order to prevent leakage when the valve is closed, a tight closure must be maintained between the valve seating and the flow control element. Two groups of sealing methods are used, metal-to-metal seating and soft seating. The greatest strength is obtained from a metal-to-metal seal. However, metal seating is subject to corrosion,

erosion, and galling. In the soft seating method, a soft and resilient material such as rubber or plastic is placed between the valve seating and the valve plug. In general, this sealing method provides a higher degree of fluid tightness and is most commonly used. However, its application is limited to the temperature and fluid compatibility requirements.

To provide an effective seal closure when the valve is closed, the force transmitted to the stem by the actuator must overcome three major resistances. These are as follows:

1. The force caused by the line pressure against the valve plug.
2. The clamping force at the seating surface which is necessary to provide fluid tightness and effective closure.
3. The frictional force imposed by the compression of packing materials on the stem.

Pearson (1978) has estimated an expression for the total axial force necessary to produce an effective valve closure:

$$F_T = \frac{\pi}{4} p\{d_o^2 + 8d_o W + 4\mu_s d_s l_s\} \qquad [4.1]$$

where F_T = total force to be imparted by the actuator,

p = operating pressure,

d_o = outside diameter of the seating surface,

μ_s = coefficient of friction between the packing materials and the stem,

d_s = diameter of the stem,

l_s = total length of the packing material, and

W = width of the seating surface.

4.2.2 Stuffing Box and Gland Seal

The most common method of stem seal is the use of a stuffing box and a compressible packing material placed into the annular space between the stem and the stuffing box. The sealing is obtained by tightening of a gland to force the packing materials to expand radially and compress against the surface of the stem. The radial pressure distribution varies exponentially throughout the packing length. The stem is fluid-tight if the radial pressure on the inner package ring equals the process pressure. In general, the radial pressure of the outermost packing ring will be considerably higher than the necessary pressure and could result in excessive shaft wear. This could also result in a more expensive actuator due to the large force necessary to produce a tight closure. In most applications, the compressive force is adjusted to give a slight leakage past the last packing ring. The packing material is normally elastic and deformable. It should also have a low coefficient of friction so as to reduce frictional forces. In addition, the packing ring should be chemically inert and compatible with the process fluids. Packing materials should also withstand the temperature and pressure requirements of the process.

The proportioning of the stuffing box and gland is an area of speculation. Various empirical formulations estimating the stem diameter, width of packing, and the required packing length have been reported. A typical stuffing box with a two-bolt gland design is shown in Figure 4.2. The following empirical suggestion was recommended by Pearson (1978) for determining the width W_s of the packing ring:

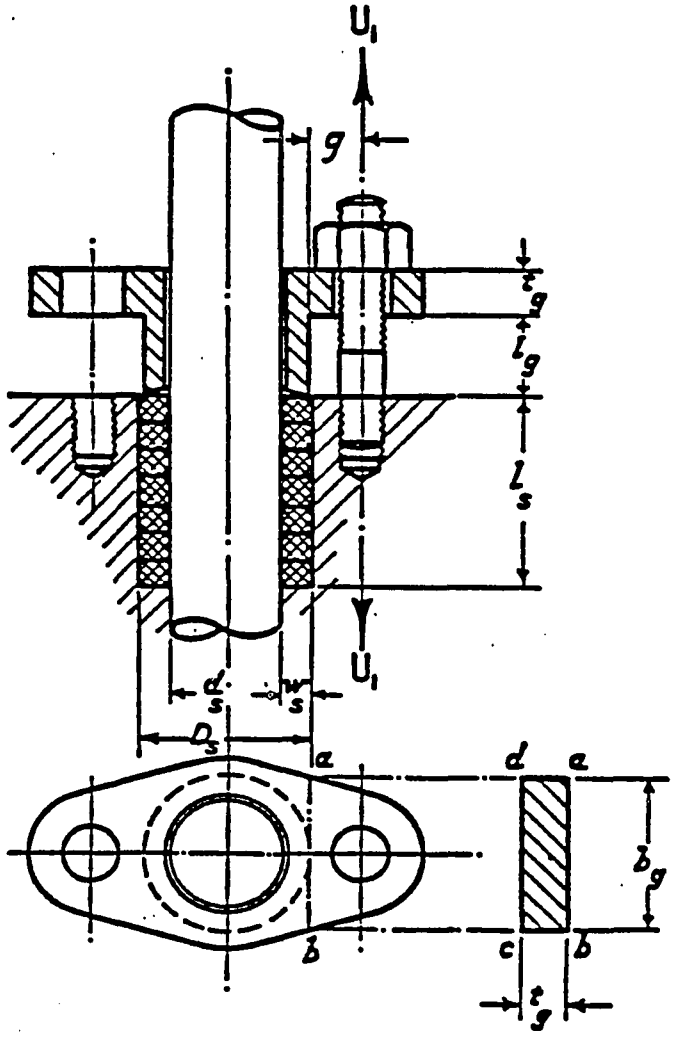

Figure 4.2 Stuffing box and gland assembly.

$$W_s = d_s/8 + 3/16 \text{ (inch)} \qquad [4.2]$$

As a rule of thumb, the optimal packing length is 1.5 d_s. In most cases, the two-bolt oval gland construction is sufficient to provide the necessary tightening force on the packing. The required size of the bolts must be sufficient to maintain the upthrust force produced by the inner valve pressure acting on the annular region between D_s and d_s and also the drag force acting on the packing. The total load shared by the two bolts is:

$$U_T = (\pi p/4)\{D_s^2 - d_s^2\} + \pi \mu_s d_s l_s p \qquad [4.3]$$

The suitable size of bolt can be determined from Appendix N of Pearson (1978).

4.2.3 Factors Governing Gasket Seal

Gaskets are frequently used as a method of sealing between the valve body and bonnet connection. To produce a tight seal, a bolt force is needed to compress the gasket materials. The force must be sufficient to counteract the hydrostatic force exerted by the internal pressure on the area bounded by the diameter of the gasket. In addition, a compressive force is required to maintain a tight closure. The total load force is given by:

$$W_m = \frac{\pi}{4} G^2 p + 2\pi b G p M \qquad [4.4]$$

where G is the diameter of gasket reactions, b is the effective gasket seating width, and M is a gasket factor depending on the gasket materials.

The selection of gasket material plays a vital role. Asbestos, plastics, graphite elastimers, and metals are commonly used with success. In general, the optimal gasket material should be deformable and compressible. The gasket material should be able to flow and fill the void volume and irregularities of the surfaces. The general criteria in the selection of packing material are also applicable to the gasket. The gasket material should be chemically inert and compatible with the process fluid. It should also withstand the temperature and pressure requirements of the process.

4.3 Mechanical Considerations

The valve body is essentially a pressure vessel. The mechanical design to satisfy temperature and pressure requirements is necessary. The thickness of the valve body can be calculated by the following formula given in Pearson (1978):

$$t_s = (pd_f/2f) + c \qquad [4.5]$$

where t_s is the shell thickness, p is the operating pressure, d_f is the diameter of the valve body at its largest point, f denotes the allowable working stress, and c is an empirical constant dependent on the material of construction. The above estimation is really applicable only where the valve diameter is large compared with the shell thickness. As an additional precaution, it is recommended to compare the results with those given by the well-known Lame's formula for a thick cylinder:

$$t_s = \frac{d_f}{2} \sqrt{\left(\frac{f + p}{f - p} \right)} - 1 \qquad [4.6]$$

CHAPTER 5

DEVELOPMENT OF A NON-PLUGGING ANNULAR CONTROL VALVE

To avoid the potential problem of valve plugging, an annular valve configuration which has a streamline flow characteristic was conceptualized. A schematic diagram of the valve geometry is shown in Figure 5.1. The objective was to model the non-Newtonian flow through the annular valve. A parametric study was performed to determine the optimal valve geometry. The parameters of interest were the annular length L_a, the conical length L_c, the conical angle φ, and the inner and outer radii of the annulus. The analysis was simplified by dividing the valve configuration into four distinct sections. Mathematical models were developed to predict the flow through each valve section. Section 1 describes the flow through an annulus formed by two concentric cylinders. Section 3 is the flow through the conical region with a tapered angle φ. Since the pressure developed by an extruder at complete valve closure can be sufficiently high to damage the machine, it is not desirable to design the valve to allow complete closure. Therefore, the valve configuration shown in Figure 5.1a is in a completely closed position. If the valve trim is displaced to a new position as shown in Figure 5.1b, section 2 can be conceptualized as the flow between an area bounded by a cylindrical valve trim of constant radius and a tapered valve body surface. Conversely, section 4 describes the flow through a conical valve trim and a valve body of constant radius.

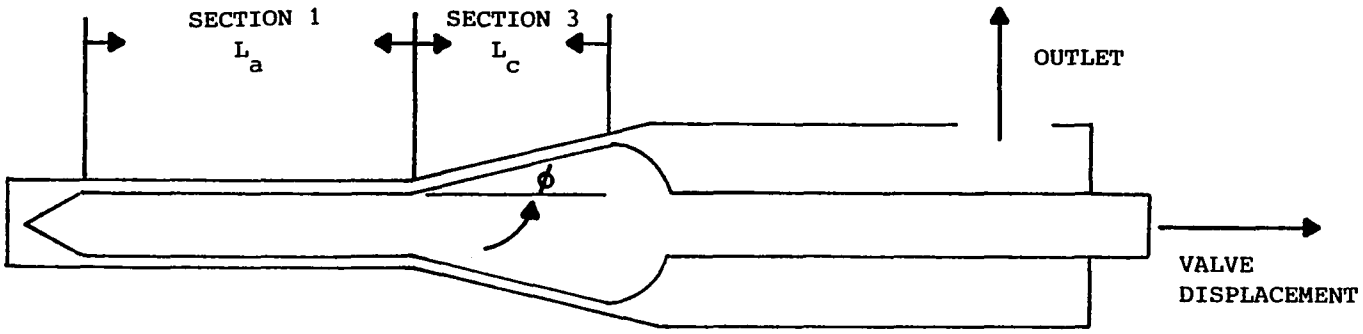

a) Valve is completely closed.

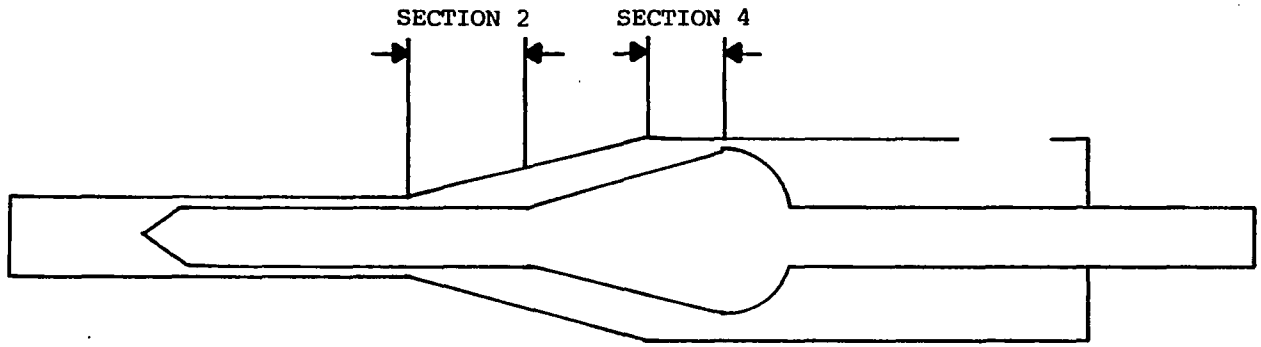

b) Valve is partially open.

Figure 5.1 Conceptualized diagram of the annular control valve.

The mathematics involved in solving the non-Newtonian flow through conical or tapered geometries are complex. To simplify the analysis, a finite-difference technique was developed. The conical geometry of sections 2, 3, and 4 was divided into incremental elements of equal length. Each element was assumed to be an annulus of constant radii. Thus, a mathematical model describing the non-Newtonian flow through a cylindrical annulus of constant radii was needed.

5.1 Isothermal Flow Between Coaxial Cylinders

For an isothermal, fully developed laminar flow along the z-direction between two coaxial cylinders of length L_a and radii of R_o and R_i, the momentum equation becomes:

$$\frac{1}{r}\frac{d}{dr}(r\tau_{rz}) = \frac{\Delta p}{L_a} \qquad [5.1]$$

The solution is:

$$\tau_{rz} = \frac{\Delta p}{2L}\left(r - \frac{(\lambda R)^2}{r}\right) \qquad [5.2]$$

where λ is a constant of integration. It is the radial distance $r = \lambda R$ at which the shear stress τ_{rz} becomes zero. For the case of power-law fluid:

$$\tau_{rz} = m\left|\frac{dv_z}{dr}\right|^{n-1}\frac{dv_z}{dr} \qquad [5.3]$$

The above two equations can be combined and integrated to give the pressure drop as a function of the volumetric flow rate. The result was given by Bernhart (1959):

$$\Delta p = \frac{2L_a m}{R_o} \left[\frac{2n + 1}{n} \frac{Q}{\pi R_o^3} \frac{1}{Y(1 - R_i/R_o)^{(2n+1)/n}} \right]^n \qquad [5.4]$$

The Fredrickson and Bird Y factor is shown in Figure 5.2 as a function of the R_o/R_i ratio and the flow behavior index n.

In order to apply Equation 5.4, the power-law parameters m and n must be determined. This requires the operating shear stress range, which can be calculated from the shear stress at the inner and outer cylinders:

$$\tau_o = \frac{R_o \Delta p}{2L_a} (1 - \lambda^2) \qquad [5.5]$$

$$\tau_i = \frac{R_o \Delta p}{2L_a} \left(\frac{R_i}{R_o} \right) \left(1 - \lambda^2 \frac{R_o^2}{R_i^2} \right) \qquad [5.6]$$

The λ was given by Bernhart (1959) and is reproduced in Figure 5.3. It is also important to note that the calculation method requires the n and m parameters to be constant over the entire range of shear stress from τ_o to τ_i. Since the shear stress is negative at τ_i and is positive at τ_o, this is clearly impossible. Therefore, the calculation is only an approximation. The approximation improves at increasing shear stress, because the flow behavior index tends to be constant over a higher range of shear stress. Since the rheological properties are more influenced by the shear stress at the outer cylinder, the shear stress at τ_o should be used.

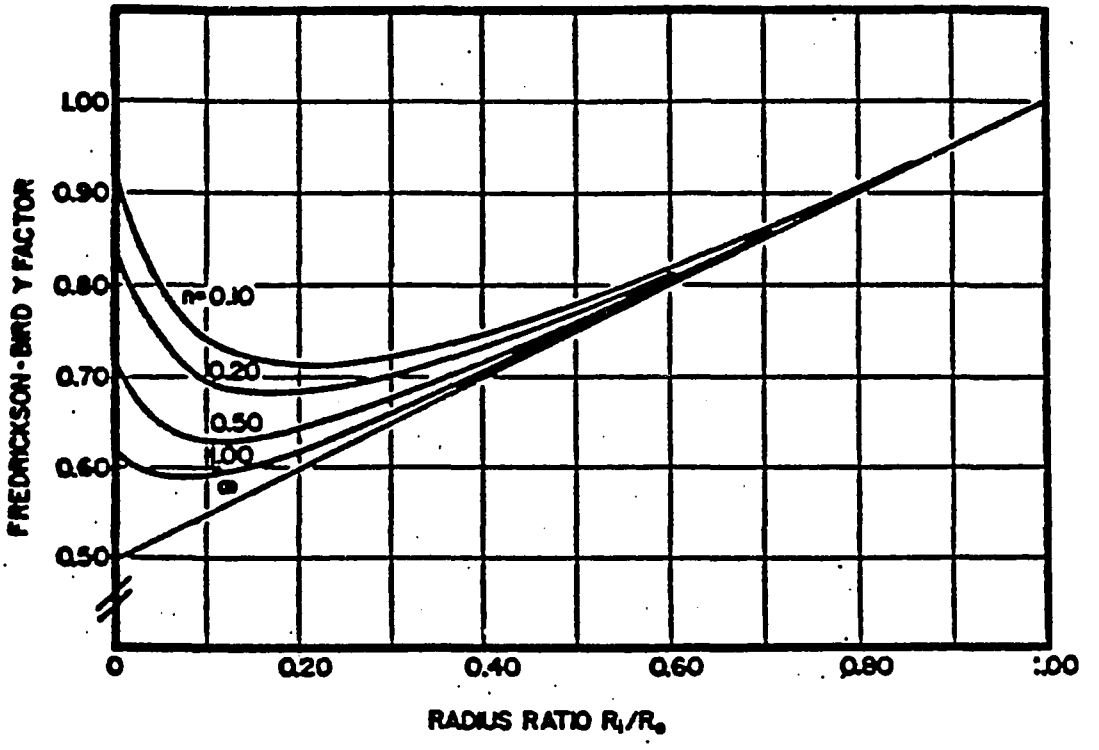

Figure 5.2 Fredrickson-Bird Y factor for flow of power-law fluids inside annulus. -- From Bernhart (1959, p. 58).

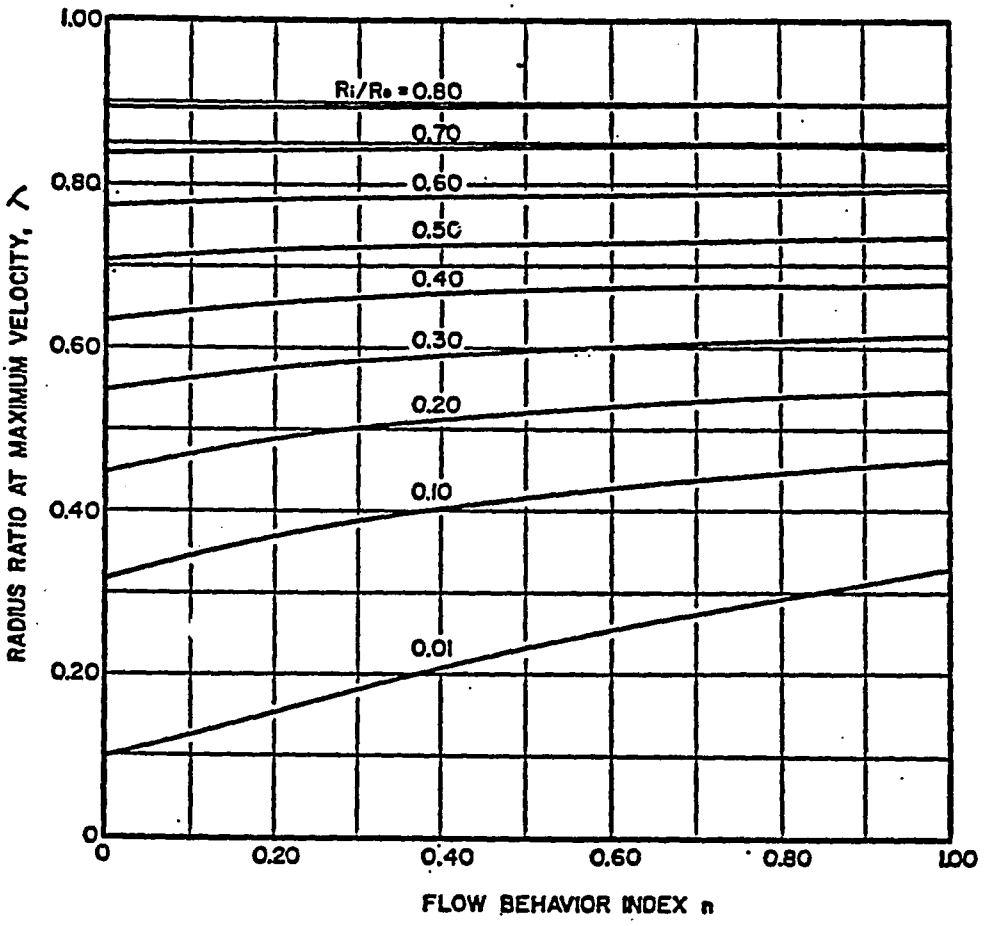

Figure 5.3 Radial position r = λR at which the shear stress is zero. -- From Bernhart (1959, p. 59).

5.2 Modeling of the Flow Through Each Valve Section

Equation 5.4 is the starting point for modeling the flow along each valve section. Mathematical expressions are needed to describe the pressure drop across each valve section as a function of valve displacement. Since section 1 is the flow through a parallel annulus, Equation 5.4 is applicable and becomes:

$$\Delta p_1 = \frac{2(L_a - x)m}{R_o} \left[\frac{2n + 1}{n} \frac{Q}{\pi R_o^3} \frac{1}{Y(1 - R_i/R_o)^{(2n+1)/n}} \right]^n \qquad [5.7]$$

where Δp_1 is the pressure drop across valve section 1, L_a is the total length of the parallel annulus, and x is the valve displacement.

For the conical geometry of section 3, the finite-difference technique is used. The method consists of representing the tapered geometry as a series of parallel annuli of equal length Δh and each with increasing diameter. The number of parallel increments j is defined by:

$$j = \frac{(L_c - x)}{\Delta h} \qquad [5.8]$$

The average inner and outer radius of each increment $\bar{R}_{ii}$ and $\bar{R}_{oi}$ is calculated by the general formulas:

$$\bar{R}_{ii} = R_i + \left[\frac{2(i - 1) + 1}{2} \right] \Delta h \tan \Theta \qquad [5.9]$$

$$\bar{R}_{oi} = R_o + \left\{ \left[\frac{2(i + 1) + 1}{2} \right] \Delta h + x \right\} \tan \Theta$$

where i = 1, 2, ..., j. The pressure drop across the entire section is the summation of the pressure drop across each annular increment:

$$\Delta p_3 = \sum_{i=1}^{j} \frac{2m\Delta h}{\bar{R}_{oi}} \left[\frac{2n+1}{n} \frac{Q}{\pi \bar{R}_{oi}^3} \frac{1}{\bar{Y}_i (1 - \bar{R}_{ii}/\bar{R}_{oi})^{(2n+1)/n}} \right]^n \qquad [5.10]$$

Section 2 describes the flow between a region bounded by a conical outside surface and a horizontal inner valve radius. The numerical procedure discussed above is applicable. The analogous results are obtained:

$$x = j\Delta h \qquad [5.11]$$

$$\tilde{R}_o = R_o + \left[\frac{2(j-1)+1}{2} \right] \Delta h \tan \Theta \qquad [5.12]$$

$$\Delta p_2 = \sum_{i=1}^{j} \frac{2m\Delta h}{\tilde{R}_{oi}} \left[\frac{2n+1}{n} \frac{Q}{\tilde{R}_{oi}} \frac{1}{\tilde{Y}_i (1 - R_i/\tilde{R}_{oi})^{(2n+1)/n}} \right]^n \qquad [5.13]$$

Conversely, section 4 is the flow through a tapered valve radius and a constant outside surface. The flow equations are:

$$x = j\Delta h \qquad [5.14]$$

$$\langle R_o \rangle = R_o + L_c \tan \Theta$$

$$\tilde{R}_i = R_i + \left[(L_c - x) + \left(\frac{2(j-1)+1}{2} \right) \Delta h \right] \tan \Theta$$

$$\Delta p_4 = \sum_{i=1}^{j} \frac{2m\Delta h}{\langle R_o \rangle} \left[\frac{2n+1}{n} \frac{Q}{\pi \langle R_o \rangle^3} \frac{1}{Y_i (1 - \tilde{R}_i/\langle R_o \rangle)^{(2n+1)/n}} \right]^n$$

Since the volumetric flow rate is the same across each valve section, the total pressure drop across the valve is the summation of pressure drop across each section:

$$\Delta p_T = \Delta p_1 + \Delta p_2 + \Delta p_3 + \Delta p_4 \qquad [5.15]$$

5.3 Installed Valve Characteristic

Once the valve dimensions are specified, the valve equations developed in the previous section can be solved. The inherent valve characteristic can be determined by fixing the volumetric flow rate and calculating the pressure drop as a function of valve displacement.

The inherent valve characteristic is valuable in describing the valve performance; however, it should be apparent that the volumetric flow rate is also affected by the valve restriction. To determine the installed valve characteristic, the extruder flow equations and the valve equations must be solved simultaneously. Due to their simplicity, the non-Newtonian extrusion equations presented by Middleman (1977) are used:

$$\pi_Q = Q/V_b WH \qquad [5.16]$$

$$\pi_p = \Delta p H^2/2\bar{\mu}_s V_b$$

$$\bar{\mu}_s = m\left(\frac{V_b}{H}\right)^{n-1}$$

It is important to recognize that the above equations are only applicable to the metering zone. The extruder flow equation and the valve equation provide two expressions with the volumetric flow rate, the pressure drop across the valve, and the pressure drop across the metering zone as the unknown variables. In order to solve the simultaneous equations, the pressure at the entrance to the metering zone must be known. The requirement is complicated by the mathematical complexity in modeling the pressure profile along the feeding and melting zones of the extruder. For simplicity, the pressure generated across the

metering zone is assumed to be equal to the pressure drop across the control valve. Thus, the simultaneous solution to the extruder and valve equations becomes possible.

A graphical procedure provides the most convenient method of solving the problem. The procedure is illustrated by the flow chart given in Figure 5.4. First, it is necessary to specify the operating conditions such as temperature and the screw speed. From the operating temperature and assumed range of shear rate at the valve, the empirical parameters n and m of the power-law model are determined from the logarithmic flow curve and Equation 2.7. The shear rate in the extruder can be calculated from:

$$\dot{\gamma} = \frac{\pi D N \cos \Theta}{H} \qquad [5.17]$$

The extruder flow, Equation 5.16, is solved by selecting values of π_Q and π_p from Figure 3.5. A screw characteristic curve of pressure drop versus volumetric flow rate is generated. In order to solve the valve equation, the appropriate valve dimensions are needed. At a particular valve opening, Equation 5.15 is solved to obtain a valve characteristic curve of pressure drop as a function of flow rate. The intersection of the valve characteristic and the screw characteristic will give the pressure drop and the flow rate at the specified valve opening. The calculated Q and Δp are used to determine the shear stress at the outer wall of the valve annulus. If the result is not within the range of the previously assumed value, then a different shear rate is estimated and the calculation is repeated to obtain the next Q and Δp pair. This procedure is reiterated until the shear rates are within range. At this

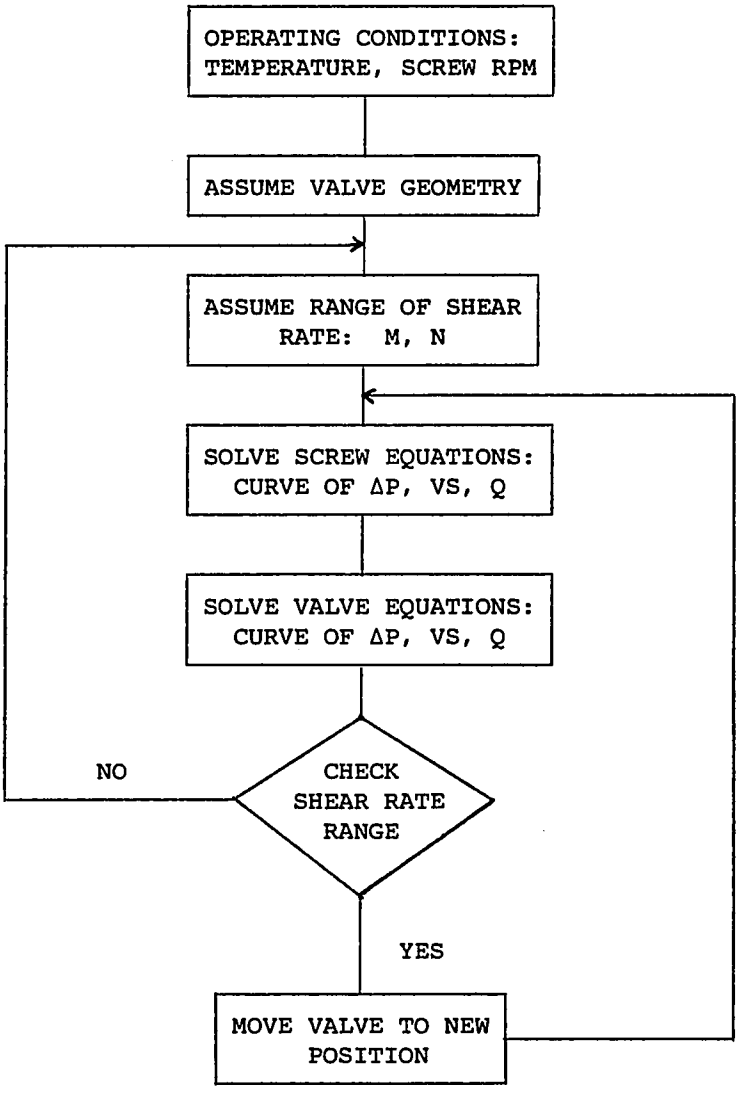

Figure 5.4 Schematic flow diagram detailing the procedure used to calculate the installed valve characteristic.

point, the valve displacement is incremented. The method is repeated to obtain the installed valve characteristic.

A series of parametric evaluations is performed to investigate the effect of various valve dimensions. The optimal valve configuration should give a linear pressure drop across the valve as a function of valve position. A FORTRAN program given in Appendix A is used for the parametric analysis. The program prompts the user for the parameters and calculates the pressure drop across each valve section as a function of valve displacement x.

5.4 Design Criterion

The design criterion was to determine the optimal valve geometry which provides a linear valve characteristic for the extrusion of biomass slurries. This analysis is complicated by the lack of reliable rheological properties of the wood slurries at the shear rate of interest. It was observed by White (1981) that wood slurries are pseudoplastic at low shear rate and that the power-law model fits the apparent viscosity data fairly well in the range of shear rate investigated. Due to this observation and also the availability of the Dow low-density polyethylene at the extruder laboratory, the rheological properties of this polymer are used for design calculation. Polyethylene is a pseudoplastic material and the power-law model is widely used to represent the viscosity data. The logarithmic flow curves for a Dow type 955 LDPE and a Dupont Alathon 3 LDPE are shown in Figure 5.5. The power-law coefficients at different shear ranges are summarized in Table 5.1. Since the viscosity of wood slurries is considerably higher than the polyethylene,

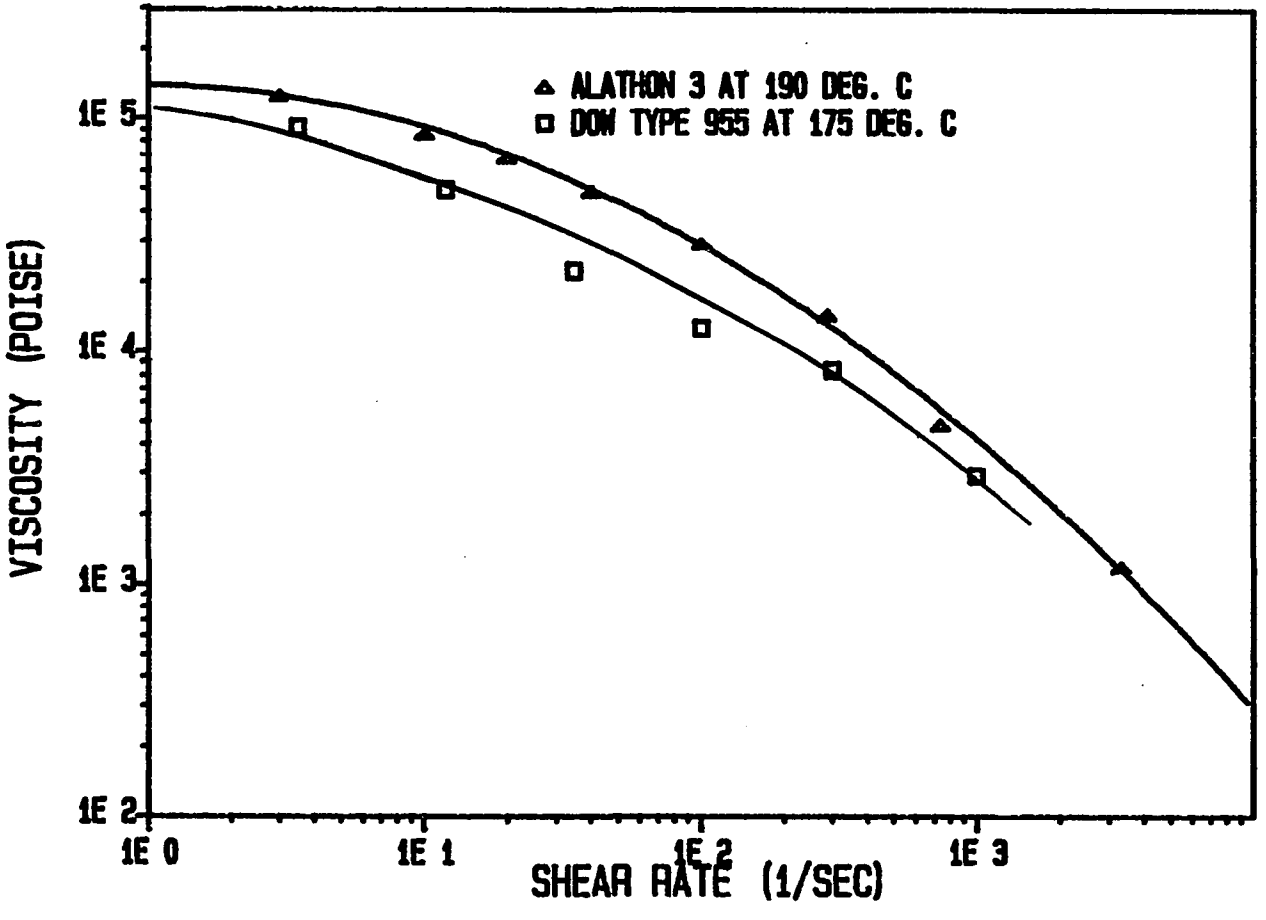

Figure 5.5 Logarithmic flow curves for a Dow type 955 LDPE and a Dupont Alathon 3 LDPE.

Table 5.1 Power-law parameters for a Dow type 955 LDPE at 175°C and a Dupont Alathon 3 LDPE at 190°C.

	$\dot{\gamma}$ (sec^{-1})	n	m ($lbf/in^2 sec^n$)	τ (lbf/in^2)
Dow	48-61	0.44	2.02	11.1-18.9
	162-484	0.62	0.81	144-37.4
	484-1614	0.24	7.95	35.1-46.8
Dupont	10-4000	0.24	13.47	23-99

flexibility in valve design and engineering judgment are needed to ensure that the same valve can be used for the extrusion of wood slurries.

5.5 Results of Parametric Evaluation

The Prodex extruder used in this research has a 1-3/4 inch diameter and L/D ratio of 24:1. In order to perform the parametric studies, the screw dimensions of the metering zone summarized in Table 5.2 are needed. The metering zone has ten helical channels with a total length of 12.5 inches. The helical screw angle Θ has a measure of 17.7°. The channel width W is 1.67 inches and the annular distance between the root of the screw flight and barrel is 0.078 inch. In all summation studies, the power-law parameters for the Dow LDPE at 170°C were used. The extruder screw was assumed to be rotating at 80 RPM.

Table 5.2 The screw dimensions for the metering zone of the Prodex extruder.

Parameter	Dimension
W	1.67 inch
H	0.078 inch
Θ	17.7°
L	12.5 inches

The large number of valve parameters necessitated a systematic approach. First, the effects of conical angle φ were examined. Figure 5.6 summarizes the simulated valve characteristic for the extrusion of a Dow LDPE resin. The results are for conical angles of 5°, 10°, 20°, and 30°; while other valve parameters remain unchanged. The pressure drop across each individual valve section is also given in Table A.1 of Appendix A. It is apparent that as the conical angle increases the installed valve characteristic becomes more exponential. This is the consequence of the large change in the pressure drop across the conical section (section 3) for a relatively small change in valve lift. Therefore, it is advisable to minimize the conical dimensions.

The next series of simulations was to study the effects of different annular size. Figure 5.7 illustrates the installed valve characteristics for two annular dimensions of 1/32 inch and 2/32 inch. The evaluation indicated the important relationship between annular spacing

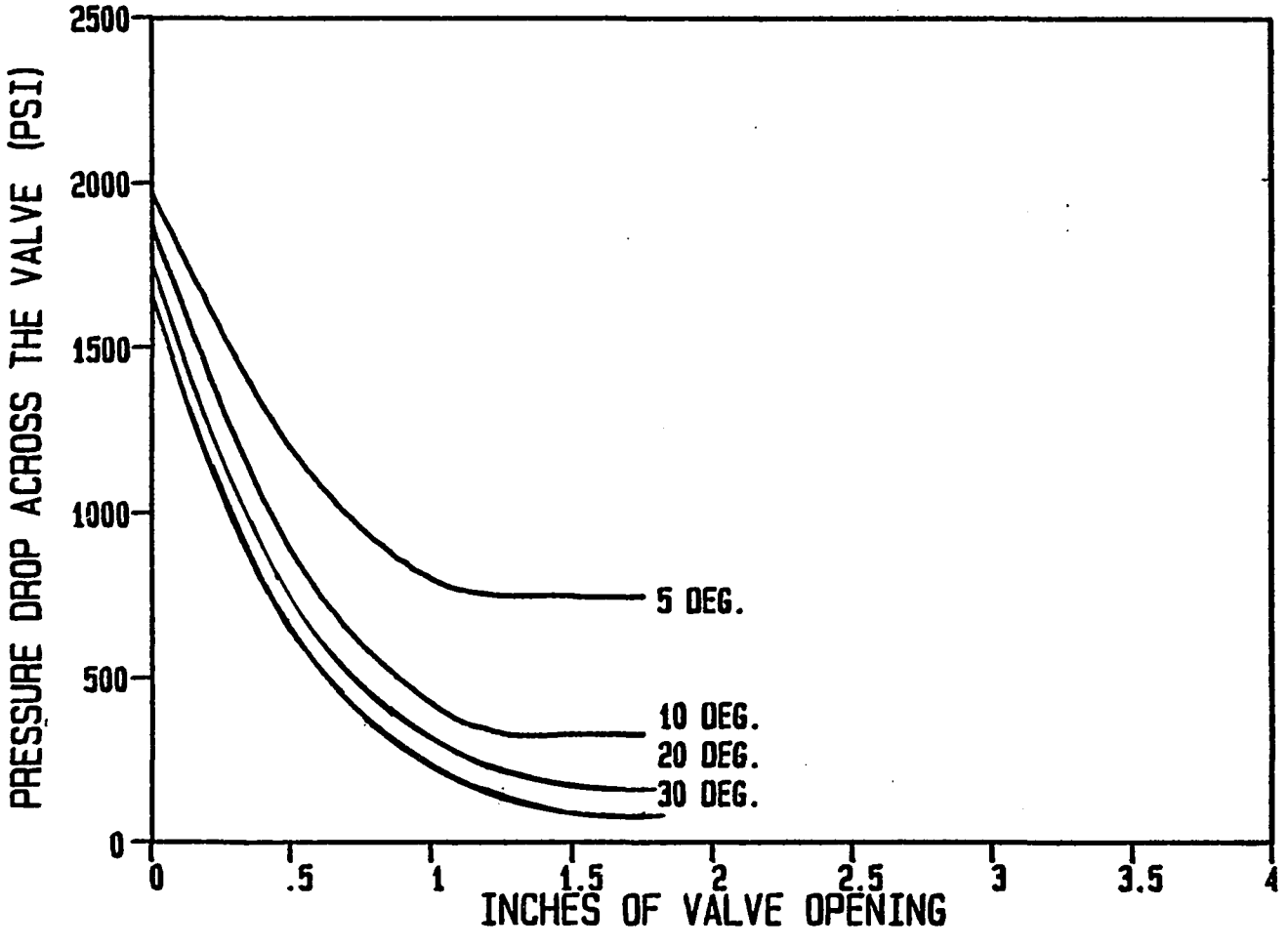

Figure 5.6 Simulated valve characteristics for different conical angle φ. -- Other valve dimensions are: R_o = 5/16, R_i = 4/16, L_a = 1, and L_c = 3 (all dimensions are in inches).

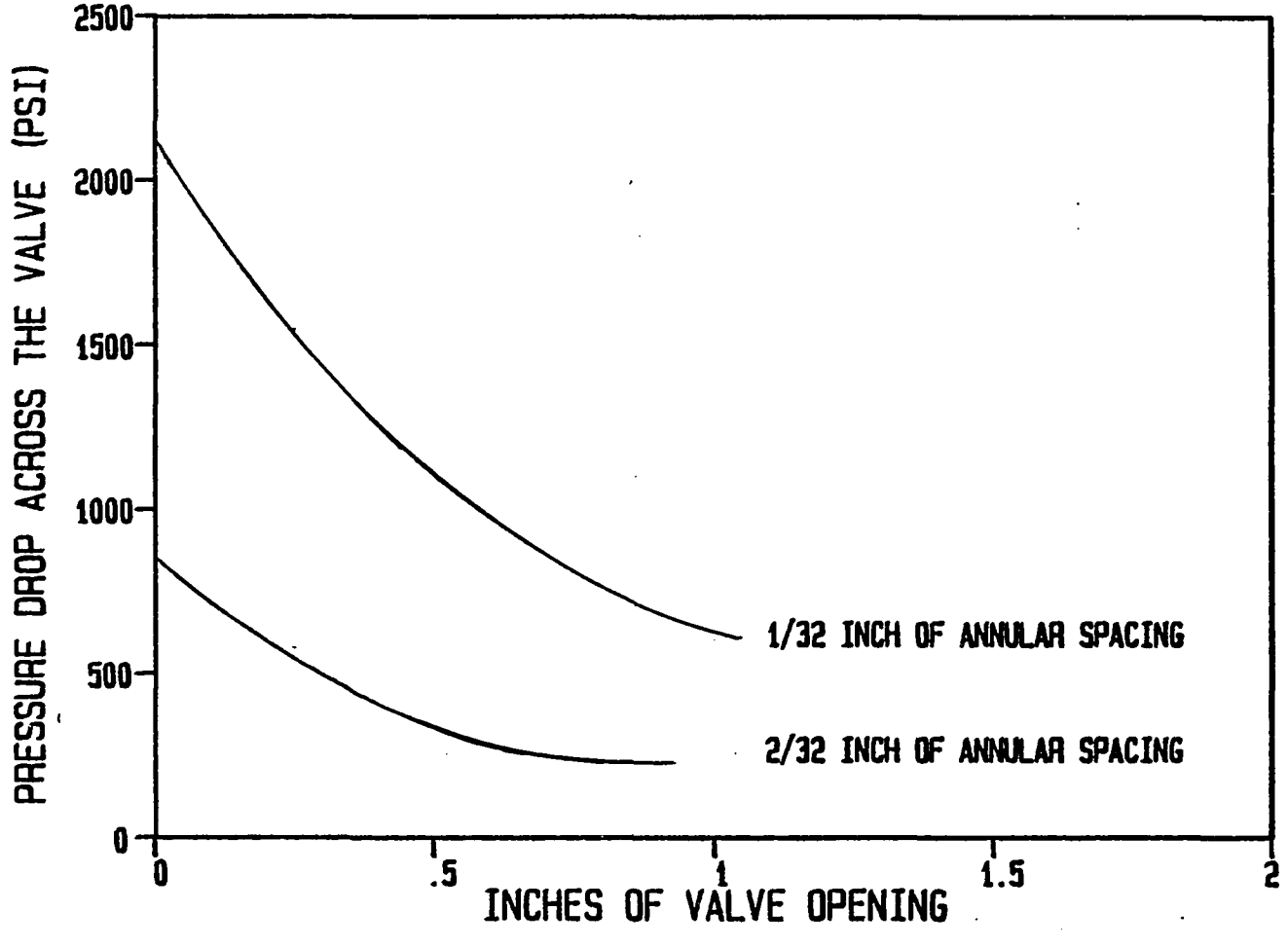

Figure 5.7 Simulated valve characteristics for two different annular spacings. -- Other value dimensions are: R_i = 1/2 inch, L_a = 3/4 inch, L_c = 1/2 inch, and φ = 10°.

and the pressure generated at the extruder outlet. An annular spacing of 1/32 inch is capable of restricting the extruder outlet pressure up to 2000 psi, while an annulus of 2/32 inch could only restrict the pressure up to 750 psi. It is also important to note that, if the annular size is too narrow, valve plugging could be a potential problem. On the other hand, if the annulus is too large, the extruder cannot develop the 3000 psi pressure required for the biomass liquefaction reaction. The two competing factors make the sizing of the annulus an important criterion.

The effect of annular radii on the valve performance is illustrated in Figure 5.8. It is evident that the dimensions of the inner and outer radii have a relatively small influence on the overall valve performance. Therefore, the geometric specifications of the annular radii should be based on mechanical consideration. The minimum trim radius must be capable of withstanding the process pressure.

The effects of annular length L_a of 3, 4, and 5 inches are summarized in Figure 5.9. It appears that as the length of the annulus increases the valve characteristics become more linear. After careful consideration, the valve configuration of Figure 5.9 with the 4-inch annulus length is selected as the optimal valve geometry. There are many factors contributing to this decision. The valve characteristic is linear and is capable of restricting the extruder outlet pressure at 1400 psi. It was mentioned that the viscosity of the wood slurries can be considerably more than that of LDPE. Consequently, it is expected that the pressure developed by the extrusion of wood slurries will be higher than 1400 psi. As a comparison, the simulated valve

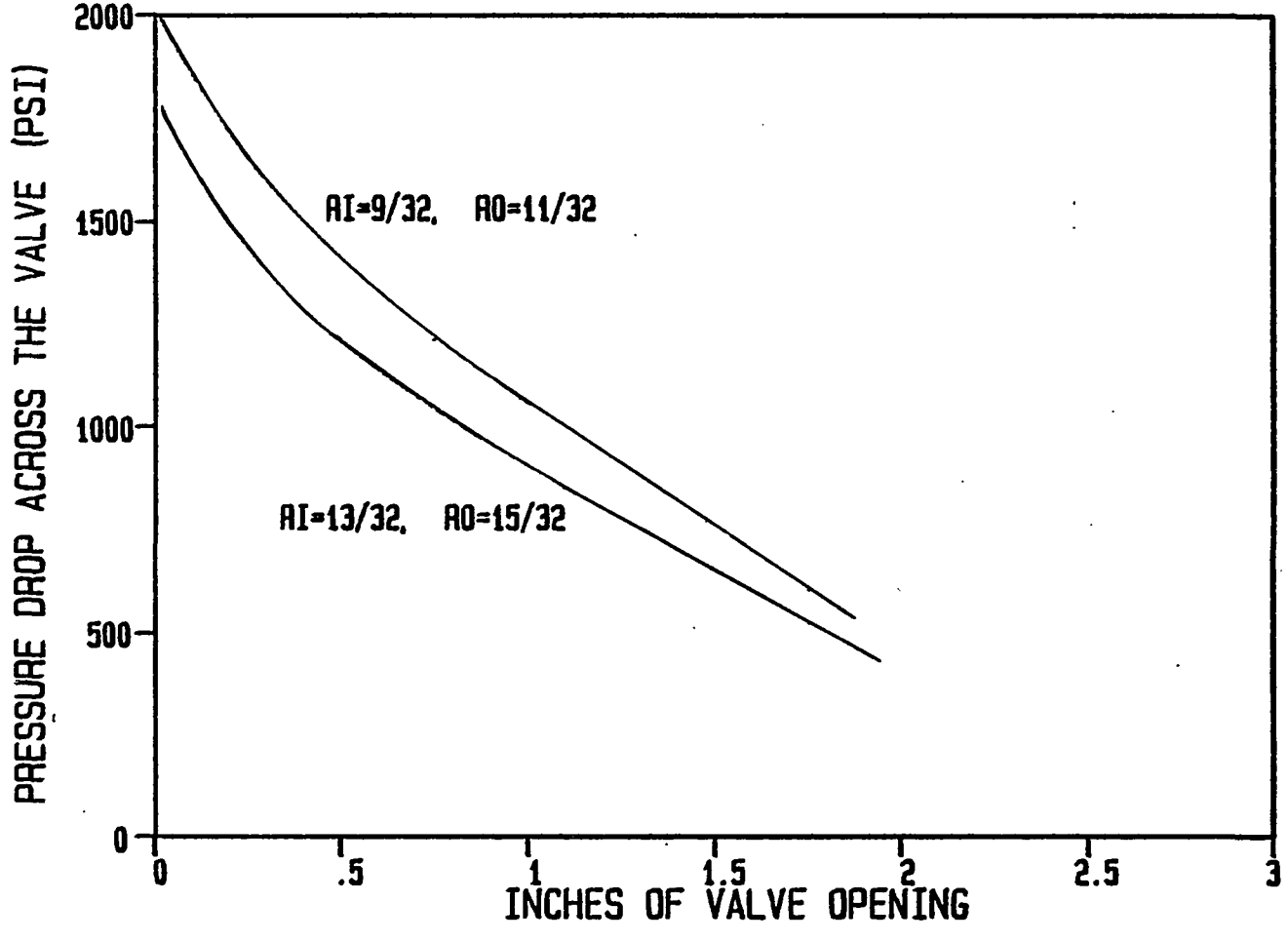

Figure 5.8 Simulated valve characteristics for different annular radii. -- Other value dimensions are: L_a = 2 inches, L_c = 2 inches, and φ = 10°.

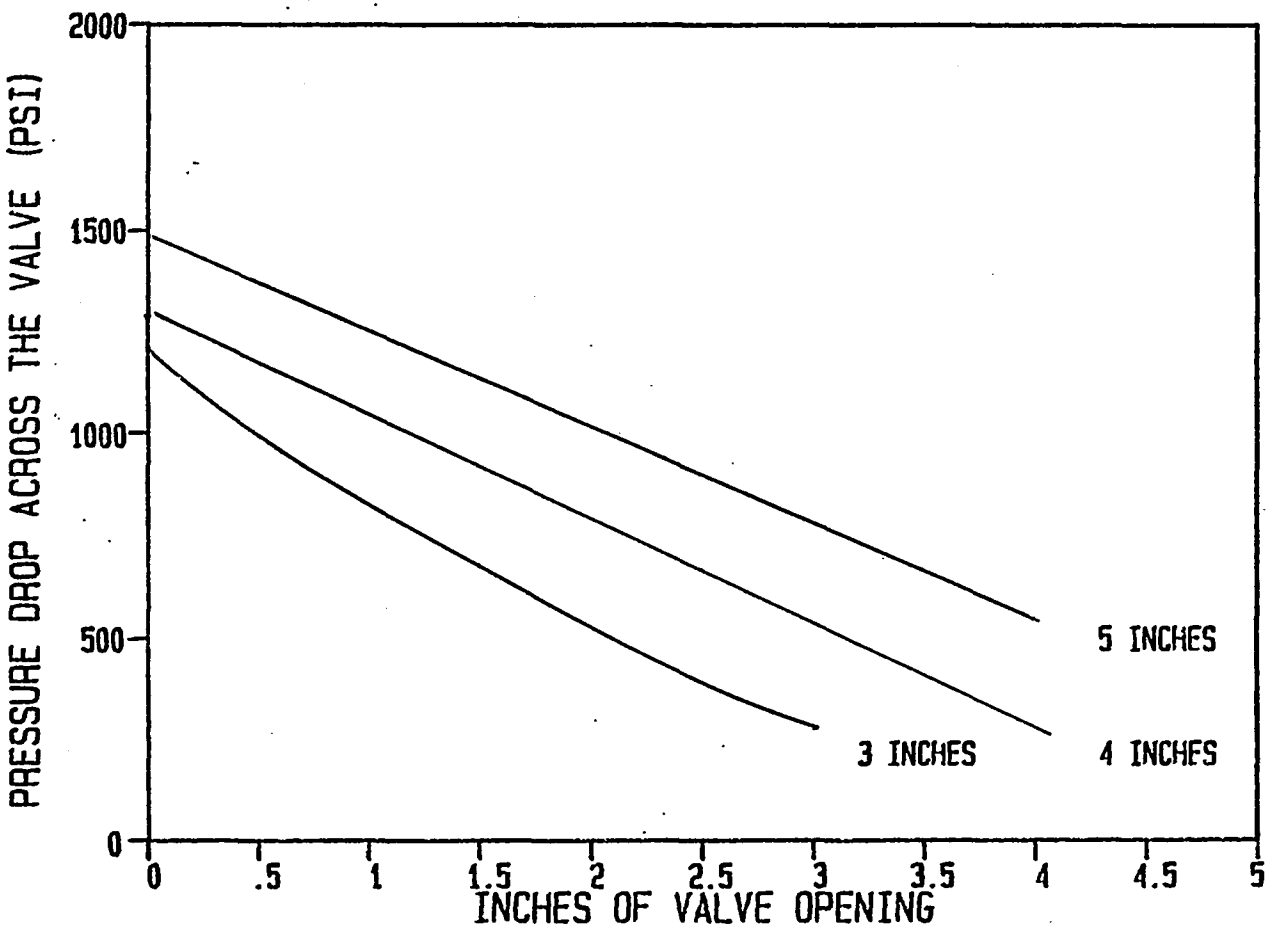

Figure 5.9 Simulated valve characteristics for different annular length L_a. -- Other valve dimensions are: R_o = 9/32 inch, R_i = 12/32 inch, L_c = 1.5 inches, and $\varphi \cong 10°$.

characteristic for a Dupont Alathon 3 LDPE at 190°C is shown in Figure 5.10. Since the Alathon 3 has a higher melt viscosity, the valve is capable of restricting the extruder output to a higher pressure. The annular spacing of 3/32 inch is viewed as the optimal dimension. It is possible that this annular size is overestimated and that a smaller annulus is more effective. This could only be determined by experimental procedure.

The schematic diagram of the control valve is shown in Figure 5.11. The valve is composed of five components: the valve body, the valve trim, the conical portion of the trim, the valve bonnet, and the stuffing box assembly. The dimensions of each component are illustrated in Figures 5.12 through Figure 5.16. The valve is constructed from 303 stainless steel. The overall length is 24 inches. The conical trim of Figure 5.13 is to be inserted into the valve trim of Figure 5.12. This arrangement allows the adjustment of the length of the concentric annulus between 3.5 inches and 4.5 inches. The valve position can be manually adjusted by turning the valve handle. Twenty turns of the valve handle represent one inch of valve adjustment. The control valve can be made automatic by the use of an actuator. Possible candidates are the electrohydraulic and the electromechanical servoactuators.

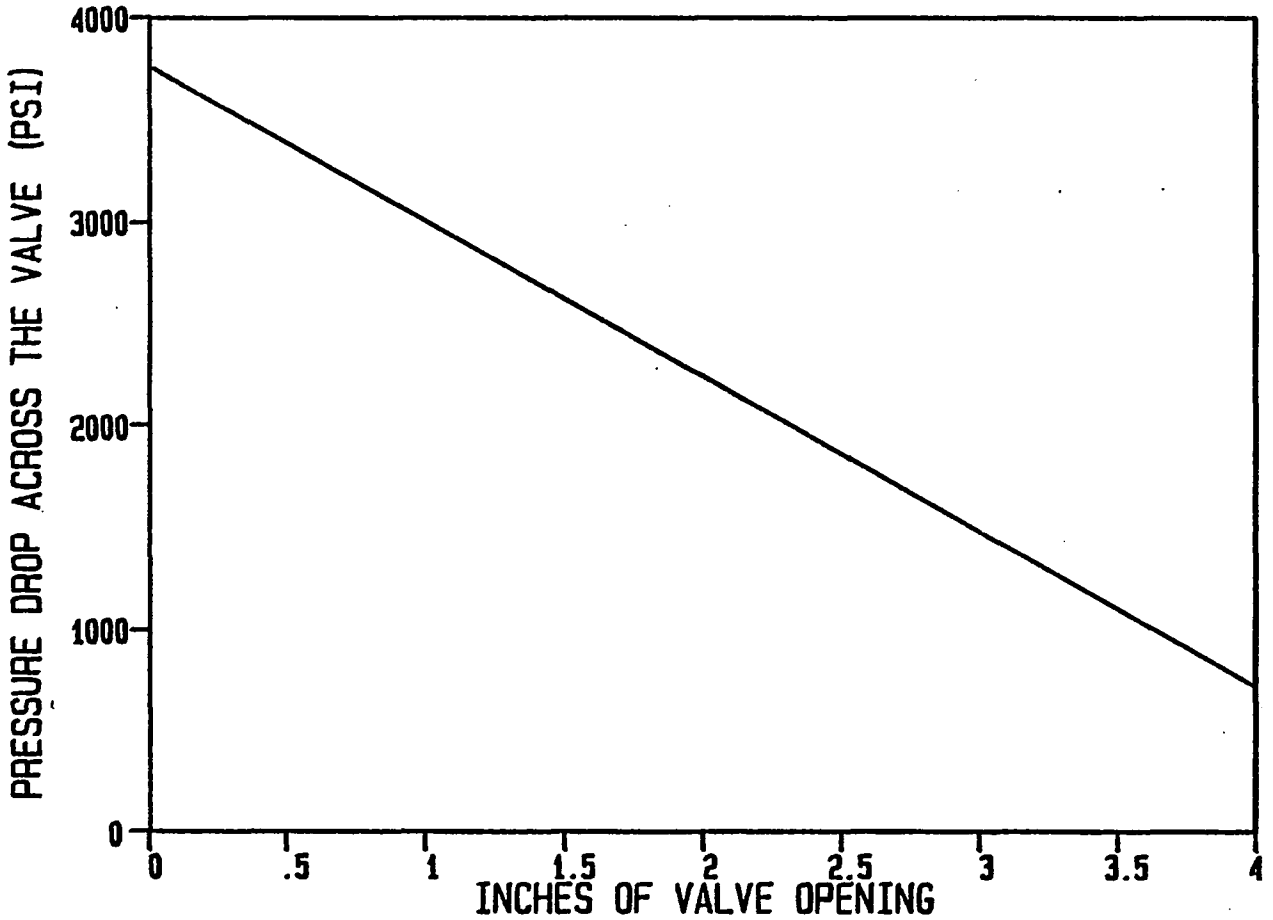

Figure 5.10 Simulated valve characteristic for the extrusion of a Dupont Alathon 3 LDPE.

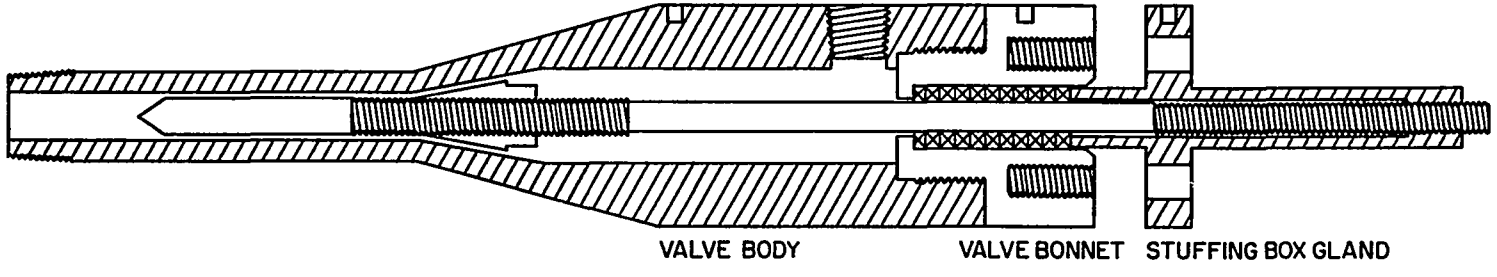

Figure 5.11 Detailed diagram of the annular valve.

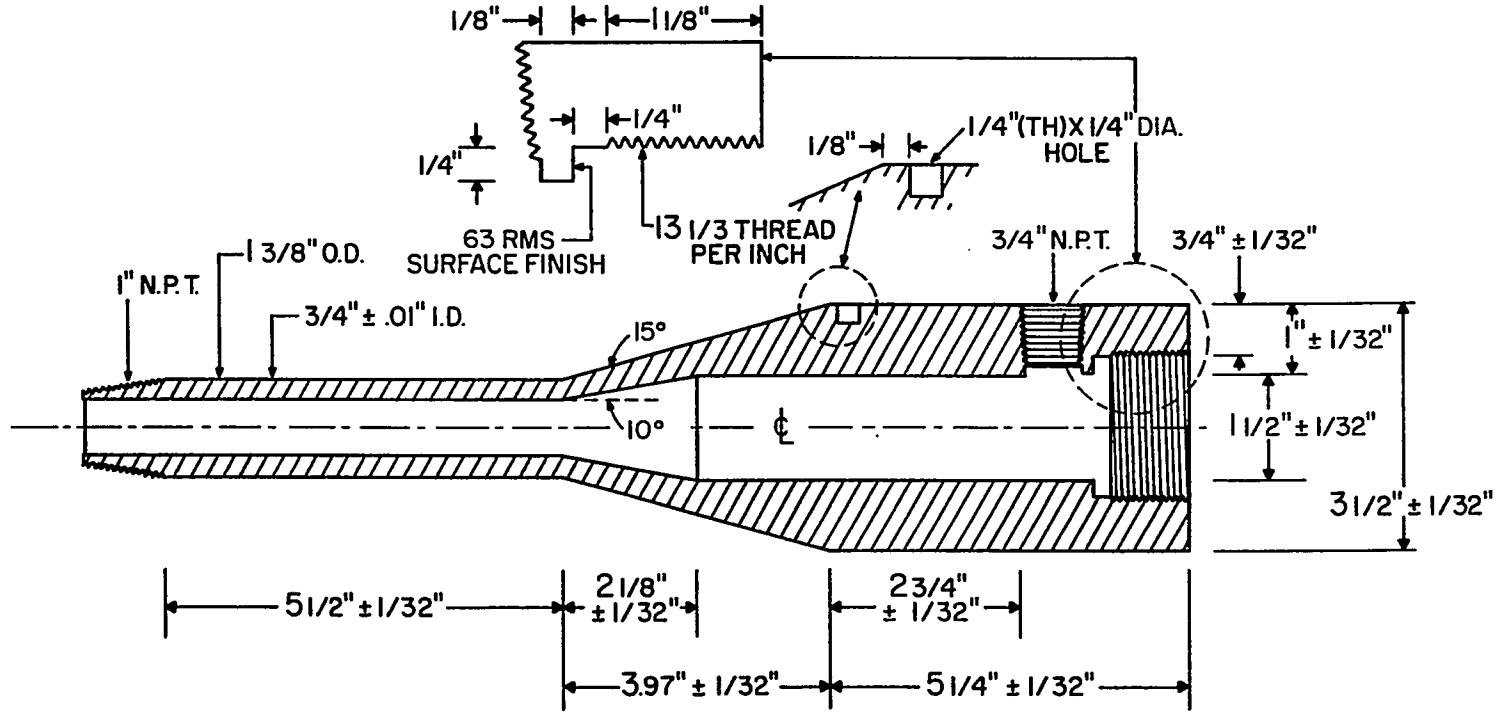

Figure 5.12 Detailed drawing of the valve body.

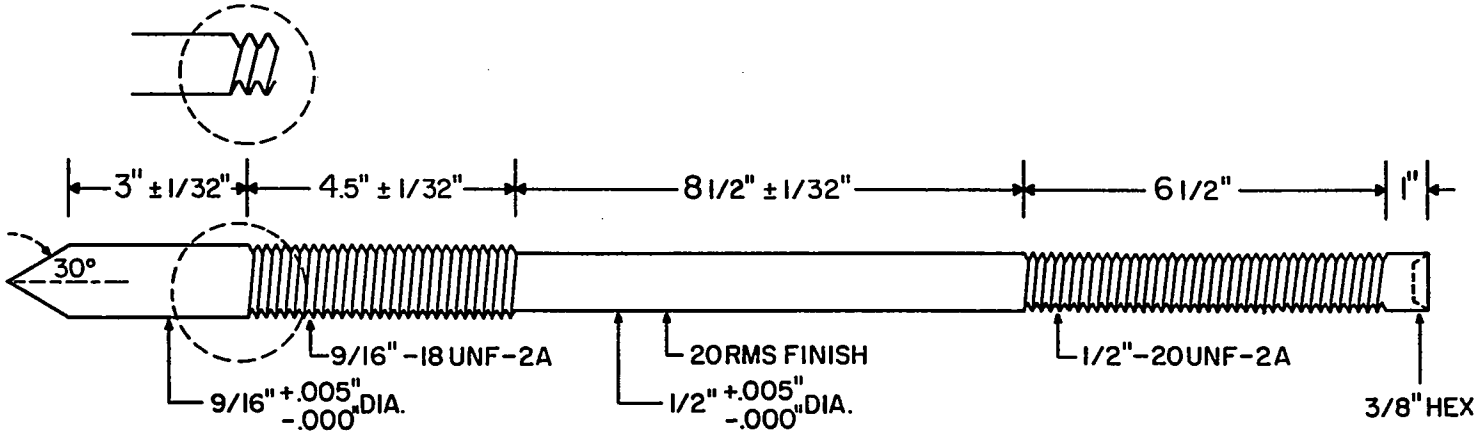

Figure 5.13 Detailed drawing of the valve trim.

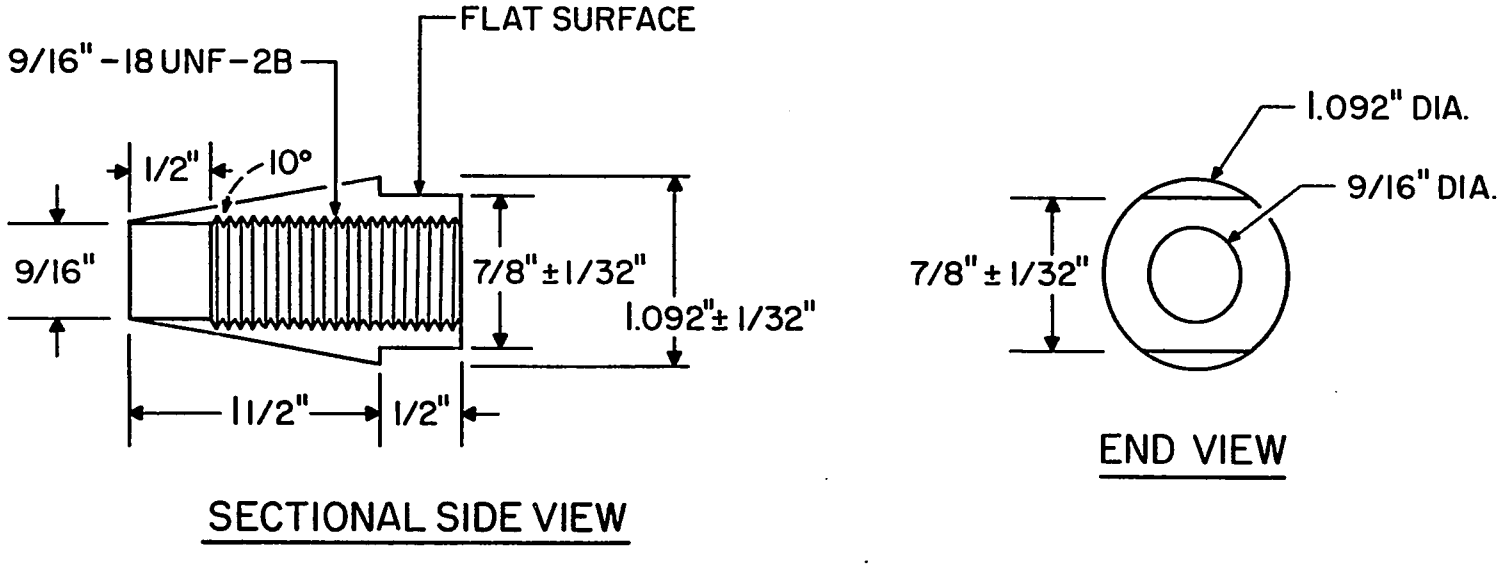

Figure 5.14 Detailed drawing of the removable conical valve plug.

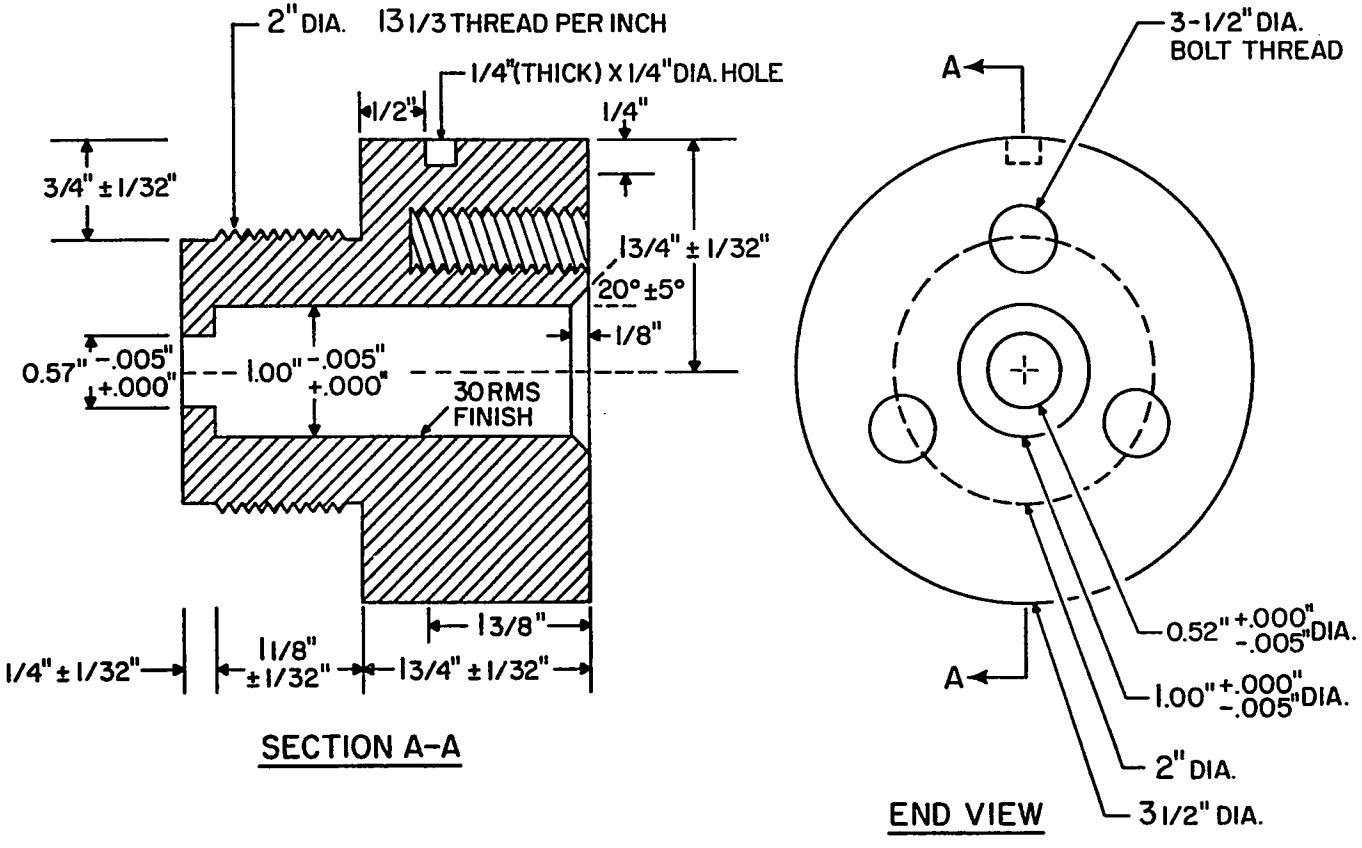

Figure 5.15 Detailed drawing of the valve bonnet.

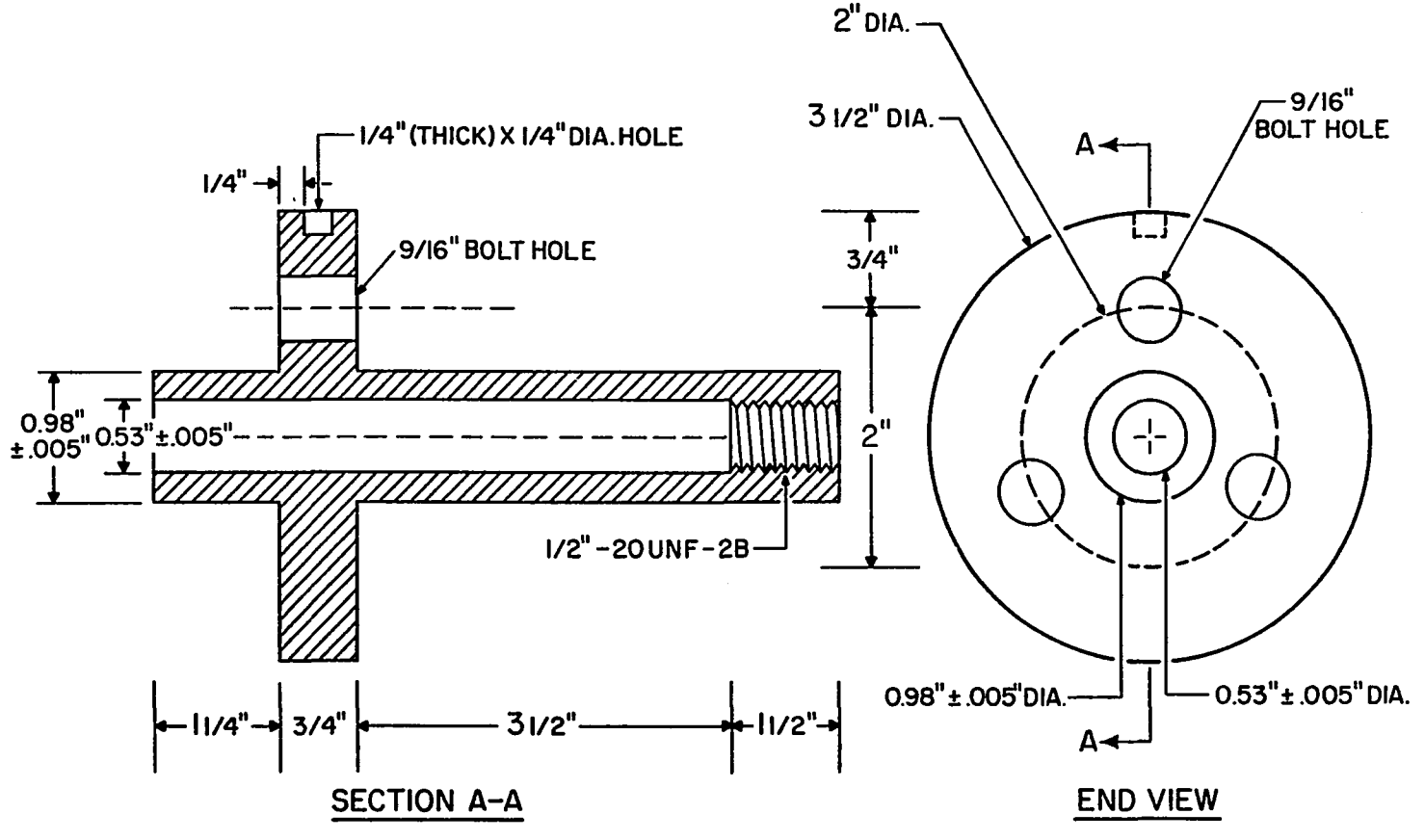

Figure 5.16 Detailed drawing of the gland assembly.

CHAPTER 6

EXPERIMENTAL PROCEDURES AND RESULTS

6.1 Description of Apparatus

Most of the experimental work was conducted with a laboratory Prodex extruder located in the Chemical Engineering Department Extruder Laboratory. The extruder has a 1-3/4 inch diameter and the screw has a L/D ratio of 24:1. It is equipped with a 7.5 HP direct current, variable speed motor. The extruder is capable of operating at pressures up to 10,000 psi and has a maximum throughput of 70 lb/hr of low-density polyethylene at 120 RPM. The machine has a screw conveyor-feeder system which conveys the polymer pellet from the feed storage tank to the extruder feed hopper. The feed box has a water circulation system to prevent the premature melting of the polymers. Electrical heating units are mounted on the extruder barrel to provide heating. Two time-proportional controllers are installed to regulate the temperature at the melting zone and at the metering region of the extruder. Electrical fan blowers are used to prevent the extruder barrel from overheating. This is usually caused by excessive viscous dissipation. The extruder screw is constructed from an alloy steel and the screw flights are hard-faced with stellite. It has nine feed channels, five transition channels, and nine metering channels. The physical dimensions of the screw were summarized in Table 5.2.

The Prodex extruder was equipped with a data acquisition system to monitor its performance. Four "Dynisco" bridge-type, strain-gauge pressure transducers and five Iron-Constantan thermocouples were inserted into the extruder at different locations. A schematic layout of the instrumentation is shown in Figure 6.1. The detail of the installation is illustrated in Figure 6.2. It consisted of a 6-inch carbon steel threaded tube filled with a high-temperature silicon grease. Thermocouples were inserted into the screw channel to obtain the melt temperature.

The annular control valve was installed at the extruder outlet as shown in Figure 6.1. An electrical heating tape was used for heating up the control valve. Due to the size of the valve, it was difficult to control the entire valve at a uniform temperature. Since most of the pressure drop occurred at the annulus, it was critical to control this annular temperature. This was accomplished by inserting a thermocouple at the outer wall of the annulus. A time-proportional controller was used to regulate this temperature.

6.2 Experimental Procedures

The experimental procedure consisted of switching on the variacs for each heating element and adjusting the extruder temperature controllers to the desirable operating conditions. It required three hours before the extruder reached operating temperature. The control valve was then insulated and the temperature controller was turned on. The control valve was allowed sufficient time to reach operating temperature. Due to the non-uniform heating of the valve, the annular

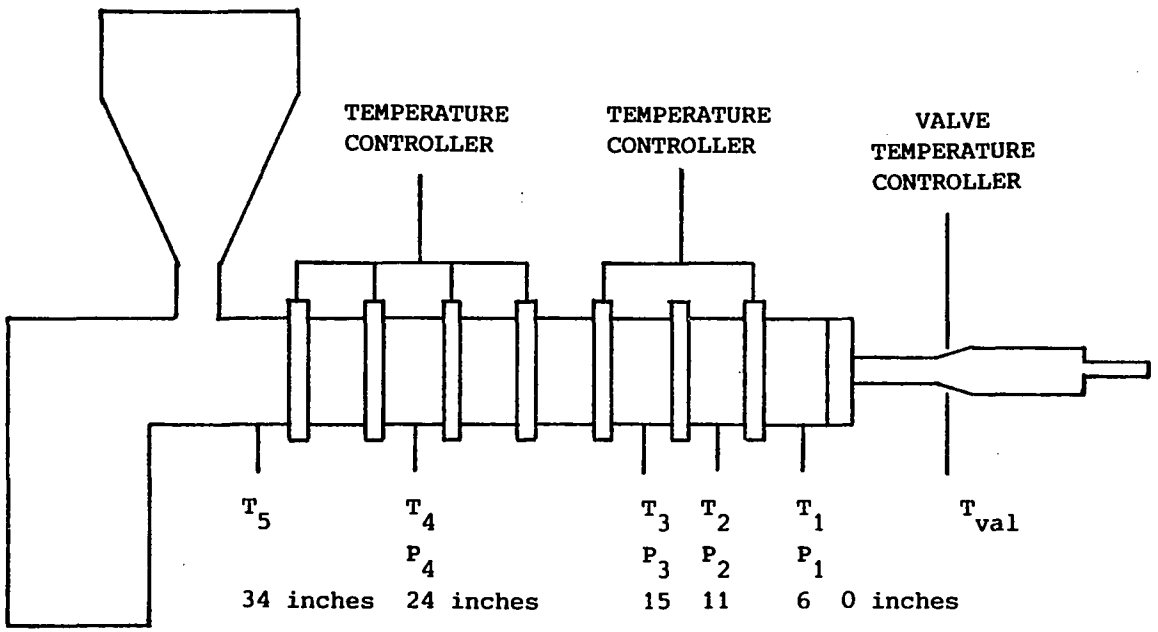

Figure 6.1 Schematic diagram of the instrumentation and apparatus layout.

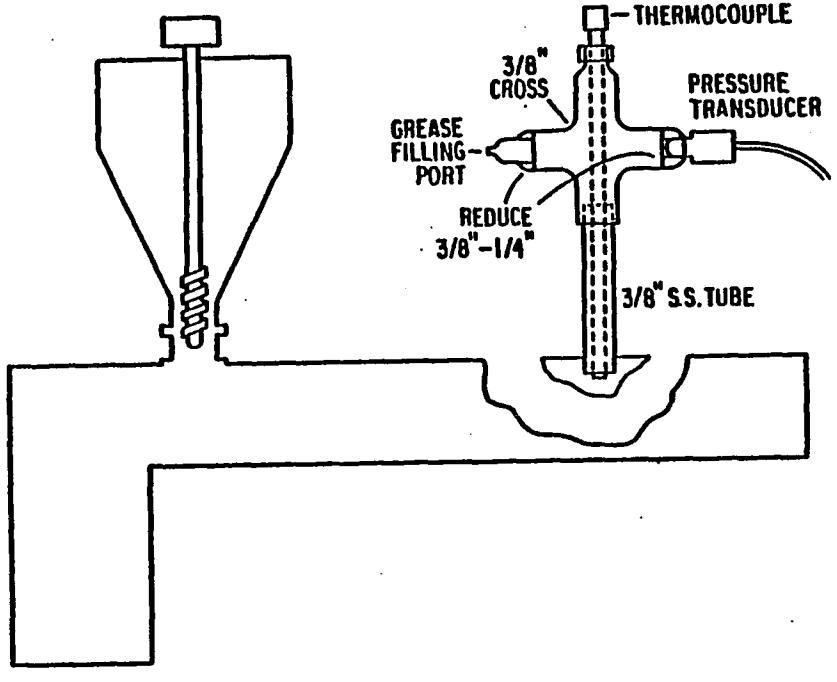

Figure 6.2 Schematic of detail mounting of instrumentation on the extruder barrel.

temperature was considerably higher than the other valve sections. At this point, it was necessary to remove the insulation around the annulus. This allowed the annular temperature to decrease to a desirable condition. This annular temperature was used as the set-point for the valve temperature controller.

The valve opening can be manually adjusted by turning the valve handle. At the beginning of each experiment, the valve was set to the closed position as shown in Figure 5.1a.

Once the extruder reached operating conditions, the variable speed drive was started and its screw speed was adjusted to a desirable RPM. The screw-conveyor motor was switched on to begin feeding polymers to the feed hopper. The cooling water to the feed box was turned on to prevent premature polymer melting. The extrusion process was allowed to reach steady state. In some cases, due to the insufficient amount of material for a long run, the experiment was started before the extruder reached steady state. It was observed that this had relatively little effect on the overall valve performance. A set of temperature and pressure measurements was then taken at each valve opening. The flow rate across the valve was also measured. The pressure generated at the extruder outlet (p_1) as a function of valve opening was plotted. Since the valve outlet was at atmospheric pressure, the pressure at the extruder outlet was equivalent to the pressure drop across the valve.

6.3 Experimental Results

The operability and performance of the control valve for the extrusion of a variety of materials were evaluated. The materials

involved were the Dow type 955 low-density polyethylene (LDPE), Albany sawdust, Albany wood flour (WF), and vacuum bottom (VB). Albany wood flour was obtained from the Department of Energy-sponsored cellulosic liquefaction process facility in Albany, Oregon. Vacuum bottom was the heavy residue produced from the distillation of the wood oil product from the Albany facility. The experimental results of extruder flow rate, pressure distribution along the metering zone, and the temperature profile of the melted polymer for the various materials are summarized in Appendix B. The pertinent and relevant results are presented in this discussion.

6.3.1 Dow Low-Density Polyethylene

The valve operating characteristic for the extrusion of the Dow LDPE was investigated. For this series of experiments, the conical portion of the valve plug was inserted on to the valve trim to provide 3-1/2 inches of valve annulus. Initially, the temperature controllers for the extruder barrel were regulated at 150°C. The temperature controller for the valve was adjusted at 175°C. Under these operating conditions, extrusion of LDPE at different screw RPM indicated that valve positioning had no effect on the pressure. The pressure at the extruder outlet was approximately 500 psi, regardless of the valve opening. Apparently, the viscosity of LDPE at this operating temperature was not sufficient to generate the pressure. Since viscosity increases with decreasing temperature, it was expected that valve performance should improve at a lower operating temperature. After several experiments, the optimal valve characteristics achievable are

illustrated in Figure 6.3. The results of extruder flow rate, pressure, and temperature readings are tabulated in Table B.1 (Appendix B). Temperature of the extruder was controlled at 150°C and the screw was rotating at a rate of 80 RPM. From the experimental results, it was evident that the valve was ineffective for the extrusion of LDPE. At best, the maximum pressure generated at the extruder outlet was 1200 psi. This occurred at a valve temperature of 100°C. The valve characteristic appeared to be linear up to 3/4 inch of opening. As the valve temperature was increased to 120°C, maximum pressure was 1000 psi. The operating range also decreased to 1/2 inch of opening. Figure 6.3 also shows the computer-simulated valve characteristic for an annular length of 3 inches. In general, the experimental result was accurate within an order of magnitude.

The flow rate across the valve as a function of valve restriction is tabulated in Table B.1. It is interesting to observe that flow rate was independent of valve position, as shown in Figure 6.4. This could be explained by the fact that drag flow was the dominant component of the total extruder flow. Consequently, a small change in pressure had little effect on the flow rate. The average flow rate observed was 370 gm/min.

The extruder flow rate can also be estimated by using the Newtonian model of Equation 3.6:

$$Q = \frac{\pi DN \cos \Theta}{2} WHF_D - \frac{WH^3}{12\mu L} \Delta p F_p \qquad [3.6]$$

From Figure 6.18 of Tadmore and Klein (1970), the drag flow and pressure flow shape factors are, for H/W of 0.04:

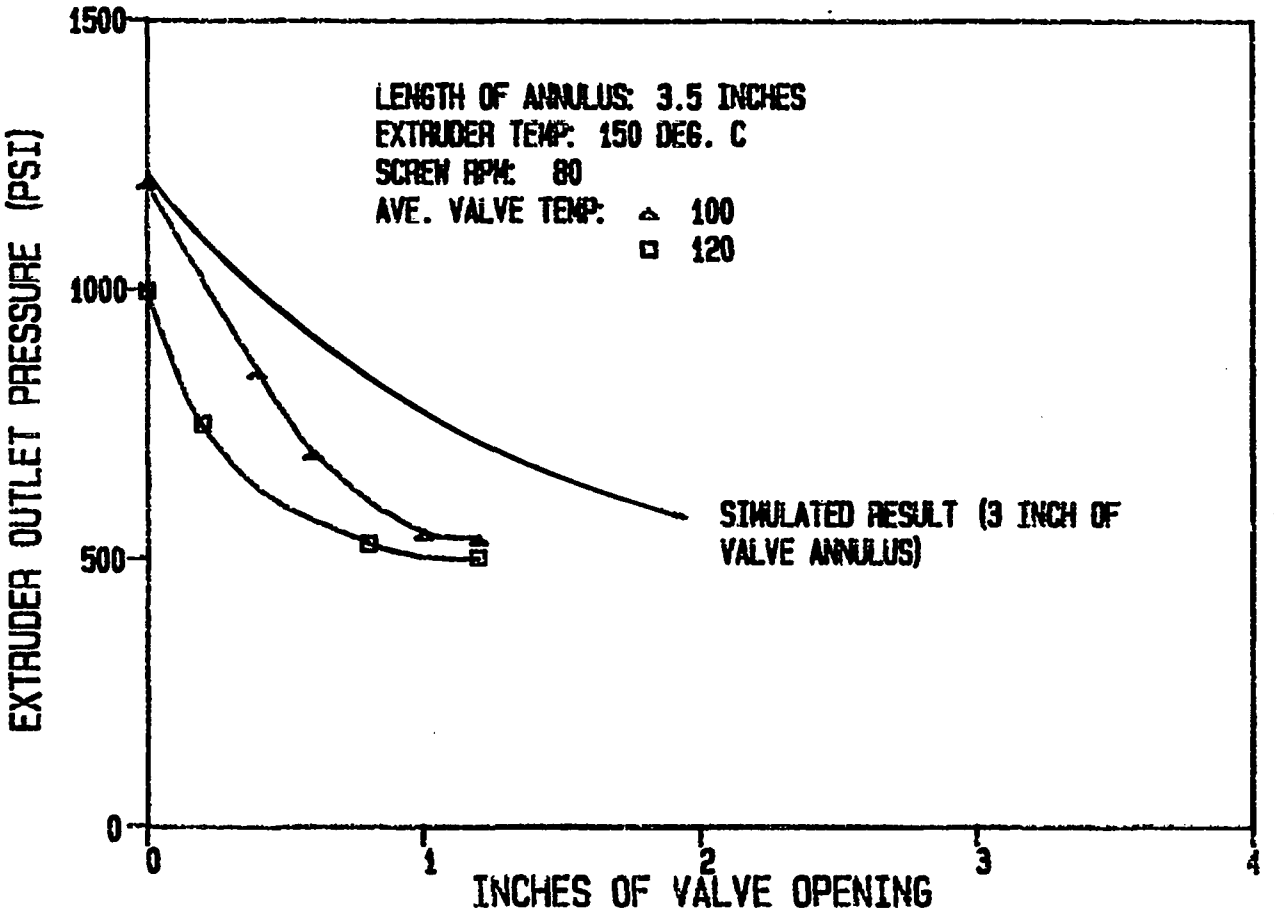

Figure 6.3 Valve characteristics for the extrusion of a Dow LDPE at different temperatures. -- Experimental data are reported in Table B.1.

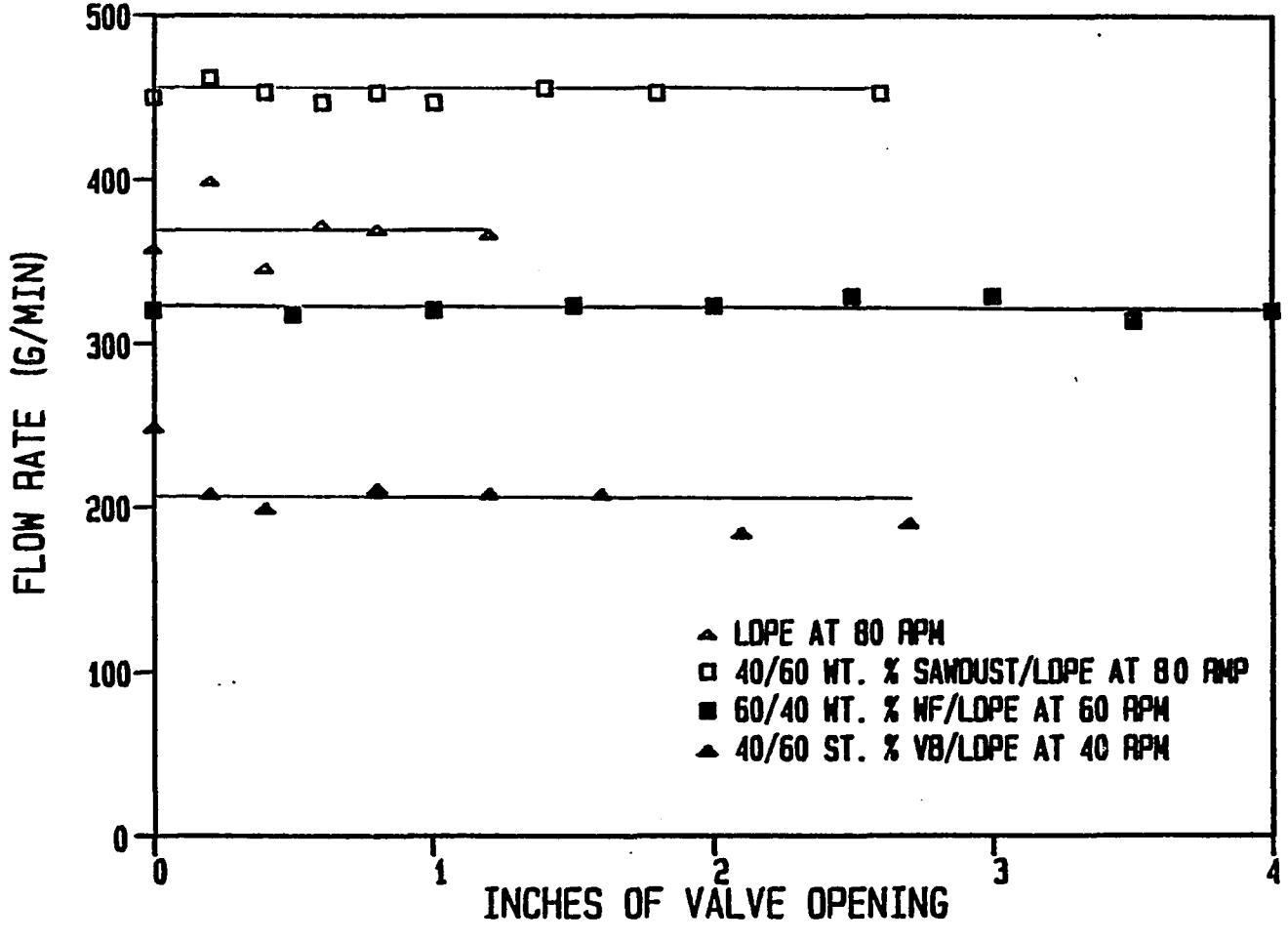

Figure 6.4 Flow rate as a function of valve opening.

$F_D = 0.97$

$F_p = 0.97$

From experimental results in Table B.1 and Figure 5.5:

$N = 80$ RPM

$\Delta p \simeq 500$ psi

$\mu = 4x10^3$ poise

Substituting the above data into Equation 3.6:

$Q = 0.44 + 0.044$ (in^3/sec)

Thus, pressure flow is only 10 percent of the total extruder flow rate. The density of LDPE is approximately 48 lb/ft^3 and the mass flow rate becomes 366 gm/min.

6.3.2 Sawdust and Polyethylene

The valve performance for the extrusion of a 40:60 wt % Albany sawdust and LDPE regrind was evaluated. Figure 6.5 depicts the valve characteristics at two different screw RPM. Other experimental results are summarized in Table B.2. The annular length was adjusted at 4-1/2 inches. Temperature of the extruder and the valve was controlled at 145°C and 110°C, respectively. In general, the valve operability showed considerable improvement over the LDPE. This was expected, since the sawdust/LDPE slurry was more viscous. At near valve closure, the effects of the conical geometry resulted in a non-linear valve characteristic. As the valve opening increased, the conical effect diminished and the valve characteristic appeared to be linear up to 2 inches of opening. At this point, further valve opening had no effect on the pressure. The valve operating range was limited to 2 inches of opening.

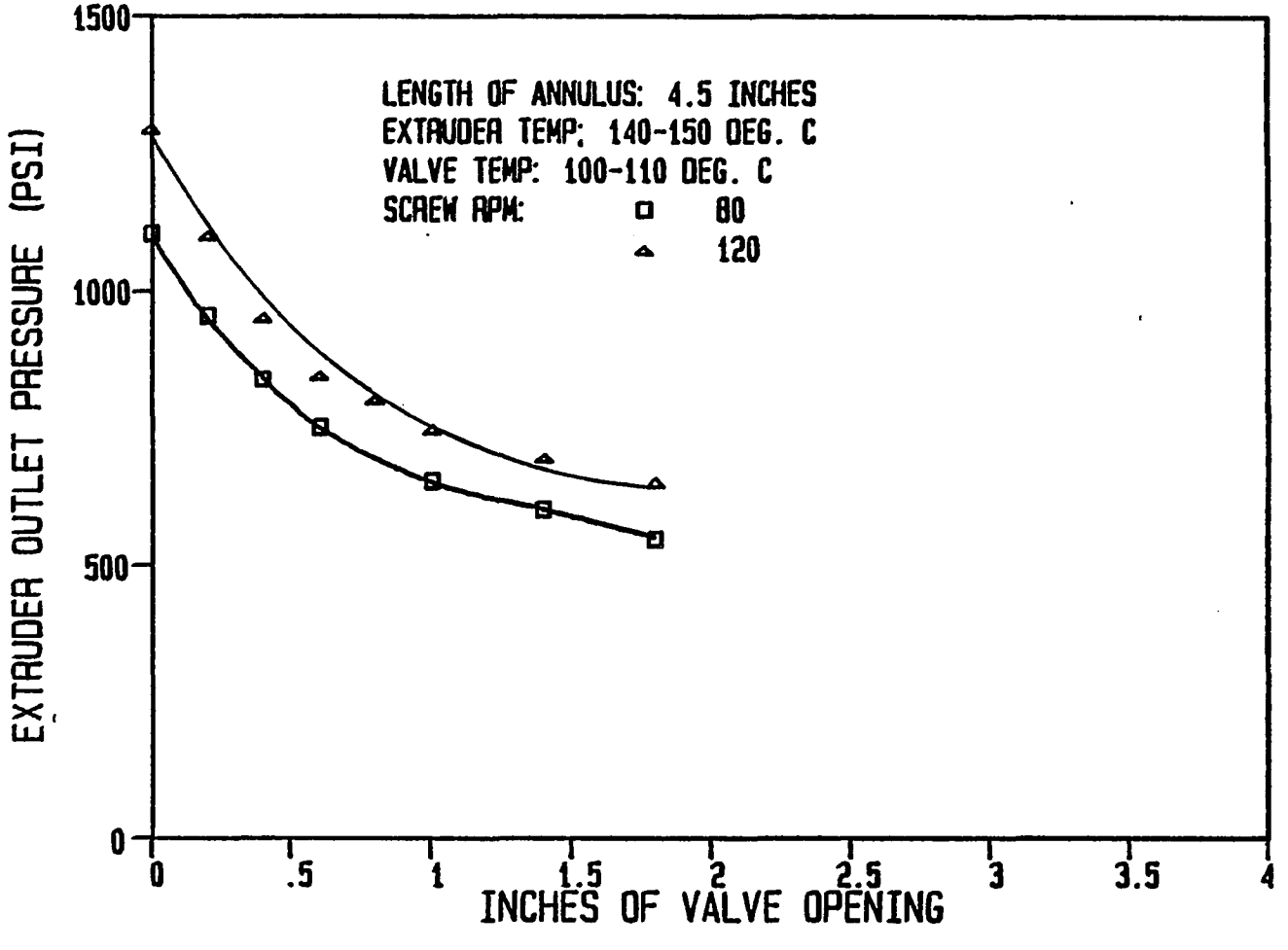

Figure 6.5 Valve characteristics for the extrusion of a 40:60 wt % sawdust/LDPE regrind at different screw RPM. -- Experimental data are reported in Table B.2.

Similar to the results obtained for LDPE, the flow rate across the valve was independent of valve opening. This was illustrated in Figure 6.4. The average flow rate as a function of screw RPM is shown in Figure 6.6. As expected by extrusion theory, the data points can be extrapolated back to the zero origin.

6.3.3 Albany Wood Flour and Polyethylene

Since the Albany wood flour/LDPE regrind is a good simulation material for the actual pumping of wood slurries into the biomass liquefaction reactor, the valve operability for different concentrations of wood flour/LDPE slurry was evaluated. Figure 6.7 illustrates the valve characteristics for the extrusion of the 40 wt %, 50 wt %, and 60 wt % wood flour slurries. The experimental conditions, flow rate, pressure, and temperature profiles of the extruder are summarized in Table B.3. The experiments were conducted with a valve annulus of 4-1/2 inches.

During the initial phase of the experiment, it was discovered that the moisture in the wood flour presented difficulties in obtaining an accurate extruder flow rate. Formation of gases inside the extruder caused an unsteady-state flow from the valve outlet. Also, a considerable amount of pressure fluctuation was observed. These problems were avoided by extruding the material once to eliminate the moisture content. The material was then reground and used again as the feedstock.

In general, the valve performance improved significantly over previous experiments. This was expected, since the viscosity of wood slurry was higher than that of sawdust. As demonstrated in Figure 6.7, a higher pressure can be generated by the extruder with the higher wood

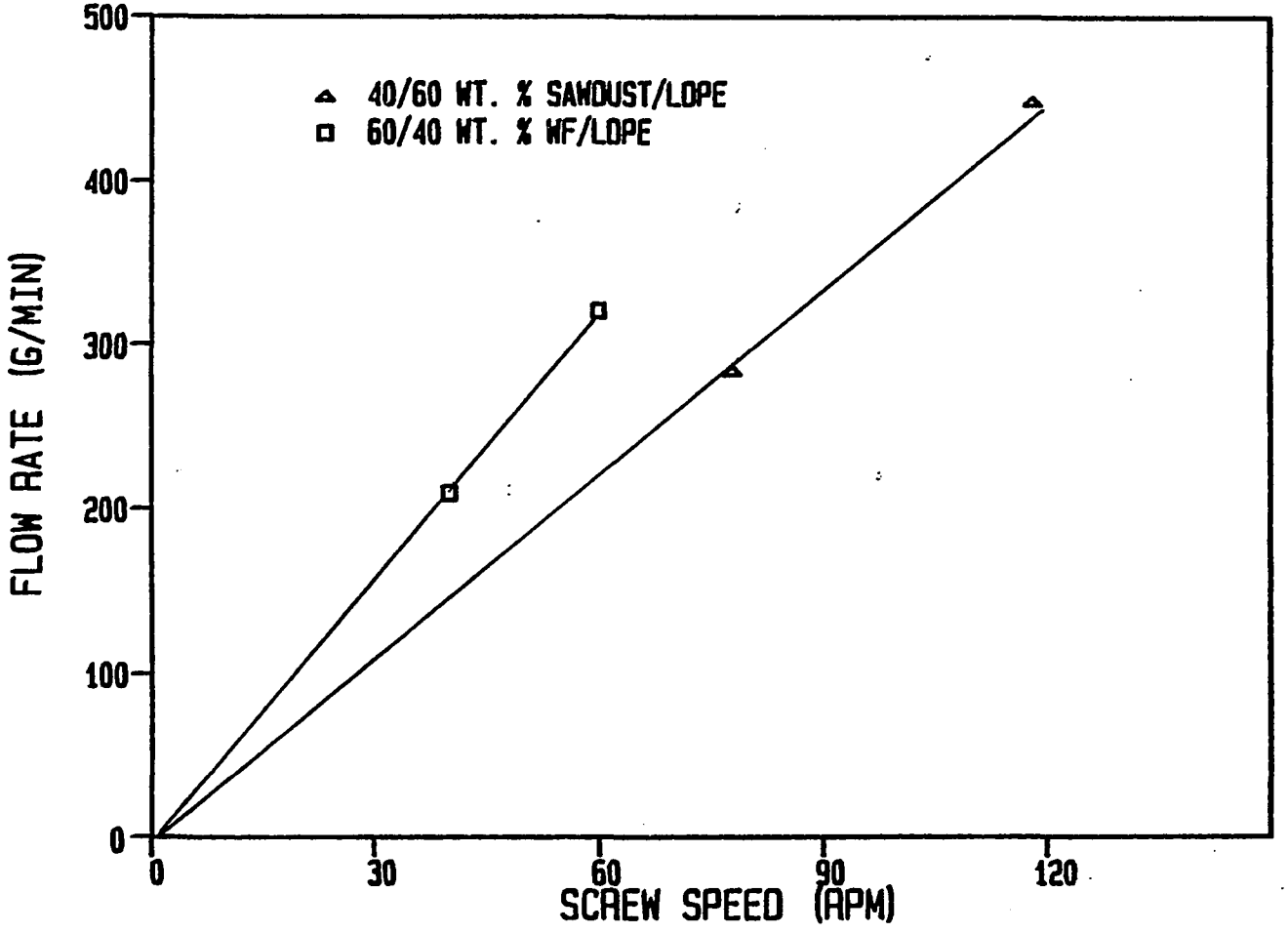

Figure 6.6 Flow rate as a function of screw RPM.

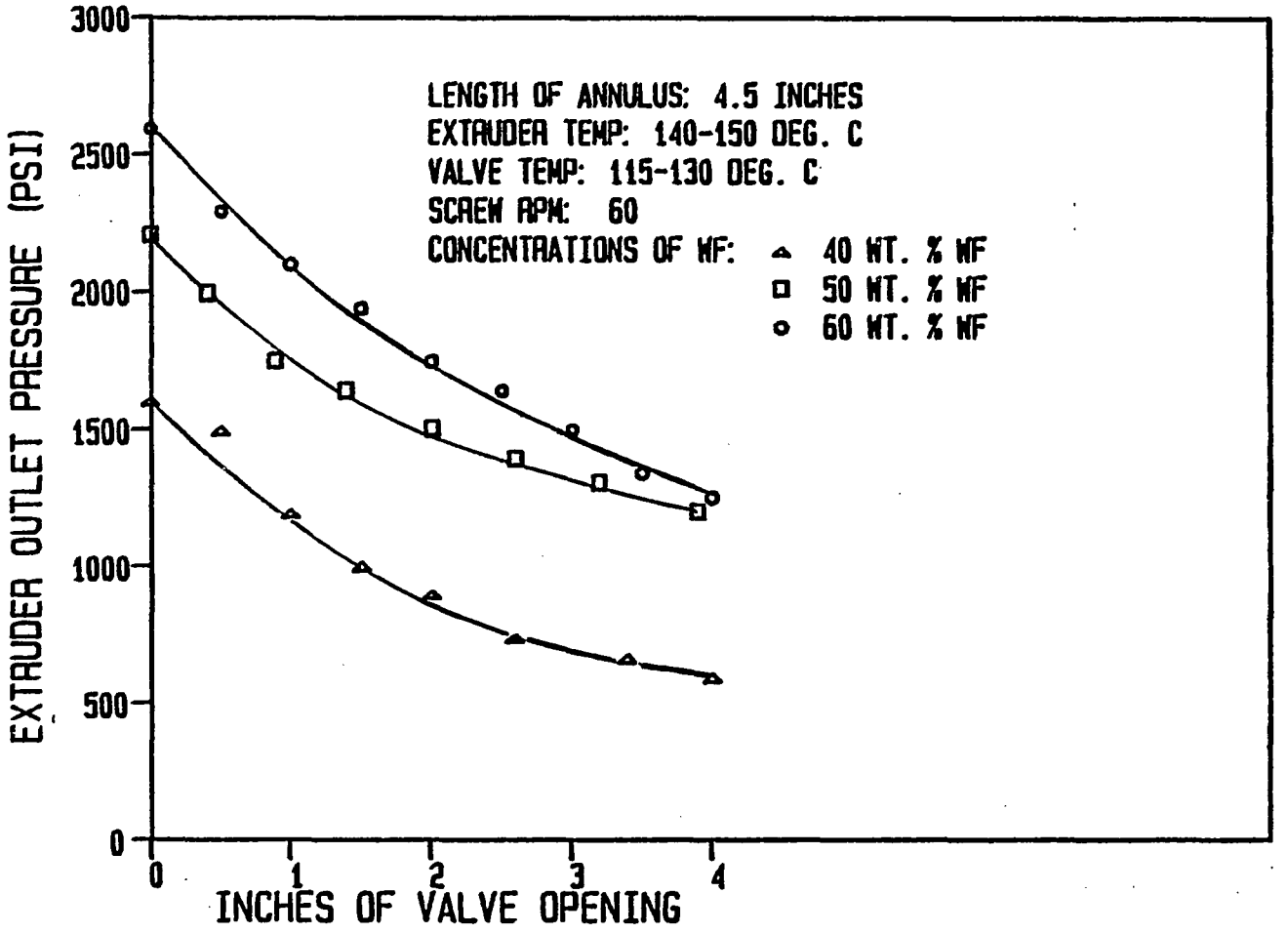

Figure 6.7 Valve characteristics for the extrusion of Albany wood flour/LDPE slurry at different concentrations. -- Experimental data are tabulated in Table B.3.

flour concentrations. For the 60 wt % wood flour slurry, the pressure at valve closure was 2600 psi, as compared to 1600 psi for the 40 wt % slurry. Initially, the combined effects of the conical and the cylindrical valve geometries produced a non-linear valve characteristic. As the valve opening was increased, the annular effect became dominant. This accounted for the linear valve characteristic at 2 inches of opening. It was also interesting to observe that the valve characteristics became more linear for the higher concentrations of wood slurry.

The effect of screw RPM on valve performance for the 60 wt % wood flour slurry was also evaluated. Figure 6.8 shows the valve characteristic at 40 RPM. For comparison, the valve performance at 60 RPM is reproduced from Figure 6.7. As expected, the pressure generated by the extruder was less at a lower screw RPM.

Valve hysteresis is another term often used to describe valve dynamics. Hysteresis can be defined as the difference in valve characteristic for complete valve travel from two opposite directions. Figure 6.9 illustrates the valve hysteresis for the extrusion of a 60 wt % wood flour slurry at 60 RPM. The maximum error observed was approximately 100 psi. This corresponded to an error of 8.3 percent for the full-scale output.

Up to this point, all the valve characteristics observed appear to have two regions, a non-linear portion and a linear portion. It was discussed that the non-linearity was caused by the conical effect at near valve closure. An experiment was conducted to verify this statement. Figure 6.10 illustrates a valve characteristic for the extrusion of a 60 wt % wood flour at 40 RPM. The conical plug was not inserted

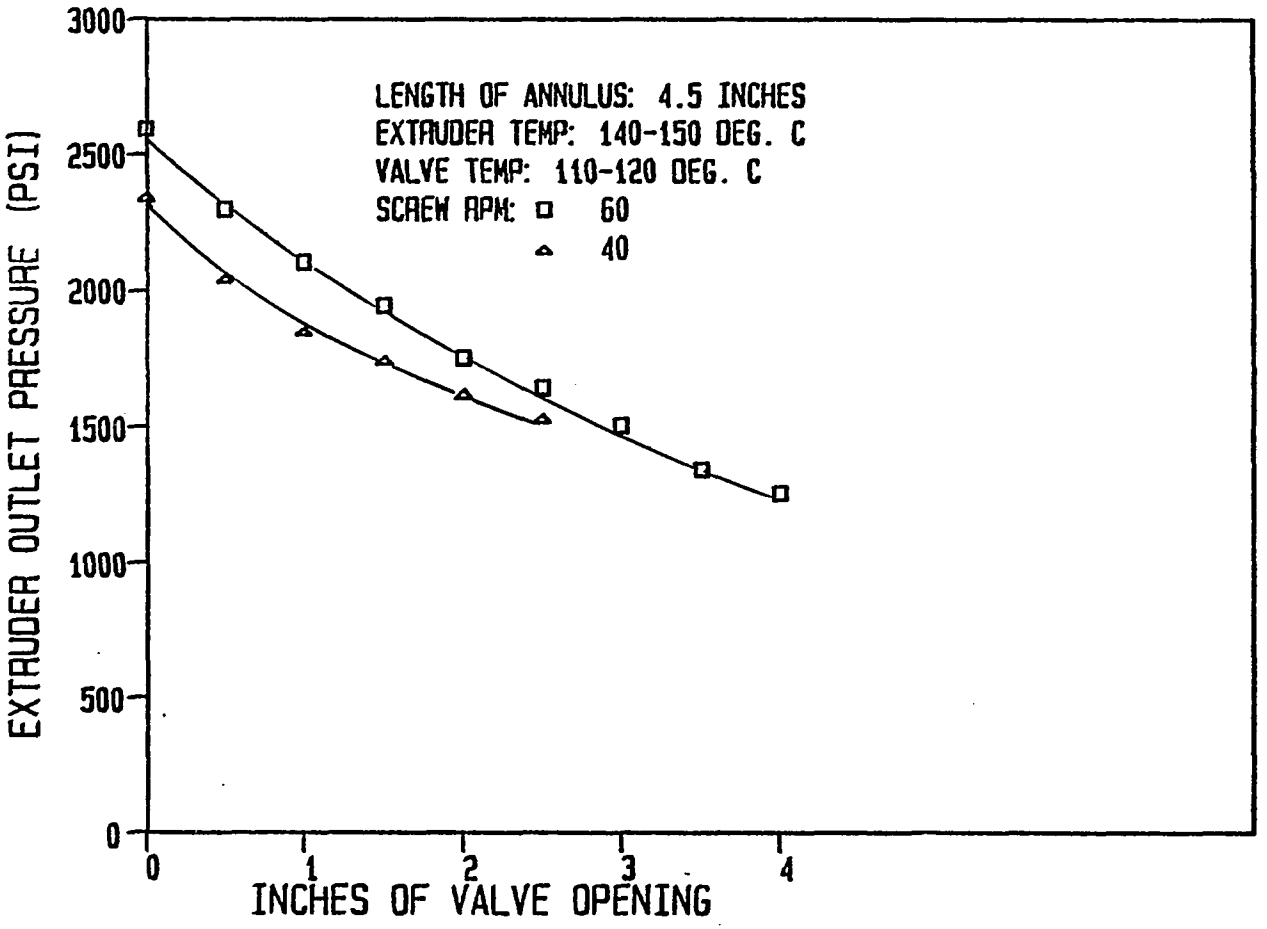

Figure 6.8 Valve characteristics for the extrusion of a 60:40 wt % WF/LDPE slurry at different RPM. -- Experimental data are tabulated in Table B.3d.

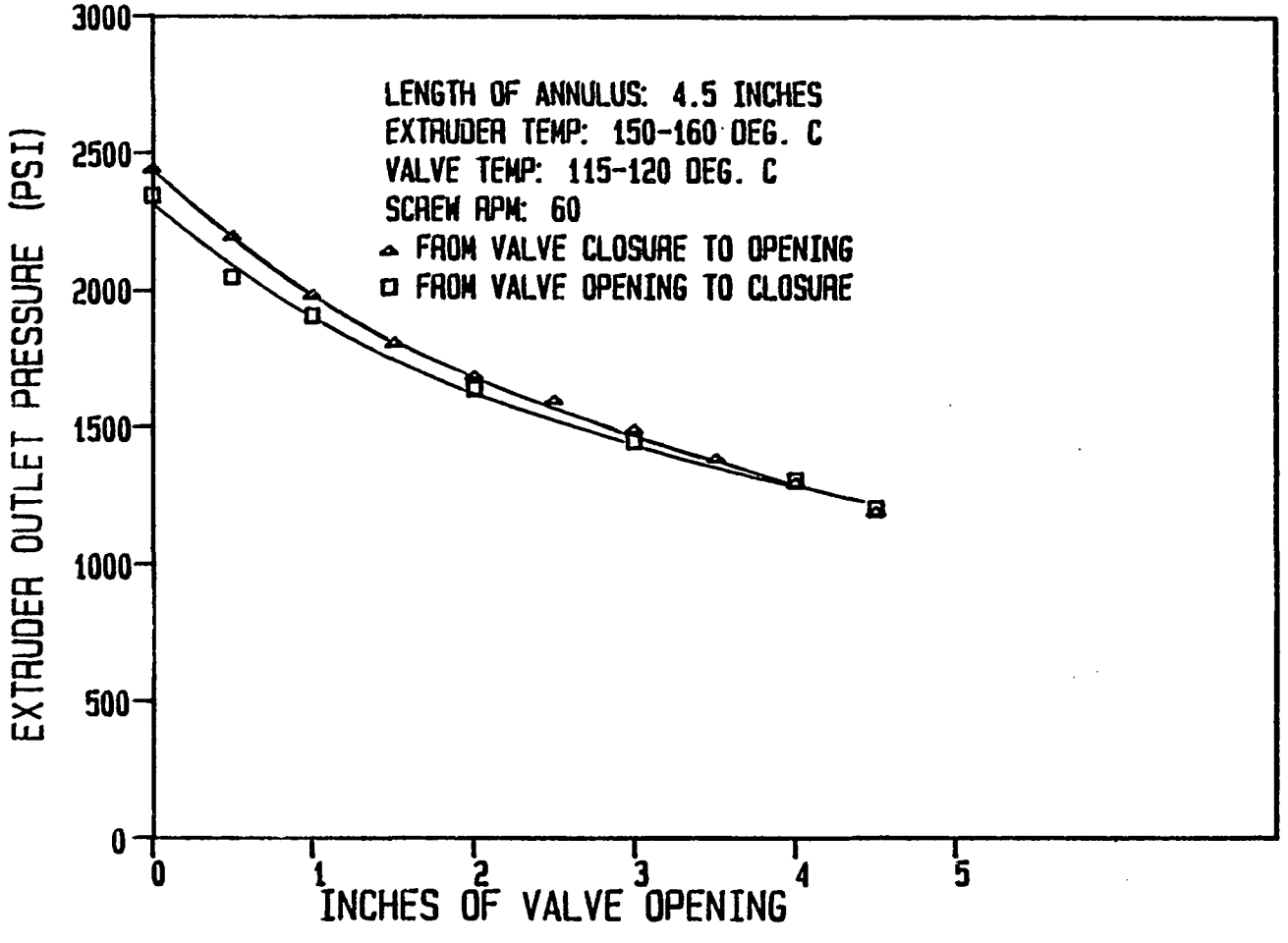

Figure 6.9 Valve hysteresis for the extrusion of a 60:40 wt % WF/LDPE at 60 RPM. -- Results for this experiment are tabulated in Table B.3e.

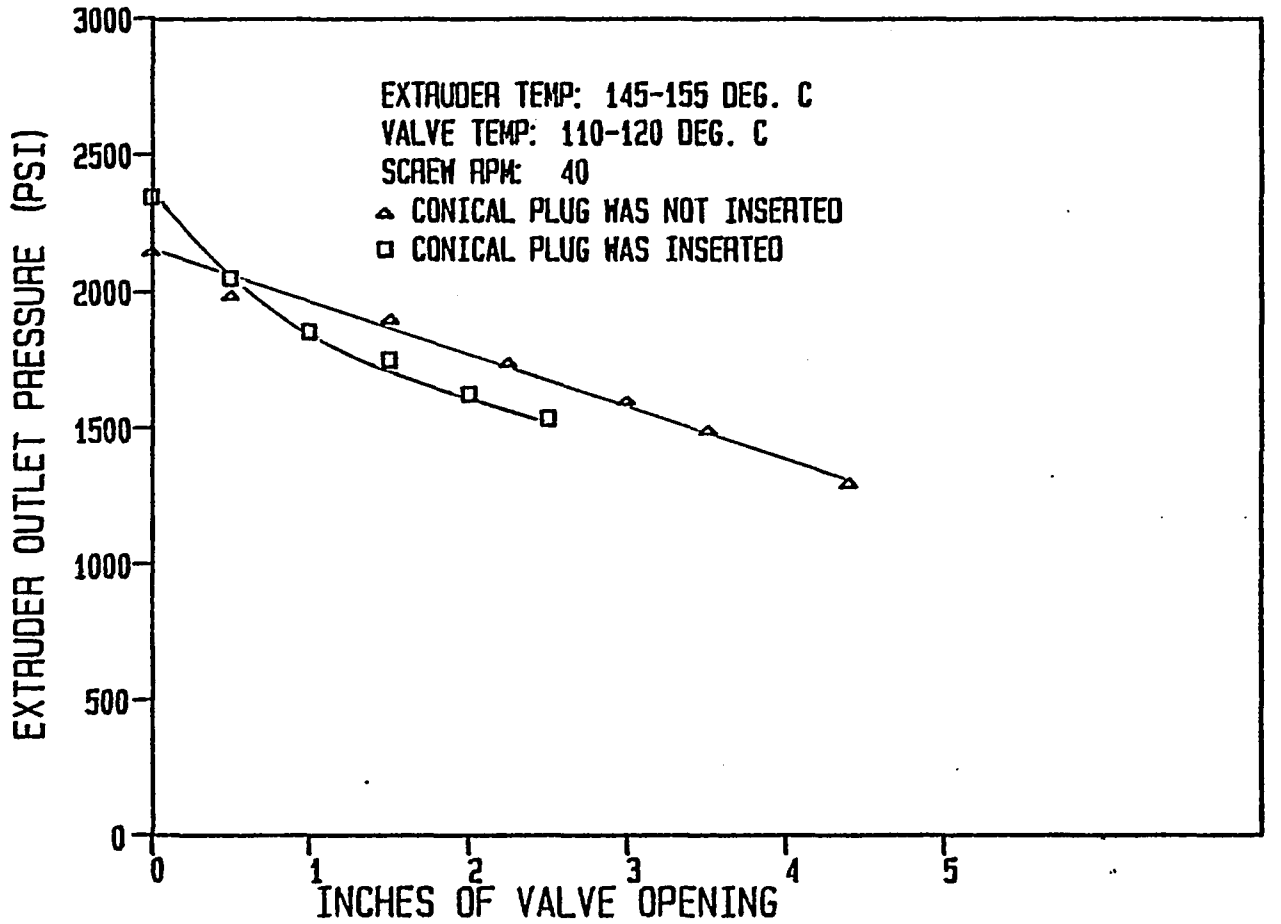

Figure 6.10 Effect of the conical geometry for the extrusion of a 60:40 wt % WF/LDPE slurry at 40 RPM. -- Results for this experiments are shown in Table B.3f.

into the valve trim. As a comparison, the valve characteristic shown in Figure 6.8 at 40 RPM was superimposed. The non-linear effect of the conical geometry is clearly demonstrated. The valve characteristic without the conical plug was linear for the complete range of valve travel.

One of the objectives in the valve development was to eliminate the problem of valve plugging. Since a temporary valve plugging will cause a decrease in the extruder flow rate and an increase in the pressure, the criteria in evaluating non-plugging performance were the steady-state flow rate and the valve characteristic. Observing from the well-behaved valve characteristics for all the experimental runs of wood slurries, valve plugging was not evident. The flow rate across the control valve as a function of valve travel is summarized in Table B.3. A plot of flow rate versus valve travel for the extrusion of the 60:40 wt % WF/LDPE was shown in Figure 6.4. Similar to the previous experiments, changing the valve restriction had no effect on the flow rate. The most important observation was the continuous and steady-state flow of material from the valve outlet. This also supported that valve plugging was not a problem. The average flow rate as a function of screw RPM was shown in Figure 6.6.

6.3.4 Albany Wood Flour and Vacuum Bottom

The valve operability for the extrusion of a 40:60 wt % wood flour and vacuum bottom slurry at 40 screw RPM is illustrated in Figure 6.11. The average temperature at the extruder and at the valve annulus were 150°C and 160°C, respectively. Comparing the results with

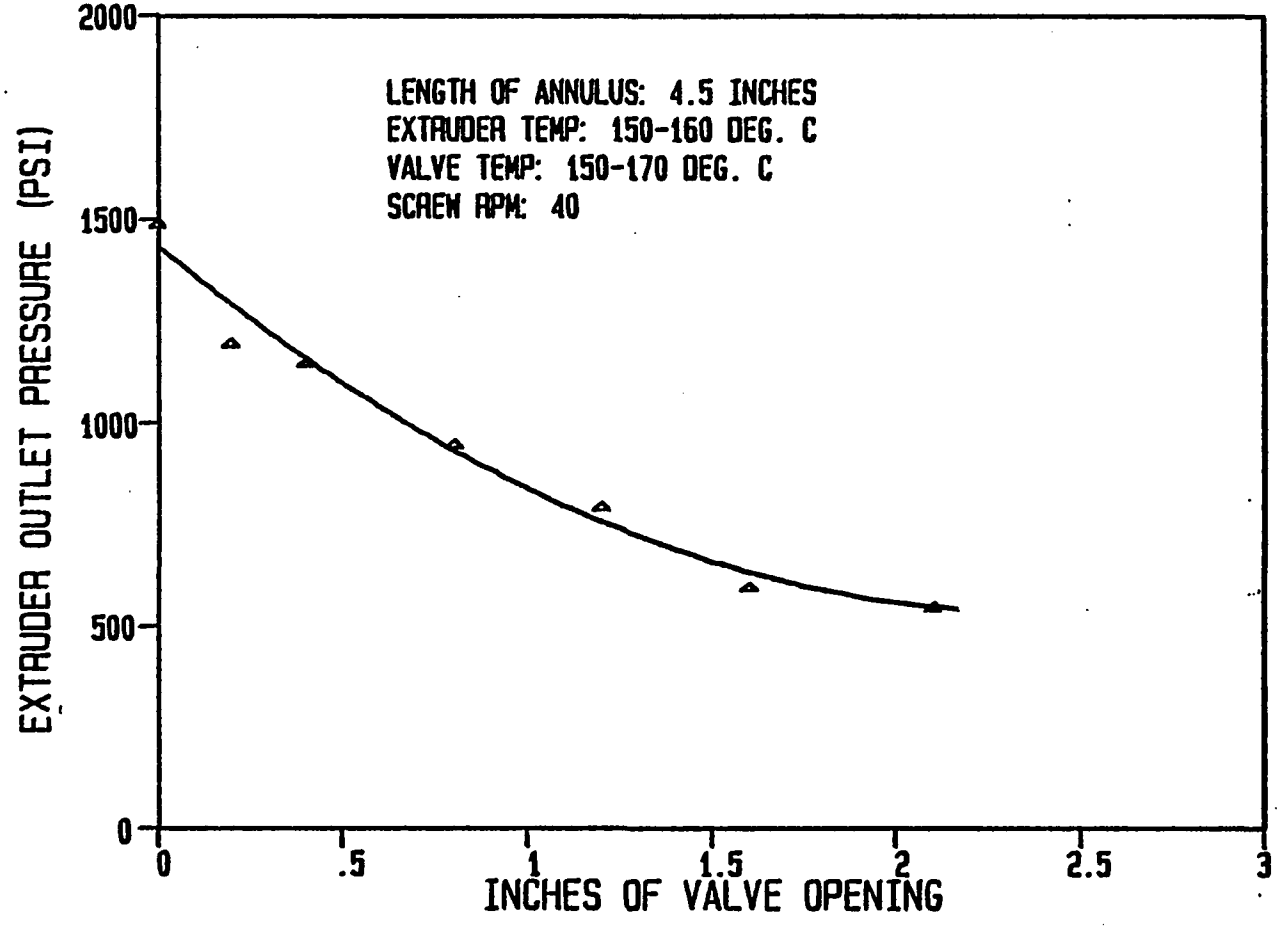

Figure 6.11 Valve characteristic for the extrusion of a 40:60 wt % WF/VB slurry at 40 RPM. -- Results for this experiment are tabulated in Table B.4.

those of wood flour/polyethylene slurry, it was evident that the control valve was more effective when used for the WF/LDPE. The pressure generated by the extruder at valve closure was less than 1600 psi. The valve operating range was decreased to 1-1/2 inches of opening. Since vacuum bottom was considered to be more viscous, it was expected that the valve performance for the extrusion of WF/VB slurry should improve. This contradiction was caused by the extreme valve temperature. The average annular valve temperature for this experiment was 160°C as compared to 120°C for the previous experiments. Evidently, this high temperature had a significant effect on reducing the melt viscosity. Consequently, the valve performance was less effective. The limited availability of vacuum bottom prevented any further experimentation at different valve temperatures. Other experimental data of flow rate, pressure, and temperature profiles are summarized in Table B.4. As expected, flow rate across the valve was not a function of valve opening. The average flow rate was 210 gm/min. Since both the pressure profile and flow rate were relatively stable over the range of valve operation, as demonstrated in Figures 6.4 and 6.11, it was concluded that valve plugging was not observed.

6.4 Viscosity of Wood Slurries

Since it is difficult to predict the viscosity of wood slurries, a simplified calculation procedure, based on the experimental results, is used. For a Newtonian flow through an annulus, the flow equation is:

$$Q = \frac{\pi \Delta p R_o^4}{8 \eta L_a} \left[(1 - k^4) - \frac{(1 - k^2)^2}{\ln (1/k)} \right] \qquad [6.1]$$

$$\tau = \frac{\Delta p R_o}{2L_a} \left[\frac{r}{R} - \frac{(1 - k^2)}{2 \ln (1/k)} \frac{R}{r} \right] \qquad [6.2]$$

where k is the ratio of inner to outer radii of the annulus. The apparent viscosity η can be calculated once the flow rate and the pressure drop across the annulus are determined. To obtain an accurate pressure drop across the annulus, it is necessary to avoid using experimental results at near valve closure, where the conical effects are dominant. It is also important to take into consideration the pressure drop across other valve members and also other imposed resistance. This is accomplished by taking two pressure drop readings at two different valve openings and subtracting their differences. This will be the actual pressure drop across the annulus.

As an example, from the linear region of the 60:40 wt % WF/LDPE valve characteristic shown in Figure 6.7, the pressure drop at 2 inches of valve opening (2-1/2 inches of annulus) is 1750 psi and at 4 inches of valve opening (1/2 inch of annulus) the pressure drop is 1250 psi. This corresponds to a Δp of 250 psi for 1 inch of annular length. From the mass flow rate in Table B.3c and the density of the 60:40 wt % WF slurry:

$$\tilde{Q} = 320 \text{ gm/min}$$

$$\rho = 73.4 \text{ lbm/ft}^3$$

$$Q = (320)\left(\frac{1}{60}\right)\left(\frac{1}{454}\right)\left(\frac{1}{73.4}\right)(123) = 0.276 \text{ in}^3/\text{sec}$$

The apparent viscosity can be calculated from Equation 6.1:

$$\eta = \frac{\pi \Delta p R_o^4}{8 L_a Q} \left[(1 - k^4) - \frac{(1 - k^2)^2}{\ln (1/k)} \right]$$

where

$$k = \frac{R_1}{R_o} = \frac{0.281}{0.375} = 0.75$$

$$\eta = \left(\frac{\pi}{8} \right) (250) (0.375^4) \left(\frac{1}{0.276} \right) (0.019(32.17)(12) \left(\frac{454}{2.54} \right)$$

$$\eta = 9.15 \times 10^3 \text{ gm/cm-sec}$$

The shear stress at the outer radius is calculated from Equation 6.2:

$$\tau = \left(\frac{250}{2} \right) (0.375) (0.24)$$

$$\tau = 11.25 \text{ lbf/in}^2 = 1.97 \times 10^6 \text{ dynes/cm}^2$$

Thus, the shear rate becomes:

$$\dot{\gamma} = \frac{\tau}{\eta} = 215 \text{ sec}^{-1}$$

A list of the calculated viscosity values is shown in Table 6.1. The data are between 0.2 million centipoise for the 40:60 sawdust/LDPE and 1.6 million centipoise for the 40:60 wt % WF/VB. In general, the results are in good agreement with those calculated by White (1981).

Table 6.1 Apparent viscosity of wood slurries.

Material	RPM	Q (gm/min)	ρ (lbm/ft^3)	$\Delta p/L_a$ (lbf/in^3)	$\dot{\gamma}$ (sec^{-1})	η (poise)
40:60 sawdust/LDPE	120	450	48	100	463	1.7×10^3
	80	275	48	125	285	3.45×10^3
40:60 WF/LDPE	60	300	65	145	227	5.02×10^3
50:50 WF/LDPE	60	292	69.2	175	208	6.62×10^3
50:40 WF/LDPE	60	320	73.4	250	215	9.15×10^3
	40	220	73.4	166	148	8.85×10^3
40:60 WF/LDPE	40	200	81	250	122	1.62×10^4

CHAPTER 7

CONCLUSIONS AND RECOMMENDATIONS

An annular valve was developed for the extrusion of biomass slurries and polymers. The objectives were to determine the required valve geometry: 1) to provide a linear installed valve characteristic and 2) to avoid the problem of valve plugging. A numerical iterative method was developed to model the non-Newtonian flow along the annular valve. The results of the parametric evaluation were used to select the optimal valve geometry.

7.1 Conclusions

The valve performance for a variety of materials was examined. As expected, the valve became more effective with materials having a higher melt viscosity. The valve was ineffective for the extrusion of Dow LDPE. It was expected that this was due to the oversizing of the valve annulus. A smaller annulus should improve the valve performance.

Considerable improvement in valve operability was observed for the extrusion of wood flour/polyethylene slurry. This was true with regard to both the higher pressure generated by the extruder and the wider valve operating range. The effects of the conical geometry and the cylindrical annulus were clearly demonstrated by the non-linear valve characteristic at near valve closure and the linearity that follows. From the well-behaved pressure profile and the steady-state flow

from the valve outlet, it was observed that valve plugging was not evident.

The valve characteristic for the extrusion of wood flour/vacuum bottom was also investigated. It appeared that the valve temperature had considerable influence on the overall valve performance. Limited availability of vacuum bottom prevented additional experiments.

7.2 Recommendations

The following recommendations and future experimentations are suggested:

1. Only the low-density polyethylene polymer was used in this study. Since LDPE has a low melt viscosity, the valve proved to be ineffective. It is strongly recommended that the valve performance for a variety of polymers should be investigated, especially those polymers having a higher logarithmic flow curve, such as Dupont Alathon 3 LDPE.
2. It is suggested that different valve geometries should be used. This could be accomplished by using the same valve body and using different trims. In this fashion, the effects of valve geometry could be evaluated to provide an optimal result. This is especially true in regard to the effects of annular spacing. It is expected that a small decrease in the spacing of the valve annulus will result in a large increase in the pressure generated by the extruder.
3. The valve characteristic for the wood flour/vacuum bottom slurry is inconclusive. It is believed that lowering the valve

temperature should improve the overall valve performance. It is also important to experiment with a higher concentration of WF/VB slurry. The limited availability of vacuum bottom has impeded this effort.

4. An actuator is required before the control valve can be implemented in the biomass liquefaction unit. The appropriate actuator should be either the electrohydraulic or electromechanical type. Due to the excessive price and lack of sufficient funding, the actuator was not purchased. Once the actuator is selected, the control valve can be integrated in the biomass liquefaction unit for additional studies.

APPENDIX A

COMPUTER CODE AND SIMULATION RESULTS

This appendix contains the computer code developed to simulate the installed valve characteristic. The mathematical models were presented in Sections 5.2 and 5.3. Runs for different sets of valve geometries were made. In all cases, the power-law parameters for a Dow type 955 low-density polyethylene at 170°C were used. The extruder screw was assumed to be rotating at 80 RPM. The results of the pressure drop across each valve section as a function of valve opening are shown in this appendix. The installed valve characteristics are illustrated in Section 5.5.

```
      PROGRAM VAL
C
C     This program is set up to determine the valve characteristic for a
C     Dow Type 955 low-density polyethylene at 715 Deg C.

C     The variables are:
C     Den         Density of polyethylene
C     vis         Fluid consistency index
C     nflowidx    Fluid behavior index
C     shear       Shear rate at the outer annular wall
C     L1          Length of the concentric annulus
C     D           Length of the conical section
C     RO          Outside radius of the concentric annulus
C     RI          Inner radius of the concentric annulus
C     angle       The conical angle
C     Q           Volumetric flow rate of the extruder
C     TPD         Total pressure drop across the valve
C     X           Inches of valve displacement
C
      DIMENSION SCREW (2,500)
      DATA DEN/40.0/
      REAL L1,n,nflowidx
      SCREW(1,1)=0.0
      DO 500 I=1,500

C     Use linear approximation to calculate the screw characteristic of
C     Fig. 3.5 for a given flow behavior index.

      IF(SCREW(1,I) .GE. 0.0 .AND. SCREW(1,I) .LE. 1.0) THEN
      SCREW(2,I)=-0.16*SCREW(1,I)+0.5
      I2=I+1
      SCREW(1,I2)=SCREW(1,I)+0.01
      ELSE
      IF(SCREW(1,I) .GT. 1.0 .AND. SCREW(1,I) .LE. 1.50) THEN
      SCREW(2,I)=-0.14*SCREW(1,I)+0.47
      I2=1+I
      SCREW(1,I2)=SCREW(1,I)+0.01
      ELSE
      IF(SCREW(1,I) .GT. 1.50 .AND. SCREW(1,I) .LE. 2.50) THEN
      SCREW(2,I)=-0.095*SCREW(1,I)+0.403
      I2=I+1
      SCREW(1,I2)=SCREW(1,I)+0.01
      ELSE
      IF(SCREW(1,I) .GT. 2.50 .AND. SCREW(1,I) .LE. 3.00) THEN
      SCREW(2,I)=-0.11*SCREW(1,I)+0.44
      I2=I+1
      SCREW(1,I2)=SCREW(1,I)+0.01
      ELSE
      IF(SCREW(1,I) .GT. 3.0 .AND. SCREW(1,I) .LE. 3.50) THEN
      SCREW(2,I)=-0.11*SCREW(1,I)+0.77
```

```
      I2=I+1
      SCREW(1,I2)=SCREW(1,I)+0.01
      ELSE
      GOTO 501
      ENDIF
      ENDIF
      ENDIF
      ENDIF
      ENDIF
500   CONTINUE

C     This loop calculates the pressure generated across the metering
C     zone and the flow rate of the extruder.
C     SCREW(1,J) = pressure
C     SCREW(2,J) = flow rate

501   DO 503 J=1,I
      SCREW(1,J)=744.0*SCREW(1,J)
      SCREW(2,J)=0.91*SCREW(2,J)*DEN*2.0833
503   CONTINUE

C     Prompt the user to enter valve dimensions

170   WRITE(6,200)
200   FORMAT('ENTER 1 TO RUN, 2 TO STOP')
      READ(5,350)J
350   FORMAT(I2)
      IF (J .EQ. 2) GOTO 160
      WRITE(6,201)
201   FORMAT('ENTER RO,RI,L1,D,ANGLE,FLOW IDX N,K,IN THIS ORDER')
      READ(5,*)RO,RI,L1,D,ANGLE,FLOWIDX,VIS
      WRITE(6,202)RO,RI,L1,D
      WRITE(2,202)RO,RI,L1,D
202   FORMAT('RO=',F5.2,5X,'RI=',F5.2,5X,'L1=',F5.2,5X,'D=',F5.2)
      WRITE(6,203)ANGLE,FLOWIDX,VIS
      WRITE(2,203)ANGLE,FLOWIDX,VIS
203   FORMAT('ANGLE=',F6.4,'FLOW INDEX N',F3.2,'K',F6.1)
      X=0.0
      RK1=RI/RO
      DO 150 I=1,17
508   K=0

C     This do loop assumes a volumetric flow rate and calculates the
C     pressure drop across each valve section and determines if the
C     pressure drop is equal to the pressure developed along the
C     metering zone.  If it is, the valve displacement is incremented
C     and the procedure is repeated.  Otherwise, a new volumetric flow
C     rate is used to recalculate the pressure drop.

      DO 504 K=1,1000
      BMASS=SCREW(2,K)
```

```
      Q=BMASS*12*12*12/(DEN*3600.0)
      PD2T=0.0
      PD3T=0.0
      PD4T=0.0
      FP3=0.0
      FD3=0.0

C     Determine the alpha value by using linear approximation to the
C     curves shown in Fig. 5.3.

      IF(RK1 .GE. 0.8) THEN
      ALPHA=0.90
      ELSE
      IF(RK1 .LT. 0.8 .AND. RK1 .GE. 0.7) THEN
      ALPHA=0.85
      ELSE
      IF(RK1 .LT. 0.7 .AND. RK1 .GE. 0.6) THEN
      ALPHA=0.78
      ELSE
      IF(RK1 .LT. 0.6 .AND. RK1 .GE. 0.5) THEN
      ALPHA=0.73
      ELSE
      ALPHA=0.67
      ENDIF
      ENDIF
      ENDIF
      ENDIF

C     This block of statements calculates the pressure drop across the
C     concentric annulus of valve section one.  Determine the
C     Fredrickson-Bird Y factor by linear approximation of the curves
C     shown in Fig. 5.2.

      IF(X .LT. L1) THEN
      IF(RK1 .GE. 0.6 .AND. RK1 .LE. 1.0) THEN
      Y=0.475*RK1+0.53
      ELSE
      IF(FLOWIDX .GE. 0.2 .AND. FLOWIDX .LE. 0.4) THEN
      Y=0.4*RK1+0.57
      ELSE
      IF(FLOWIDX .GT. 0.4 .AND. FLOWIDX .LE. 0.6) THEN
      Y=0.5*RK1+0.51
      ELSE
      Y=0.6*RK1+0.45
      ENDIF
      ENDIF
      ENDIF
      N=(FLOWIDX*2+1)/FLOWIDX
      TEMP=(N*Q/((RO**3)*3.14*Y*((1.0-RK1)**N)))**FLOWIDX
      PD1=2.0*(L1-X)*VIS*TEMP/RO
      ELSE
```

```
      PD1=0
      ENDIF
      XTEMP-0.25
      RO1=RO

C     If the valve displacement is greater than the length of the
C     concentric annulus, the pressure drop across valve section one is
C     zero.

      IF(X .LE. L1) THEN
      X1=X
      ELSE
      X1=L1
      ENDIF

C     This do loop calculates the pressure drop across valve section two
C     of Fig. 6.1.

      DO 400 J=1,1000
      IF(XTEMP .LE. X1) THEN

C     Calculate the average outside radius for each incremental annulus.

      R2AVE=(RO2+RO1)/2.0
      RO1=RO2
      RK2=RI/R2AVE

C     Calculate the Fredrickson-Bird Y factor.

      IF(RK2 .GE. 0.6 .AND. RK2 .LE. 1.0) THEN
      Y1=0.475*RK2+0.525
      ELSE
      IF(FLOWIDX .GE. 0.2 .AND. FLOWIDX .LE. 0.4) THEN
      Y1=0.4*RK2+0.57
      ELSE
      IF(FLOWIDX .GT. 0.4 .AND. FLOWIDX .LE. 0.6) THEN
      Y1=0.5*RK2+0.51
      ELSE
      Y1=0.6*RK2+0.45
      ENDIF
      ENDIF
      ENDIF

C     Calculate the pressure drop across for each incremental annulus.

      TEMP1=((N*Q)/((R2AVE**3)*Y1*3.14*((1.0-RK2)**N)))**FLOWIDX
      PD2=2.0*0.25*VIS*TEMP1/R2AVE
      XTEMP=XTEMP+0.25
      PD2T=PD2+PD2T
      ELSE
      GOTO 300
```

```
      ENDIF
400   CONTINUE
300   XTEMP1=X+0.25
      RO1=RO+TAN(ANGLE)*X
      RI1=RI

C     This do loop calculates the pressure drop across valve section
C     three.

      DO 401 J=1,1000
      IF(XTEMP1 .LE. D) THEN

C     Calculate the average inside and outside radii for each
C     incremental annular element.

      RO2=RO+TAN(ANGLE)*XTEMP1
      RI2=RI+TAN(ANGLE)*(XTEMP1-X)
      RO3AVE=(RO2+RO1)/2.0
      RI3AVE=(RI1+RI2)/2.0
      RO1=RO2
      RI1=RI2
      RK3=RI3AVE/RO3AVE
      IF(RK3 .GE. 0.6 .AND. RK3 .LE. 1.0) THEN
      Y2=0.475*RK3+0.53
      ELSE
      IF(FLOWIDX .GE. 0.2 .AND. FLOWIDX .LE. 0.4) THEN
      Y2=0.4*RK3+0.57
      ELSE
      IF(FLOWIDX .GT. 0.4 .AND. FLOWIDX .LE. 0.6) THEN
      Y2=0.5*RK3+0.51
      ELSE
      Y2=0.6*RK3+0.45
      ENDIF
      ENDIF
      ENDIF
      TEMP2=(N*Q/((RO3AVE**3)*Y2*3.14*((1.0-RK3)**N)))**FLOWIDX
      PD3=2.0*0.25*VIS*TEMP2/RO3AVE
      FP2=6.28*RI1*TAN(ANGLE)*0.25*((PD3/2.0)+620.0)
      FD2=PD3*RK3*A*B*3.14*(1.0-(0.8/RK3)**2)
      FD3=FD3+FD2
      FP3=FP3+FP2
      XTEMP1=XTEMP1+0.25
      PD3T=PD3T+PD3
      ELSE
      GOTO 301
      ENDIF
401   CONTINUE

C     This block of statements is used to calculate the pressure drop
C     across valve section four.  If valve displacement X is less than
C     the conical length D only the conical effect occurs.
```

```
      IF(X .LE. D) THEN
      XTEMP1=0.25
      XTEMP=(D-X)+0.25

C     Calculate the average inside radius.

      R4O=RO+D*TAN(ANGLE)
      RI1=RI+(D-X)*TAN(ANGLE)

C     This do loop calculates the pressure drop for each incremental
C     annular element.

      DO 402 J=1,1000
      IF(XTEMP1 .LE. X) THEN
      RI2=RI+XTEMP*TAN(ANGLE)
      RIAVE=(RI2+RI1)/2.0
      RK4=RIAVE/R4O
      RI1=RI2
      IF(RK4 .LE. 0.2) THEN
      Y4=0.62
      ELSE
      Y4=0.53+RK4*0.47
      ENDIF
      TEMP3=(N*Q/((R4O**3)*Y4*3.14*((1.0-RK4)**N)))**FLOWIDX
      PD4=2.0*0.25*VIS*TEMP3/R4O
      PD4T=PD4T+PD4
      XTEMP1=XTEMP1+0.25
      XTEMP=XTEMP+0.25
      ELSE
      GOTO 302
      ENDIF
402   CONTINUE
      ELSE

C     If the valve displacement is greater than the conical length, both
C     the concentric valve trim and conical plug need to be considered.

      XX=X-D
      R4O=RO+TAN(ANGLE)*D
      RK6=RI/R4O
      IF(RK6 .LE. 0.2) THEN
      Y6=0.62
      ELSE
      Y6=0.53+RK6*0.43
      ENDIF

C     Calculate the pressure drop due to the concentric annulus.

      TEMP3=(N*Q/((R4O**3)*Y6*3.14*((1.0-RK6)**N)))**FLOWIDX
      PD6=2.0*XX*VIS*TEMP3/R4O
      XTEMP1=0.25
```

```
      RI1=RI
      R4O=RO+TAN(ANGLE)*D

C     This do loop calculates the pressure drop for the conical valve
C     trim.

      DO 403 J=1,1000
      IF(XTEMP1 .LE. D) THEN
      RI2=RI+TAN(ANGLE)*XTEMP1
      RK4=(RI1+RI2)/(2.0*R4O)
      RI1=RI2
      IF(RK4 .LE. 0.2) THEN
      Y4=0.62
      ELSE
      Y4=0.53+0.47*RK4
      ENDIF
      TEMP3=(N*Q/((R4O**3)*Y4*3.14*((1.0-RK4)**N)))**FLOWIDX
      PD4=2.0*0.25*VIS*TEMP3/R4O
      PD4T=PD4T+PD4
      XTEMP1=XTEMP1+0.25
      ELSE
      PD4T=PD4T+PD6
      GOTO 302
      ENDIF
403   CONTINUE
      ENDIF

C     Summation of the pressure drop for all valve sections.

301   TPD=PD1+PD2T+PD3T+PD4T

C     Calculate the error between the pressure drop across the valve and
C     the pressure generated in the metering zone.  If the difference is
C     greater than 100 psi, a new volumetric flow rate is assumed and
C     the procedure is repeated.  If the error is less than 100 psi, the
C     valve position is incremented.

      ERROR=TPD-SCREW(1,K)
      IF(ABS(ERROR) .LE. 100.0) THEN
      GOTO 505
      ENDIF
504   CONTINUE

C     Calculate the shear rate to determine if the assumed shear rate is
C     within range.

505   IF((L1-X) .LE. 0.00) THEN
      SHEAR=0.00
      GOTO 507
      ELSE
      SHEAR=RO*TPD*(1-(ALPHA)**2)/(2*(L1-X))
```

```
      ENDIF
      IF(SHEAR .LE. 14.4) THEN
      NFLOWIDX=0.44
      VIS=2.02
      ELSE
      IF(SHEAR .GT. 14.4 .AND. SHEAR .LE. 35.1) THEN
      NFLOWIDX=0.62
      VIS=0.81
      ELSE
      IF(SHEAR .GT. 35.1 .AND. SHEAR .LE. 47.0) THEN
      NFLOWIDX=0.62
      VIS=0.81
      ELSE
      GOTO 507
      ENDIF
      ENDIF
      ENDIF
      IF(NFLOWIDX .EQ. FLOWIDX) THEN
      GOTO 507
      ELSE
      FLOWIDX=NFLOWIDX
      GOTO 508
      ENDIF
507   WRITE(2,100)X,PD1,PD2T,PD3T,PD4T,PD5,TPD
      WRITE(2,101)BMASS,SHEAR,FLOWIDX,VIS
      WRITE(6,100)X,PD1,PD2T,PD3T,PD4T,PD5,TPD
100   FORMAT(5X,F8.2,5X,F8.2,5X,F8.2,5X,F8.2,5X,F8.2,5X,F8.2,5X,F8.2)
101   FORMAT(5X,F8.2,5X,F8.2,5X,F8.2,5X,F8.2)

C     Increment the valve position by 0.25 inch.

      X=X+0.25
150   CONTINUE
      GOTO 170
160   STOP
      END
```

Table A.1 Pressure drop across each valve section as a function of valve displacement for different conical angles. -- Other valve dimensions are: R_o = 5/16, R_i = 4/16, L_a = 1, and L_c = 2 (all dimensions are in inches).

Conical Angle φ	Valve Displacement, x (inches)	Pressure Drop across Each Valve Section (psi) Δp_1	Δp_2	Δp_3	Δp_4	Total Pressure Drop Δp_T
5°	0.0	582	0	1396	0	1980
	0.25	533	121	780	81	1510
	0.50	396	206	462	140	1203
	0.75	216	274	296	189	977
	1.00	0	337	202	235	775
	1.25	0	365	131	255	752
	1.50	0	385	85	271	742
10°	0.0	612	0	1273	0	1885
	0.25	592	98	451	52	1195
	0.50	446	152	212	83	894
	0.75	247	191	118	106	664
	1.00	0	222	71	124	418
	1.25	0	179	55	96	331
	1.50	0	188	37	102	327
	1.75	0	195	25	107	327
	2.00	0	200	16	111	327
20°	0.0	650	0	1095	24	1746
	0.25	630	62	178	35	900
	0.50	492	85	62	41	675
	0.70	267	99	30	46	435
	1.00	0	111	15	48	174
	1.25	0	113	9	48	170
	1.75	0	114	5	49	169
	2.00	0	115	0	50	168
30°	0.0	678	0	968	0	1646
	0.25	600	38	80	12	730
	0.50	507	49	24	16	590
	0.75	275	56	11	18	356
	1.00	0	62	6	20	88
	1.25	0	62	3	20	87

Table A.2 Pressure drop across each valve section as a function of valve displacement for different annular spacings. -- Other valve dimensions are: R_i = 1/2 inch, L_a = 3/4 inch, L_c = 1/2 inch, and φ = 10°.

Annular Spacing (inches)	Valve Displacement, x (inches)	Pressure Drop across Each Valve Section (psi)				Total Pressure Drop
		Δp_1	Δp_2	Δp_3	Δp_4	Δp_T
1/32	0.0	1298	0	823	0	2121
	0.25	1182	177	78	164	1551
	0.50	704	264	0	248	1216
	0.75	0	264	0	356	620
2/32	0.0	479	0	304	0	783
	0.25	353	89	50	82	574
	0.50	186	129	0	122	308
	0.75	0	129	0	154	283

Table A.3 Pressure drop across each valve section as a function of valve displacement for different inner and outer annular radii. -- Other valve dimensions are: L_a = 2 inches, L_c = 2 inches, and φ = 10°.

Inner and Outer Radii (inches)	Valve Displacement, x (inches)	Pressure Drop across Each Valve Section (psi)				Total Pressure Drop
		Δp_1	Δp_2	Δp_3	Δp_4	Δp_T
R_i = 9/32	0.0	1105	0	857	0	1963
R_o^i = 11/32	0.25	1150	81	268	53	1553
	0.50	1052	120	112	79	1363
	0.75	920	143	54	95	1213
	1.00	779	162	15	110	1080
	1.25	617	178	3	120	933
	1.50	443	197	0	135	784
	1.75	236	215	0	148	603
	2.00	0	235	0	161	394
R_i = 13/32	0.0	975	0	802	0	1780
R_o^i = 15/32	0.25	996	71	247	51	1365
	0.50	905	104	102	75	1190
	0.75	796	125	50	91	1065
	1.00	669	141	26	103	940
	1.25	534	156	14	115	820
	1.50	375	169	7	125	678
	1.75	197	182	0	136	519
	2.00	0	195	0	146	342

Table A.4 Pressure drop across each valve section as a function of valve displacement for different annular length L_a. -- Other valve dimensions are: R_i = 9/32 inch, R_o = 12/32 inch, L_c = 1.5 inches, and $\varphi = 10°$.

Annular Length L_a (inches)	Valve Displacement, x (inches)	Pressure Drop across Each Valve Section (psi)				Total Pressure Drop
		Δp_1	Δp_2	Δp_3	Δp_4	Δp_T
3.0	0.0	840	0	358	0	1200
	0.5	768	60	59	43	930
	1.0	633	90	12	75	810
	1.5	490	107	0	90	687
	2.0	320	119	0	100	539
	2.5	131	130	0	110	377
	3.0	0	140	0	131	271
4.0	0.0	1000	0	313	0	1313
	0.5	937	60	50	40	1080
	1.0	834	80	20	65	1000
	1.5	714	100	0	77	891
	2.0	581	110	0	87	779
	2.5	447	120	0	100	668
	3.0	289	129	0	112	600
	3.5	114	137	0	126	377
	4.0	0	145	0	141	207
5.0	0.0	1190	0	293	0	1485
	0.5	1140	51	50	45	1286
	1.0	1049	71	10	61	1191
	1.5	940	82	0	71	1093
	2.0	828	90	0	80	998
	2.5	709	100	0	89	898
	3.0	578	114	0	100	762
	3.5	444	123	0	113	680
	4.0	287	131	0	127	535

APPENDIX B

TABULATED EXPERIMENTAL RESULTS

The experimental data are summarized in this appendix. The data reported are screw rotational speed, valve opening (20 turns represent one inch of valve movement), pressure profile along the metering zone, temperature profile of the melt, average temperature of the valve at the outer wall of the annulus, extruder temperature controller readings, and the mass flow rate. The nomenclature used are identified in Figure 6.1.

It is also important to mention that in some experimental runs a temperature correction was necessary. It was discovered that, during installation and subsequent replacement of the carbon-steel tubes, thermocouples T_1 and T_3 were not inserted correctly into the polymer melt. In reference to thermocouple T_2, which was placed into the polymer melt, thermocouples T_1 and T_3 were 1 cm and 3 cm away from the polymer melt. Consequently, these measurements were not a good representation of the melt temperature.

To estimate these temperature differences, the extruder was allowed sufficient heating time to reach steady state. A set of thermocouple readings was made prior to the beginning of each experiment. Since the extruder was at steady state, the temperature of the melted polymer across the metering zone should be the same. Any error in thermocouple readings was assumed to be attributed to the misplacement of the thermocouples. As expected, temperatures T_1 and T_3 were between

5-15°C lower than T_2. These temperature differences were added to each subsequent reading.

Table B.1 Experimental results for the extrusion of a Dow LDPE at 80 RPM. -- An annular length of 3½ inches was used.

# of Turns	Inches of Valve Opening	Pressure Profile (psi)				Temperature Profile (°C)					Average Valve Temperature (°C)	Extruder Temperature Controllers (°C)		Flow Rate (gm/min)
		P_1	P_2	P_3	P_4	T_1	T_2	T_3	T_4	T_5		T_{met}	T_{melt}	
0	0.0	1000	1350	890		131	130	123	133	88	115	145	150	358
4	0.2	750	1150	890		134	132	125	134	88	110	145	150	400
8	0.4	700	1150	900		134	132	125	134	89	110	145	150	348
12	0.6	530	1000	890		134	132	125	134	89	113	145	150	378
16	0.8	530	1000	850						88	110	145	150	370
24	1.2	530	750			134		125	134	88	110			368

Table B.2a Experimental data for the extrusion of a 40:60 wt % sawdust/LDPE at 80 RPM. -- An annular length of 4½ inches was used.

# of Turns	Inches of Valve Opening	Pressure Profile (psi)				Temperature Profile (°C)					Average Valve Temperature (°C)	Extruder Temperature Controllers (°C)		Flow Rate (gm/min)
		P_1	P_2	P_3	P_4	T_1	T_2	T_3	T_4	T_5		T_{met}	T_{melt}	
0	0.0	1100					136	132		75	100			266
4	0.2	950	930								100	145	140	284
8	0.4	840	730				138	134		75	95		150	286
12	0.6	750	710								100			264
20	1.0	650	630				138	134		75	95			244
28	1.4	600	630								95	150	140	280
36	1.8	550					138	134		75		150	135	274
44	2.2	550	500											272
52	2.6	500					138	134		75				264
74	3.7	410					138	134		75		150	135	306

Table B.2b Experimental data for the extrusion of a 40:60 wt % sawdust/LDPE slurry at 120 RPM. -- An annular length of 4½ inches was used.

# of Turns	Inches of Valve Opening	Pressure Profile (psi)				Temperature Profile (°C)					Average Valve Temperature (°C)	Extruder Temperature Controllers (°C)		Flow Rate (gm/min)
		P_1	P_2	P_3	P_4	T_1	T_2	T_3	T_4	T_5		T_{met}	T_{melt}	
0	0.0	1300	1200	690							95	145	140	450
4	0.2	1100	1200	690							95			462
8	0.4	950	1200	690		139		131			100	145	140	454
12	0.6	850	1100	600		139		132			98	145	140	446
16	0.8	800	950	600		139	148	132		79		150	140	454
20	1.0	750	900	600		139	149	132		79		150	145	448
28	1.4	700	900	500		139	149	134		79				456
36	1.8	650	850	500		139	149	134		79		150	145	452
52	2.6	650	800	500		139	149	135		79		150	145	

Table B.3a Experimental results for the extrusion of a 40:60 wt % WF/LDPE slurry at 60 RPM. -- An annular length of 4½ inches was used.

# of Turns	Inches of Valve Opening	Pressure Profile (psi)				Temperature Profile (°C)					Average Valve Temperature (°C)	Extruder Temperature Controllers (°C)		Flow Rate (gm/min)
		P_1	P_2	P_3	P_4	T_1	T_2	T_3	T_4	T_5		T_{met}	T_{melt}	
0	0.0	1600	1650	2350		116	121	120	136	69	120-130	150	150	287
10	0.5	1500	1500	2170	1300							150	150	298
20	1.0	1200	1370	2170	800	136	143	130	134	81		155	150	300
30	1.5	1000	1200	2100	1000	138	143	130	132	81		160	150	302
40	2.0	900	1100	2050	1120	141	145	132	134	83		160	150	302
54	2.7	740	950	2050	1100	143	145	136	143	84		160	150	304
68	3.4	670	780	1900	1100	147	148	138	143	86				286

Table B.3b Experimental results for the extrusion of a 50:50 wt % WF/LDPE mixture at 60 RPM. -- An annular length of 4½ inches was used.

# of Turns	Inches of Valve Opening	Pressure Profile (psi)				Temperature Profile (°C)					Average Valve Temperature (°C)	Extruder Temperature Controllers (°C)		Flow Rate (gm/min)
		P_1	P_2	P_3	P_4	T_1	T_2	T_3	T_4	T_5		T_{met}	T_{melt}	
0	0.0	2200	2300	2650	2500	128	121	119	136	64	125	150	150	286
8	0.4	2000	2200	2600	2500	133	132	119	141	66		150	150	288
18	0.9	1750	2000	2600	2500	133	134	126	141	68		150	150	298
28	1.4	1650	2000	2550	2450	133	136	130	141	70		150	155	294
40	1.0	1500	1800	2490	2400	133	136	131	141	70	120	150	155	294
52	2.6	1400	1750	2450	2350	133	136	131	141	70		150	155	292
64	3.2	1300	1600	2350	2350	133	136	133	141	70	119	150	155	290
78	3.9	1200	1550	2350	2300	133	136	134	141	70		150	155	294
90	4.5	1100	1500	2350	2300	133	136	134	141	70	117	155	155	291
102	5.1	1000	1400	2300	2150	133	136	134	141	70		155	155	294

Table B.3c Experimental data for the extrusion of a 60:40 wt % WF/LDPE at 60 RPM. -- An annular length of 4½ inches was used.

# of Turns	Inches of Valve Opening	Pressure Profile (psi)				Temperature Profile (°C)					Average Valve Temperature (°C)	Extruder Temperature Controllers (°C)		Flow Rate (gm/min)
		P_1	P_2	P_3	P_4	T_1	T_2	T_3	T_4	T_5		T_{met}	T_{melt}	
0	0.0	2600	2800	3000	3130	126	132	126	141	64	121	150	140	320
10	0.5	2300	2700	3000	2900	128	138	129	145	65				318
20	1.0	2100	2500	3000	2900	130	139	133	147	66	119	155	155	320
30	1.5	1950	2300	2900	2900	135	143	135	147	68		150	160	324
40	2.0	1750	2200	2800	3000	135	145	139	150	70	114	150	160	324
50	2.5	1650	2100	2800	2800	137	147	142	152	70		155	165	328
60	3.0	1500	2000	2600	2800	138	147	144	152	68	129	155	165	328
70	3.5	1350	1900	2600	2800	138	147	146	152	70				316
80	4.0	1250	1800	2600	2800	138	147	146	152	70				320

Table B.3d Experimental data for the extrusion of a 60:40 wt % WF/LDPE slurry at 40 RPM. -- An annular length of 4½ inches was used.

# of Turns	Inches of Valve Opening	Pressure Profile (psi)				Temperature Profile (°C)					Average Valve Temperature (°C)	Extruder Temperature Controllers (°C)		Flow Rate (gm/min)
		P_1	P_2	P_3	P_4	T_1	T_2	T_3	T_4	T_5		T_{met}	T_{melt}	
0	0.0	2350	2800	2900	3500	126	123	114	136	38	107	150	140	202
10	0.5	2050	2600	2600	3400	126	123	114	136	68		150	145	214
20	1.0	1850	2500	2400	3200	126	123	116	136	68		150	145	208
30	1.5	1750	2340	2200	3100	126	125	119	136	68		150	150	214
40	2.0	1620	2300	2200	3200	126	127	121	136	68	130	150	145	208
50	2.5	1530	2100	1800	3200	126	123	121	136	68		150	145	214

Table B.3e Experimental data for the extrusion of a 60:40 wt % WF/LDPE slurry at 60 RPM. -- An annular length of 4½ inches was used.

# of Turns	Inches of Valve Opening	Pressure Profile (psi)				Temperature Profile (°C)					Average Valve Temperature (°C)	Extruder Temperature Controllers (°C)		Flow Rate (gm/min)
		P_1	P_2	P_3	P_4	T_1	T_2	T_3	T_4	T_5		T_{met}	T_{melt}	
0	0.0	2450	3100	3400	3400	132	134	126	140	64	125	150	145	320
10	0.5	2200	2600	3160	to	134	138	130	143	66		160	155	306
20	1.0	2000	2450	3000	3000	134	138	131	147	68	113	160	160	318
30	1.5	1820	2400	2810		132	139	135	148	70				326
40	2.0	1700	2300	2750		132	141	144	150	70	119	160	160	322
50	2.5	1600	2200	2750		132	141	144	150	70	116	160	160	326
60	3.0	1500	2200	2750		132	143	144	148	70		160	160	
70	3.5	1400	2100	2750		132	145	144	145	70				338
80	4.0	1300	2000	2700		132	143	144	145	68	120			
90	4.5	1200	1800	2600		136	145	144	147	70				338
80	4.0	1300	1970	2740		137	147	144	147	68	128	165	160	
60	3.0	1450	2200	2800		137	145	146	150	70	120	165	160	348
40	2.0	1650	2300	2800		136	145	146	150	73				334
20	1.0	1900	2550	2950		136	145	149	154	73	120	165	165	
10	0.5	2050	2700	3180							119	165	165	330
0	0.0	2350	3000	3250										

Table B.3f Experimental data for the extrusion of a 60:40 wt % WF/LDPE slurry at 40 RPM. -- The conical cone was not used.

# of Turns	Inches of Valve Opening	Pressure Profile (psi)				Temperature Profile (°C)					Average Valve Temperature (°C)	Extruder Temperature Controllers (°C)		Flow Rate (gm/min)
		P_1	P_2	P_3	P_4	T_1	T_2	T_3	T_4	T_5		T_{met}	T_{melt}	
0	0.0	2150	2600	3050	3000	128	130	126	136	60	119	140	150	212
10	0.5	2000	2500	2800	2900	126	130	126	136	60		140	150	214
30	1.5	1900	2400	2800	3000	123	130	126	134	60		140	148	214
45	2.25	1750	2250	2740	2900	121	130	126	136	60		145	150	218
60	3.0	1600				123	133	134	138	62		145	150	222
70	3.5	1500	2050	2650	2700	128	136	134	139	62		150	155	222
90	4.5	1300	1900	2650	2900	128	136	136	140	64	108	150	150	218
100	5.0	1150	1800	2610	3000	123	133	138	141	62				

Table B.4 Experimental data for the extrusion of a 40:60 wt % WF/VB slurry at 40 RPM. -- An annular length of 4½ inches was used.

# of Turns	Inches of Valve Opening	Pressure Profile (psi)				Temperature Profile (°C)					Average Valve Temperature (°C)	Extruder Temperature Controllers (°C)		Flow Rate (gm/min)
		P_1	P_2	P_3	P_4	T_1	T_2	T_3	T_4	T_5		T_{met}	T_{melt}	
0	0.0	1500	2700		1500	132	147	140	145	71	150-170	150	150	250
4	0.2	1200	1600	1700	1200	136	150	142	147	74		155	150	210
8	0.4	1150.	1500	1420	800	138	150	144	147	74		155	150	200
16	0.8	950	1300	1200	670	140	149	148	150	74		160	150	212
24	1.2	800	1100	900	530	140	152	148	150	76		160	155	208
32	1.6	600	1000	840	530	140	152	148	150	76		160	155	200
42	2.1	550				140	150	148	150	76		160	155	186
54	2.7	500	700	600	300							160	155	190

NOMENCLATURE

Roman

b	Effective gasket seating width, inches
d_f	Diameter of the valve body, inches
d_s	Diameter of the stem, inches
d_o	Outside diameter of the seating surface, inches
D	Inside diameter of the extruder barrel, inches
e	Width of the screw flight, inches
E	Activity energy, kcal/gm mole
f	Allowable working stress, lbf/sec^2
F_D	Shape factor for drag flow
F_P	Shape factor for pressure flow
F_T	Total force to be imparted by the actuator, lbf
g	Gravitational acceleration, ft/sec^2
G	Diameter of gasket reaction, inches
H	Screw channel depth, inches
k	Ratio of inner to outer radii of the annulus
l_s	Total length of the packing, inches
L	Length of the metering zone, inches
L_a	Length of the valve annulus, inches
L_c	Length of the conical valve trim, inches
m	Consistency index, $lbf/sec^n\text{-}in^2$
M	Gasket factor
n	Fluid behavior index

N	Screw speed, RPM
p	Pressure, lbf/sec^2
Q	Volumetric flow rate, $inch^3/sec$
R_i	Inside radius of the valve annulus, inches
R_o	Outside radius of the valve annulus, inches
T	Temperature of the melt, °C
T_{melt}	Temperature controller reading of the melting zone, °C
T_{met}	Temperature controller reading of the metering zone, °C
T_{val}	Temperature of the valve at the annulus, °C
U_T	Total force required to seal the packing, lbf
v_x	Cross-channel velocity, ft/sec
v_z	Down channel velocity, ft/sec
V_b	Screw velocity along the helical axis, ft/sec
W	Channel width, inches
W_m	Total load required to hold gasket in place, lbf
x	Axial valve displacement, inches
Y	Fredrickson and Bird factor
z	Screw channel coordinate axis, inches

Greek

$\dot{\gamma}$	Shear rate, sec^{-1}
δ_f	Radial clearance between the crest of the screw flight and the barrel, inches
η	Apparent non-Newtonian viscosity, $lbf\text{-}sec/in^2$
Θ	Helical angle of the screw
λ	Radial distance at which the shear stress is zero

μ	Newtonian viscosity, lbf-sec/in^2
μ_s	Coefficient of friction
ρ	Density, lb/ft^2
τ	Shear stress, lbf/in^2
φ	Tapered angle of the conical trim

REFERENCES

Agur, E. E., and J. Vlachopoulous. 1982. Numerical simulation of a single-screw plasticating extruder. Polymer Engineering Science, 22, 1084.

Battelle Labs. 1981. Proceedings of the 13th Biomass Thermochemical Conversion Contractors Meeting. Arlington, Virginia, October 27-29.

Bernhart, E. C. 1959. Processing of Thermoplastic Materials. New York: Reinhold Publishing Corporation.

Booy, M. C. 1981. The influence of non-Newtonian flow on effective viscosity and channel efficiency in screw pumps. Polymer Engineering Science, 21, 93.

Cogswell, F. N. 1973. The influence of pressure on the viscosity of polymer melts. Plastics and Polymers, 41, 39.

Donovan, R. C. 1971. A theoretical melting model for plasticating extruders. Polymer Engineering Science, 11, 247.

Eyring, H., S. Glasstone, and K. Lardle. 1941. Theory of Rate Processes. New York: McGraw-Hill.

Griffith, R.M. 1962. Fully developed flow in screw extruder. Theoretical and experimental study. Industrial and Engineering Chemistry Fundamentals, 1, 180.

Lindt, J. T. 1985. Mathematical modeling of melting of polymers in a single-screw extruder. A critical review. Polymer Engineering Science, 25, 585.

Maddock, B. H. 1959. A visual analysis of flow and mixing in extruder screws. Society of Plastics Engineers Journal, 15, 383.

McKelvey, J. M. 1962. Polymer Processing. New York: Wiley.

Middleman, S. 1977. Fundamentals of Polymer Processing. New York: McGraw-Hill.

Mount, E. M., J. G. Walson, and C. I. Chung. 1982. Analytical melting model for extrusion: Melting rate of fully compacted solid polymer. Polymer Engineering Science, 22, 729.

Patterson, W. I., P. Branchi, and J. Paris. 1979. Valve control of extruder output. Society of Plastics Engineering (37th Annual Technical Conference), 25, 166.

Pearson, G. H. 1978. Valve Design. London: Mechnical Engineering Publications Ltd.

Semjonow, V. 1965. Rheology Acta, 4, 133.

Shirato, M., T. Murase, and M. Iwata. 1983. Pressure profile in a power-law fluid in constant-pitch, straight-taper and decreasing-pitch screw extruders. International Chemical Engineering, 23, 323.

Skelland, A. H. P. 1967. Non-Newtonian Flow and Heat Transfer. New York: Wiley.

Tadmore, Z., and G. Gogos. Principles of Polymer Processing. New York: Wiley.

Tadmore, Z., and J. Klein. 1970. Engineering Principles of Plasticating Extrusion. New York: Van Nostrand Reinhold Company.

White, D. H. 1981. Economic analysis of extruder feeder-preheater-reactor systems. Special report to the Department of Energy, Department of Chemical Engineering, University of Arizona, Tucson, August 31.